POLITECNICO DI MILANO

Scuola di Ingegneria Industriale e dell'Informazione
Corso di Laurea Magistrale in Ingegneria Elettrica

POLITECNICO
MILANO 1863

Generation of Scenarios for the Validation of Dynamic Mode Decomposition

Relatore: Prof. Alberto Berizzi

Correlatore: Andrea Vicario

Tesi di Laurea Magistrale di:

Su Can Matr.10572736

Xu Yini Matr.10572963

Anno Accademico 2018-2019

Acknowledgment

First of all, we would like to thank our supervisor Prof. Alberto Berizzi for his availability and professionalism given to us during these months, it has been a pleasure to be his graduated students.

A special gratitude to Andrea Vicario for his precious help in the simulation of this thesis. We wish him all the best in his PhD period.

Thanks for all of the classmates we have met in these years. We would always remember the time we spent together in the campus, going through exams, laughing and sharing life stories.

We would like to thank Xi'an Jiaotong University and Politecnico di Milano. With this double-degree program, we have got the chance to study abroad. The experience in Milan gives us a general expression of Italy and Europe. The food, the people and the scenery here would be unforgettable memories for us.

Thanks for all of our families. You never failed to make your contribution to the success of this work. Thanks for your time and patient for listening to subjects you didn't actually know.

Thanks for Duan Chongwei, Liu Cheng, Hu Rui, Wang Xing and Chen Renqing. We are very lucky to have you all. Thanks for the fantastic days we spent in Rubattino and Gauss.

ABSTRACT

Power systems are complex dynamic systems. Once a power system loses stability, serious consequences may occur within a few seconds. The development of dynamic monitoring technique makes it possible to characterize global behaviors of the power system with data-driven methods.

The thesis focuses on a new framework for electromechanical oscillations identification from observational data, based on dynamic mode decomposition (DMD) algorithm. Our work consists of modal estimates with conventional method and a data-base generation for DMD analysis.

Firstly, a simple two-area testing system is simulated in the DIgSILENT PowerFactory software. The eigenvalues and oscillation modes of the test system are calculated and identified with the use of model-based analysis method.

Secondly, with a Matlab script simulating the stochastic load deviation in real time, selected variables of the system are measured in different scenarios, which provides a data-base for the validation of DMD.

Lastly, DMD algorithm is applied to identify oscillation modes in two typical events. The comparison between the results obtained by DMD algorithm and model-based method can validate the effectiveness of DMD algorithm for the electromechanical modes identification.

Key words：Electromechanical Oscillation；Mode Identification；DMD；

SOMMARIO

Le reti elettriche di potenza sono sistemi dinamici complessi. Una perdita di stabilità da parte della rete può comportare gravi conseguenze nel giro di pochi secondi. Lo sviluppo di tecniche di monitoraggio in tempo reale, basate sull'analisi dei dati, consentirebbe di caratterizzare i comportamenti globali della rete.

La tesi si concentra su una nuova tecnica per l'identificazione delle oscillazioni elettromeccaniche direttamente da dati osservati, basata sull'algoritmo noto come Dynamic Mode Decomposition (DMD). Il nostro lavoro consiste in un'analisi modale con metodo tradizionale e la generazione di un data-base per l'analisi attraverso la DMD.

Viene inizialmente simulato un semplice sistema di test a due aree attraverso il software DIgSILENT PowerFactory. Gli autovalori e i modi oscillatori del sistema di test sono quindi calcolati e identificati con l'uso di un metodo model-based.

Successivamente, grazie ad uno script Matlab che simula la deviazione stocastica del carico stocastico in tempo reale, le principali variabili del sistema vengono acquisite in diversi scenari, per generare così una base di dati per la convalida della DMD.

Infine, l'algoritmo DMD viene applicato per identificare le oscillazioni in due eventi dinamici distinti. Il confronto tra i risultati ottenuti con l'analisi modale e la DMD conferma l'efficacia di quest'ultimo per l'identificazione delle oscillazioni elettromeccaniche.

Key words：Oscillazioni elettromeccaniche；Identificazione dei Modi；DMD；

CONTENTS

1 Introduction

1.1 Background and Significance of Research

Power systems are complex dynamic systems. On the one hand, they must always guarantee the necessary power quality and quantity, on the other hand, they are constantly disturbed.

Time, place, type and severity of the disturbances are random. Once a power system loses stability, serious consequences may occur within a few seconds, causing great economic losses and social impact. Therefore, dynamic power system theory is the basis of power system planning, design and operation, so it has a great significance for a safe and stable operation.

Power system stability may be broadly defined as the property of a power system to remain in a state of operating equilibrium under normal operating conditions and to regain an acceptable state of equilibrium after being subjected to a disturbance. Instability in a power system may be manifested in different ways, depending on the system configuration and operating mode. Traditionally, the stability problem has been the preservation of synchronous operations. Since power systems rely on synchronous machines, a necessary condition for a satisfactory system operation is that all generators remain in synchronism or, colloquially, “in step”. This aspect of stability is influenced by the dynamics of generator rotor angles and power-angle relationships.

For convenience in analysis and to achieve useful insight into the nature of stability problems, it is usual to characterize the rotor angle stability phenomena in terms of the small-signal stability and transient stability.

Small-signal (or small-disturbance) stability is the ability of the power system to maintain synchronism under small disturbances. Such disturbances occur continually on the system because of small variations in loads and generation. The disturbances are considered sufficiently small for a linearization of system equations. In large power systems, variable generation schemes and the stochastic characteristics of loads cause a higher probability of appearance of electromechanical oscillations, refers to inter-area modes (0.1-1 Hz) and local modes (1-5 Hz). These events may cause unsecured operations of the system and the possibility of generator outages and blackouts.

At present, there are mainly two research methods for electromechanical oscillations analysis of the power system.

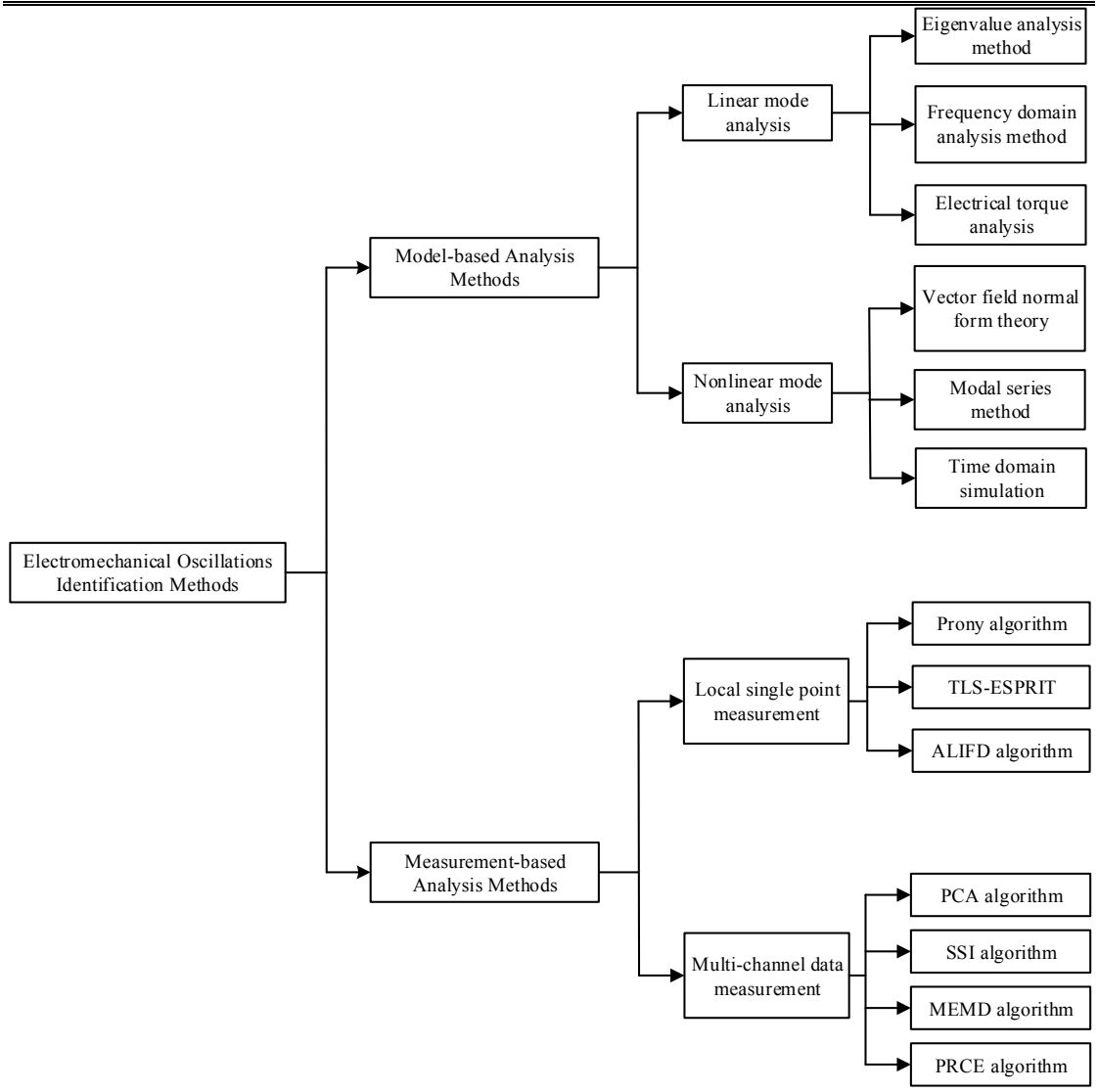

Figure 1.1 Methods of electromechanical oscillation identification

The first one is the model-based analysis method, which is to obtain the system-wide differential and algebraic equations by establishing the electromechanical transient models for all components. The system stability is then analyzed according to the first theorem of Lyapunov stability. However, this method is suitable only for offline analysis and depends on the accuracy of models and parameters. The second one is based on real-time measurement. The recent application of wide area measurement system (WAMS) provides strong support to measurement-based power system stability analysis. The oscillation phenomenon of the system is therefore analyzed by the signal processing technique. Advanced mathematical methods, such as Prony algorithm, Adaptive Local Iterative Filter Decomposition (ALIFD) algorithm and Principal Component Analysis (PCA) algorithm can be used.

- Prony algorithm: In this method, the sample function is constructed through sampled data to determine the order of the signal and the autoregressive coefficient.

The eigenvalue corresponding to the oscillation mode is obtained, and the oscillation characteristic parameter identification is realized. Prony algorithm has a good effect on extracting the steady oscillation mode of the power system, which is widely applied in large-scale power grids.

- ALIFD algorithm: Firstly, the smoothed intrinsic mode function (IMF) component is extracted based on ALIFD decomposition. With the use of Hilbert transform, the oscillation feature parameters are identified. The advantage of this method is that the false modal problem decomposed by EMD algorithm can be avoided. It is applicable to real-time measured signals, and truly reflects the inherent oscillation characteristics of various non-stationary power oscillation signals coupled by multi-mode.
- Principal Components Analysis: PCA is a technique exploited in the multivariate statistics that allows to transform a number of possibly correlated variables into a smaller set of variables called principal components. The goal of PCA is to compute the most significant transformation in order to express variation among a high number of variables through a reduced number of components.

Therefore, it is of great significance for the improvement of real-time monitoring and control of power system oscillation to well and truly identify oscillation modes and parameters based on filed measurement.

1.2 Aim of the Research

The necessity of new tools to identify in real time the oscillations and the behavior of the buses following an event leads Terna to commission this study.

The study focuses on a new method for electromechanical oscillations identification based on Dynamic Mode Decomposition (DMD). Based on recent studies, DMD can be used to analyze the global behavior of electromechanical oscillation. The core objective of DMD algorithm is to find the low dimensional approximate matrix.

A low dimensional approximate matrix is supposed to be obtained from measurements, whose eigenvalues and the corresponding eigenvector could be employed to describe the oscillation features. At this point, the electromechanical oscillation modes would be extracted without knowing the underlying dynamics.

Our work is to first analyze the well-known Kundur testing grid using the model-based method with the DIgSILENT PowerFactory software. Then, generate typical dynamic events of the system and obtain real-time measurement information, which will be used as a data base for DMD to validation to its effectiveness.

1.3 Scope of the Thesis

The other chapters of this research are organized as follow:

- Chapter 2 provides a general description of power system dynamics and small-signal stability phenomena including fundamental concepts and classification.
- Chapter 3 describes the tested system, selected variables and all the events, which offers data base and validation for dynamic model decomposition algorithm.
- Chapter 4 describes the dynamic model decomposition theory and makes comparison between the results of model-based analysis method and dynamic model decomposition method.
- Chapter 5 presents the conclusions of the thesis and highlights some possible future studies.

2 Power System Stability: Small-Signal Stability

2.1 Introduction

The aim of this chapter is to provide a general presentation of power system stability problems concerning classification and physical aspects. It is very important to understand the different types of instability and how they are related to each other. According to the background in Chapter 1, our focus is the electromechanical oscillation problem, which belongs to small-signal stability. Fundamental concepts of small-signal stability are explained in this chapter, as a theoretical groundwork for the subsequent simulations.

2.2 Power System Stability Problem

Power systems are the largest and most complex man-made dynamic systems, which are continuously subjected to perturbations and experience transitions from one operating state to another also in form of oscillations [1]. Instability in a power system may be manifested in different ways depending on the system configuration and operating mode. Traditionally, the stability problem has been the preservation of synchronous operations. This aspect of stability is influenced by the dynamics of generator rotor angles and power-angle relationship.

Classification of the stability problem is presented in Figure 2.1.

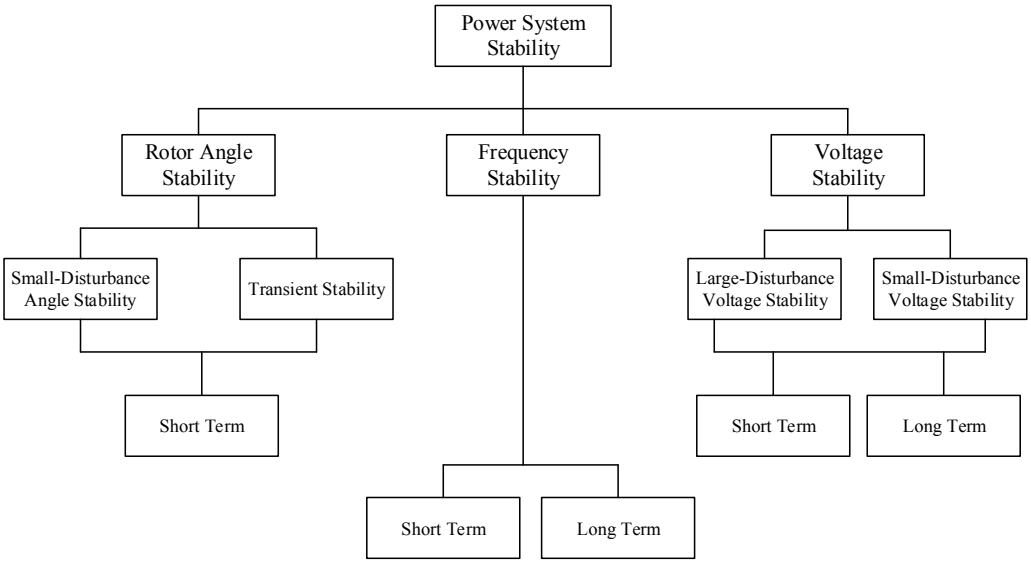

Figure 2.1: Classification of power system stability [2]

Classification of the stability problem is presented in Figure 2.1.

2.2.1 Voltage Stability

Voltage stability refers to the ability of a power system to maintain the nominal voltage at all buses in the system after being subjected to a disturbance from a given initial condition.

However, the major factor contributing to voltage instability is the voltage drop that occurs when active and reactive power flow through inductive reactance of the transmission grid; this limits the capability of the transmission network for power transfer and voltage support, which are limited when some of the generators hit their field or armature current time-overload capability limits[1]. Voltage stability is threatened when a disturbance increases the reactive power demand beyond the sustainable capacity of the available reactive power resources.

2.2.2 Frequency Stability

Frequency stability refers to the ability of a power system to maintain steady frequency following a severe system upset resulting in a significant unbalance between real power generation and load. It depends on the ability to maintain or restore equilibrium between system generation and load, with minimum unintentional loss of load. Instability may occurs in the form of sustained frequency swings leading to tripping of generating units and/or loads [4].

Any unbalance between generation and load demand causes deviation of the system frequency with respect to the nominal value. The system frequency is a global quantity, any unbalance affects the operation of all the synchronous machines of the power system. Any change in the angular frequency leads to a variation of the electromagnetic torque and finally unbalance between the electromagnetic torque and the mechanical torque of the synchronous machines.

The change in the angular frequency is given by[19]

$$\Delta\omega = \frac{\Delta P}{2H_{sys}} \tag{2-1}$$

Where ΔP is the active power unbalance and H_{sys} is the system inertia calculated as the summation of inertias of all the turbine generators in the power system.

2.3 Rotor Angle Stability

Rotor angle stability refers to the ability of inter-connected synchronous machines of a power system to remain in synchronism after being subjected to a disturbance. The stability problem involves the study of the electromechanical oscillations inherent in

power systems. It depends on the ability to maintain or restore equilibrium between electromagnetic and mechanical torque of each synchronous machine in the system. Instability may occurs in the form of increasing angular swings of some generators leading to their loss of synchronism with the others.

2.3.1 The stability phenomena

Stability is a condition of equilibrium between opposing forces. The mechanism by which interconnected synchronous machines maintain synchronism with one another is through restoring forces, which act whenever there are forces tending to accelerate or decelerate one or more machines with respect to other machines.

Under steady-state conditions, there is an equilibrium between the input mechanical torque and the output electrical torque of each machine, and the rotor speed remains constant. If the system is perturbed this equilibrium will be upset, resulting in acceleration or deceleration of the rotors of the machines according to the laws of motion of a rotating body. If one generator temporarily runs faster than another, the angular position of its rotor will advance relative to that of the slower machine. The resulting angular difference transfer part of the load from the slow machine to the fast machine, depending on the power-angle relationship. This tends to reduce the speed difference and hence the angular separation. The power-angle relationship, as discussed above, is highly nonlinear. Beyond a certain threshold, the load transfer is reduced, leading to loss of synchronism and instability.

In electric power systems, the change in electrical torque of a synchronous machine following a perturbation can be resolved into two components:

$$\Delta T_e = T_S \Delta\delta + T_D \Delta\omega \tag{2-2}$$

where

- $T_S \Delta\delta$ is the component of torque change in phase with the rotor angle perturbation $\Delta\delta$ and is referred as the synchronizing torque component;
- T_S is the synchronizing torque coefficient.
- $T_D \Delta\omega$ is the component of torque in phase with the speed deviation $\Delta\omega$ and is referred as the damping torque component;
- T_D is the damping torque coefficient.

System stability depends on the existence of both components of torque for all of the synchronous machines. Lack of enough synchronizing torque results in instability through an aperiodic drift in rotor angle. On the other hand, lack of sufficient damping torque results in oscillatory instability. It is usual to characterize the rotor angle stability phenomena in terms of the small-signal stability and transient stability. In this thesis,

we are concerned about the former one.

2.3.2 Small-signal Stability

Small-signal (or small-disturbance) stability is the ability of the power system to maintain synchronism under small disturbances. Such disturbances occur continually on the system because of small variations in loads and generation. Disturbances are considered sufficiently small for linearization of system equations to be permissible for purposes of analysis. The nature of system response to small disturbances depends on several of factors including the initial operating point, the transmission system strength, and the type of generator excitation controls used. For a generator connected radially to a large power system, in the absence of automatic voltage regulators (i.e., with constant field voltage) the instability is due to lack of sufficient synchronizing torque. This results in instability through a non-oscillatory mode, as shown in Figure (a). With continuously acting voltage regulators, the small-disturbance stability problem is ensuring sufficient damping of system oscillations. Instability is normally through oscillations of increasing amplitude. Figure (b) illustrates the nature of generator response with automatic voltage regulators.

In today's practical power systems, small-signal stability is largely a problem of insufficient damping of oscillations. The following types of oscillations can be detected in power system:

1) *Local modes or machine-system modes*, associated with the swinging of units at a generating station with respect to the rest of the power system. The term *local* is used because the oscillations are localized at one station or a small part of the power system.
2) *Interarea modes*, associated with the swinging of many machines in one part of the system against machines in other parts. They are caused by two or more groups of the closely coupled machines being interconnected by weak ties.
3) *Control modes*, associated with generating units and other controls. Poorly tuned exciters, speed governors, HVDC converters and static var compensators are the usual causes of instability of these modes.
4) *Torsional modes*, associated with the turbine-generator shaft system rotational components. Instability of torsional modes may be caused by interaction with excitation controls, speed governors, HVDC controls, and series-capacitor-compensated lines.

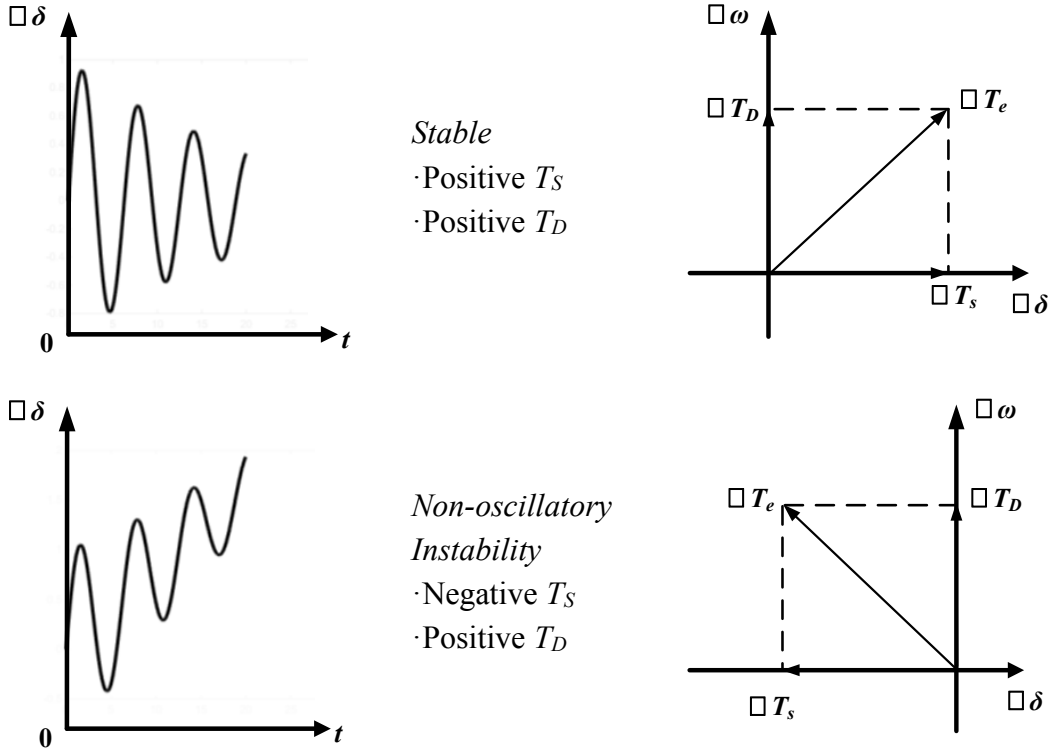

(a) With constant field voltage

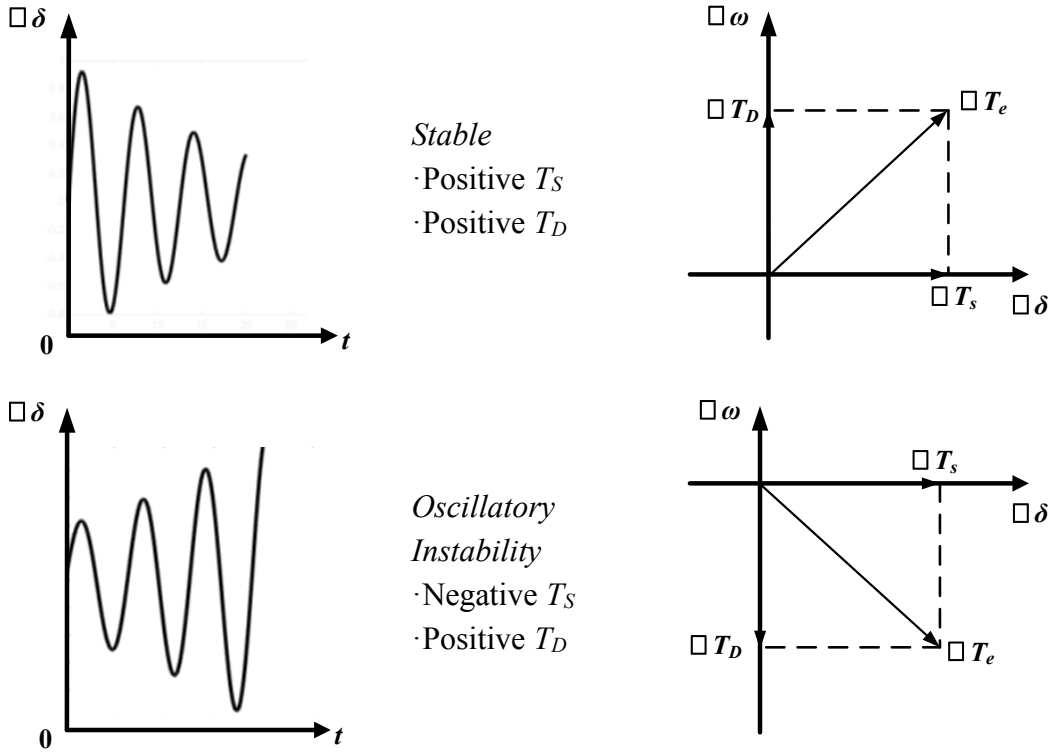

(b) With excitation control

Figure2.2 Nature of small-signal response

2.4 Fundamental concepts of stability of dynamic system

2.4.1 State-Space Representation

The behavior of a dynamic system, such as a power system, may be described by a set of *n* first order nonlinear ordinary differential equations of the following form:

$$\dot{x}_i = f_i\left(x_1, x_2, \ldots, x_n; u_1, u_2, \ldots, u_r; t\right) \quad i = 1, 2, \ldots, n \tag{2-3}$$

where *n* is the order of the system and *r* is the number of inputs. This can be written in the following form by using vector-matrix notation:

$$\dot{\mathbf{x}} = \mathbf{f}\left(\mathbf{x}, \mathbf{u}, t\right) \tag{2-4}$$

where

$$\mathbf{x} = \begin{bmatrix} x_1 \\ x_2 \\ \vdots \\ x_n \end{bmatrix}, \quad \mathbf{u} = \begin{bmatrix} u_1 \\ u_2 \\ \vdots \\ u_n \end{bmatrix}, \quad \mathbf{f} = \begin{bmatrix} f_1 \\ f_2 \\ \vdots \\ f_n \end{bmatrix}$$

The column vector **x** is referred as the state vector, and its entries x_i as state variables. The column vector **u** is the vector of inputs to the system. These are the external signals the influence the performance of the system. Time is denoted by *t*, and the derivative of a state variable *x* with respect to time is denoted by $\dot{x}$. If the derivatives of the state variables are not explicit functions of time, the system is said to be autonomous. In this case, Equation (2-4) simplifies to

$$\dot{\mathbf{x}} = \mathbf{f}\left(\mathbf{x}, \mathbf{u}\right) \dot{\mathbf{x}} = \mathbf{f}\left(\mathbf{x}, \mathbf{u}\right) \tag{2-5}$$

We are often interested in output variables which can be observed on the system. These may be expressed in terms of the state variables and the input variables in the following form:

$$\mathbf{y} = \mathbf{g}\left(\mathbf{x}, \mathbf{u}\right) \tag{2-6}$$

where

$$\mathbf{y} = \begin{bmatrix} y_1 \\ y_2 \\ \vdots \\ y_n \end{bmatrix}, \quad \mathbf{g} = \begin{bmatrix} g_1 \\ g_2 \\ \vdots \\ g_n \end{bmatrix}$$

The column vector **y** is the vector of outputs, and **g** is a vector of nonlinear functions relating state and input variables to output variables.

2.4.2 The concept of state

The concept of state is fundamental to the state-space approach. The state of a system represents the minimum amount of information about the system at any instant in time t_0 that is necessary so that its future behavior can be determined without reference to the input before t_0.

Any set of n linearly independent system variables may be used to describe the state of the system. These are referred to as the state variables, they form a minimal set of dynamic variables that, along with the inputs to the system, provide a complete description of the system behavior. Any other system variables may be determined from a knowledge of the state.

The state variables may be physical quantities in a system such as angle, speed, voltage, or they may be abstract mathematical variables associated with the differential equations describing the dynamics of the system. The choice of the state variables is not unique. This does not mean that the state of the system at any time is not unique; only that the means of representing the state information is not unique. Any set of state variables we may choose will provide the same information about the system. If we over specify the system by defining too many state variables, not all of them will be independent.

The system state may be represented in an n-dimensional Euclidean space called the state space. When we select a different set of state variables to describe the system, we are in effect choosing a different coordinate system.

Whenever the system is not in equilibrium or whenever the input is non-zero, the system state will change with time. The set of points traced by the system state in the state space as the system moves is called the state trajectory.

2.5 Stability of a dynamic system

The concept of state is fundamental for the state-space approach, since the state variables account for the amount of information at time $t=t_0$ that is necessary to have in order to predict the behavior of the system for $t > t_0$ [13]. State variables can be physical quantities (e.g., angle, speed or voltage) or abstract mathematical variables associated with the differential equations describing the dynamics of the system, or variable related to controls.

Another important aspect is the concept of equilibrium points, where all the derivatives of vector $\mathrm{d}\boldsymbol{x}/\mathrm{d}t$ are zero; the equilibrium point is therefore described by the equation

$$f\left(\boldsymbol{x}_0=0\right) \qquad (2\text{-}7)$$

where $\boldsymbol{x}_0$ is the state vector $\boldsymbol{x}$ at the equilibrium point. Let us now consider $\boldsymbol{u}_0$, which is the input vector corresponding to the equilibrium point about which the steady-state stability is to be investigated. Equation (2-4) becomes

$$\dot{\boldsymbol{x}}_0 = f\left(\boldsymbol{x}_0, \boldsymbol{u}_0\right) = 0 \tag{2-8}$$

It is possible to perturb the system from the above state by letting

$$\boldsymbol{x} = \boldsymbol{x}_0 + \Delta\boldsymbol{x}_0 \tag{2-9}$$

$$\boldsymbol{u} = \boldsymbol{u}_0 + \Delta\boldsymbol{u}_0 \tag{2-10}$$

where $\triangle$ represents a small deviation. After some calculations that can be found in [13] and after doing the same for equation (2-6), we get

$$\Delta\frac{d\mathbf{x}}{dt} = \mathbf{A}\Delta\mathbf{x} + \mathbf{B}\Delta\mathbf{u} \tag{2-11}$$

$$\Delta\mathbf{y} = \mathbf{C}\Delta\mathbf{x} + \mathbf{D}\Delta\mathbf{u} \tag{2-12}$$

Where

$$A=\begin{bmatrix} \frac{\partial f_1}{\partial x_1} & \cdots & \frac{\partial f_1}{\partial x_n} \\ \vdots & \cdots & \vdots \\ \frac{\partial f_n}{\partial x_1} & \cdots & \frac{\partial f_n}{\partial x_n} \end{bmatrix}$$

$$B=\begin{bmatrix} \frac{\partial f_1}{\partial u_1} & \cdots & \frac{\partial f_1}{\partial u_n} \\ \vdots & \cdots & \vdots \\ \frac{\partial f_n}{\partial u_1} & \cdots & \frac{\partial f_n}{\partial u_n} \end{bmatrix}$$

$$\mathrm{C}=\begin{bmatrix} \frac{\partial g_1}{\partial x_1} & \cdots & \frac{\partial g_1}{\partial x_n} \\ \vdots & \cdots & \vdots \\ \frac{\partial g_n}{\partial x_1} & \cdots & \frac{\partial g_n}{\partial x_n} \end{bmatrix}$$

$$\mathrm{D}=\begin{bmatrix} \frac{\partial g_1}{\partial u_1} & \cdots & \frac{\partial g_1}{\partial u_n} \\ \vdots & \cdots & \vdots \\ \frac{\partial g_n}{\partial u_1} & \cdots & \frac{\partial g_n}{\partial u_n} \end{bmatrix} \tag{2-13}$$

where

$\triangle \boldsymbol{x}$ is the state vector of dimension n

$\triangle \boldsymbol{y}$ is the output vector of dimension m

$\triangle \boldsymbol{u}$ is the input vector of dimension r

A is the state or plant matrix of size $n \times n$

B is the control or input matrix of size $n \times r$

C is the output matrix of size $m \times n$

D is the feed forward matrix which defines the proportion of input which appears directly in the output, size $m \times n$

Taking the Laplace transform of equations (2-11) and (2-12), we get the state equations in the frequency domain, whose block diagram is represented in Figure 2.3, where the initial conditions are assumed to be zero.

$$s\Delta \boldsymbol{x}(s) - \Delta \boldsymbol{x}(0) = A\Delta \boldsymbol{x}(s) + B\Delta \boldsymbol{u}(s) \tag{2-14}$$

$$\Delta \boldsymbol{y}(s) = C\Delta \boldsymbol{x}(s) + D\Delta \boldsymbol{u}(s) \tag{2-15}$$

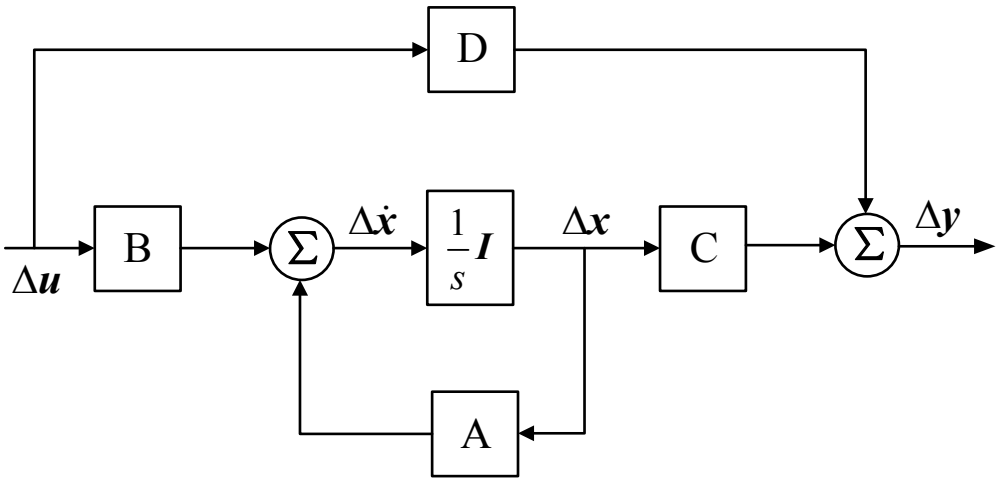

Figure 2.3 Block diagram of the states-space representation. [3]

The same happens for equation (2-16) obtaining

$$\Delta \boldsymbol{y}(s) = C\frac{adj(s\boldsymbol{I} - A)}{\det(s\boldsymbol{I} - A)}\left[\Delta \boldsymbol{x}(0) + B\Delta \boldsymbol{u}(s)\right] + D\Delta \boldsymbol{u}(s) \tag{2-16}$$

The poles of $\Delta \boldsymbol{x}(s)$ and $\Delta \boldsymbol{y}(s)$ are the roots of the equation

$$\det(s\boldsymbol{I} - A) = 0 \tag{2-17}$$

Equation (2-22) is called characteristic equation of matrix **A**.

According to Lyapunov's first method[1], which said a linear system is asymptotically stable if and only if all its eigenvalues have negative real part. The

stability analysis needs just a simple algebraic equation solution in order to evaluate the eigenvalues of the system [2]. These ones can be found considering that eigenvalues of a matrix are given by the values of the scalar parameter λ for which non-zero solutions to the equation exist:

$$A\Phi = \lambda\Phi \tag{2-18}$$

To find the eigenvalues, it is better to write equation (2-23) as

$$\left(A - \lambda I\right)\Phi = 0 \tag{2-19}$$

whose non-zero solution is

$$\det\left(A - \lambda I\right) = 0 \tag{2-20}$$

that is the same as equation (2-18).

The time dependent characteristic of a mode corresponding to complex eigenvalue λ_i is given by $e^{\lambda it}$; for this reason, the stability of the system is determined by the eigenvalues as follows:

- A real eigenvalue corresponds to a non-oscillatory mode. A negative real eigenvalue represents a decaying mode. A positive real eigenvalue represents aperiodic instability.
- Complex eigenvalues occur in conjugate pairs, and each pair corresponds to an oscillatory mode. For example

$$\left(a + jb\right)e^{(\sigma - j\omega)t} + \left(a - jb\right)e^{(\sigma + j\omega)t} \tag{2-21}$$

has the form

$$e^{\sigma t}\sin\left(\omega t + \theta\right) \tag{2-22}$$

that represents a damped sinusoid for negative values of σ.

The real component of the eigenvalues gives the damping, while the imaginary part component gives the frequency of oscillation ω. A negative real part represents a damped oscillation whereas a positive real part represents oscillations of increasing amplitude. For a complex pair of eigenvalues

$$\lambda = \sigma \pm j\omega \tag{2-23}$$

The frequency of oscillation in Hertz is given by

$$f = \frac{\omega}{2\pi} \tag{2-24}$$

that represents the damped frequency. The damping ratio is given by

$$\xi=\frac{-\sigma}{\sqrt{\sigma^2+\omega^2}} \tag{2-25}$$

2.6 Properties of matrix A

For any eigenvalue found from equation (2-21), the *n*-column vector Φ_i that satisfies equation (2-19) is called right eigenvector of A associated with λ_i For this reason, we can rewrite equation (2-19) as

$$A\Phi_i = \lambda\Phi_i \tag{2-26}$$

In the same way, considering a n-row vector Ψ_i that satisfies

$$\Psi_i A = \lambda_i \Psi_i \tag{2-27}$$

is called left eigenvector associated with λ_i. Left and right eigenvectors related to different eigenvalues are orthogonal. It means that, if $\lambda_i \neq \lambda_j$

$$\Psi_j \Phi_i = 0 \tag{2-28}$$

On the other hand, considering normalized eigenvectors related to the same eigenvalue, we have that

$$\Psi_i \Phi_i = 1 \tag{2-29}$$

Let us now consider a zero input system ($\triangle \boldsymbol{u}$=0). We can rewrite equation (2-6) as

$$\Delta \dot{\boldsymbol{x}} = A\Delta \boldsymbol{x} \tag{230}$$

The goal is to eliminate the coupling between the state variables in order to better study the motion of the system; to do this, a new vector z is introduced so that

$$\Delta \boldsymbol{x} = \Phi z \tag{2-31}$$

where Φ is defined as

$$\Phi=\begin{bmatrix}\Phi_1 & \Phi_2 & \cdots & \Phi_n\end{bmatrix} \tag{2-32}$$

Inserting equation (2-33) in equation (2-32) we obtain

$$\Phi \dot{z} = A\Phi z \tag{2-33}$$

and the new state equation can be written as

$$\dot{z} = \Phi^{-1} A\Phi z \tag{2-34}$$

Introducing **Λ** as a diagonal matrix with the eigenvalues λ_1, λ_2,⋯, λ_n as diagonal elements, equation (2-34) becomes

$$\dot{z} = \Lambda z \tag{2-35}$$

where Λ is defined as

$$\Lambda=\Phi^{-1} A\Phi \tag{2-36}$$

According to equation (1.35), the response in terms of the original state vector is given by

$$\Delta \boldsymbol{x}(t) = \Phi z(t) = \begin{bmatrix} \Phi_1 & \Phi_2 & \cdots & \Phi_n \end{bmatrix} \begin{bmatrix} z_1(t) \\ z_2(t) \\ \vdots \\ z_n(t) \end{bmatrix} \tag{2-37}$$

keeping into consideration equation (1.33) in matrix form, that

$$z(t) = \Phi^{-1} \Delta x(t) = \Psi \Delta x(t) \tag{2-38}$$

2.6.1 Mode shape

Variables $\Delta x_1, \Delta x_2, \cdots, \Delta x_n$ are the original state variables that represent the dynamic performance of the system, while variables $z_1, z_2, \cdots, z_n$ are the transformed state variables such as each of them is connected with only one mode. From equation (2-39) it is possible to notice that the right eigenvector gives the mode shape, that is the relative activity of the state variables when a particular mode is excited; on the other hand, from equation (2-40) we can see that the left eigenvector identifies which combination of the original state variables displays only the i^{th} mode.

Thus, the k^{th} element of Φ_i measures the activity of the variable x_k in the i^{th} mode, while the k^{th} element of Ψ_i weights the contribution of this activity to the i^{th} mode.

2.6.2 Participation factor

One problem exploiting right and left eigenvectors individually for identifying the relationship between the states and the modes is that the elements of the eigenvectors are dependent on units and scaling associated with the state variables. A solution for this problem is represented by the participation matrix P defined as the k^{th} state variables in i^{th} the mode.

$$P = \begin{bmatrix} P_1 & P_2 & \cdots & P_n \end{bmatrix} \tag{2-39}$$

with

$$p_i = \begin{bmatrix} p_{1i} \\ p_{2i} \\ \vdots \\ p_{ni} \end{bmatrix} = \begin{bmatrix} \Phi_{1i}\Psi_{1i} \\ \Phi_{2i}\Psi_{2i} \\ \\ \Phi_{ni}\Psi_{ni} \end{bmatrix} \qquad (2\text{-}40)$$

The generic element $p_{ki=}\Phi_{ki}\Psi_{ki}$ is the so called participation factor, which describes the relative participation of the Participation factors are good indicators for the relative participations of the related states in the respective modes.

2.6.3 Controllability and Observability

The system response in the presence of input was given as

$$\Delta\dot{\mathbf{x}} = \mathbf{A}\Delta\mathbf{x} + \mathbf{B}\Delta\mathbf{u} \qquad (2\text{-}41)$$

$$\Delta\mathbf{y} = \mathbf{C}\Delta\mathbf{x} + \mathbf{D}\Delta\mathbf{u} \qquad (2\text{-}42)$$

Expressing them in terms of the transformed variables $\mathbf{z}$ defined by (2-46)

$$\mathbf{\Phi}\dot{\mathbf{z}} = \mathbf{A}\mathbf{\Phi}\mathbf{z} + \mathbf{B}\Delta\mathbf{u} \qquad (2\text{-}43)$$

$$\Delta\mathbf{y} = \mathbf{C}\mathbf{\Phi}\mathbf{z} + \mathbf{D}\Delta\mathbf{u} \qquad (2\text{-}44)$$

The state equations in the “normal form”(decoupled) may therefore be written as

$$\dot{\mathbf{z}} = \mathbf{\Lambda}\mathbf{z} + \mathbf{B}'\Delta\mathbf{u} \qquad (2\text{-}45)$$

$$\Delta\mathbf{y} = \mathbf{C}'\mathbf{z} + \mathbf{D}\Delta\mathbf{u} \qquad (2\text{-}46)$$

where

$$\mathbf{B}' = \mathbf{\Phi}^{-1}\mathbf{B}$$
$$\mathbf{C}' = \mathbf{C}\mathbf{\Phi}$$

Referring to Equation (2-49), if the i^{th} row of matrix $\mathbf{B}'$ is zero, the inputs have no effect on the i^{th} mode. In such a case, the i^{th} mode is said to be uncontrollable.

From Equation (2-46), we see that the i^{th} column of the outputs. If the column is zero, then the corresponding mode is unobservable. This explains why some poorly damped modes are sometimes not detected by observing the transient response of a few monitored quantities.

The $n \times r$ matrix $\mathbf{B}' = \mathbf{\Phi}^{-1}\mathbf{B}$ is referred to as the model controllability matrix, and the $m \times n$ matrix $\mathbf{C}' = \mathbf{C}\mathbf{\Phi}$ as the mode observability matrix.

By inspecting $\mathbf{B}'$ and $\mathbf{C}'$ we can classify modes into controllable and observable; controllable and unobservable; uncontrollable and observable; uncontrollable and unobservable.

2.7 Characteristics of small-signal stability problems

In large power systems, small-signal stability problems may be either local or global in nature.

2.7.1 Local problems

Local problems involve a small part of the system. They may be associated with rotor angle oscillations of single generator or a single plant against the rest of the power system. Such oscillations are called local plant mode oscillations. The stability problems related to such oscillations are similar to those of a single-machine infinite bus system. Most commonly encountered small-signal stability problems are of this category.

Local problems may also be associated with oscillations between the rotors of a few generators close to each other. Such oscillations are called intermachine or interplant mode oscillations. Usually, the local plant mode and interplant mode oscillations have frequencies in the range of 0.7 to 2.0 Hz.

Other possible local problems include instability of modes associated with controls of equipment such as generator excitation systems, HVDC converters, and static var compensators. The problems associated with control modes are due to inadequate tuning of the control systems [6]. In addition, these controls may interact with the dynamics of the turbine-generator shaft system, causing instability of torsional mode oscillations [7].

Analysis of local small-signal stability problems requires a detailed representation of a small portion of the complete interconnected power system. The rest of the system representation may be appropriately simplified by use of simple models and system equivalents. Usually, the complete system may be adequately represented by a model having several hundred states at most.

2.7.2 Global Problems

Global small-signal stability problems are caused by interactions among large groups of generators and have widespread effects. They involve oscillations of a group of generators in one area swinging against a group of generators in another area. Such oscillations are called interarea mode oscillations.

Large interconnected systems usually have two distinct forms of interarea oscillations:

a) A very low frequency mode involving all the generators in the system. The system is essentially split into two parts, with generators in one part swinging against machines in the other part. The frequency of this mode o oscillation is on the order of 0.1-0.3Hz.

b) Higher frequency modes involving subgroups of generators swinging against each other. The frequency of these oscillations is typically in the range of 0.4Hz to 0.7 Hz.

2.7.3 Factors influencing interarea modes of oscillation

The characteristics of interarea modes of oscillation are very complex and significantly differ from the characteristics of local plant modes. Load characteristics, in particular, have major effect on the stability of interarea modes. The manner in which excitation systems affect interarea oscillations depends on the types and locations of the exciters, and on the characteristics of loads [2].

Speed-governing systems normally do not have a very significant effect on interarea oscillations. However, if they are not properly tuned, they may decrease damping of the oscillations slightly. In extreme situations, this may be sufficient to aggravate the situation significantly. In the absence of any other convenient means of increasing the damping, adjustment of blocking of the governors may provide some relief [4].

A mode of oscillation in one part of the system may interact with a mode of oscillation in a remoter part due to mode coupling. This occurs when the frequencies of the two modes are nearly equal [4]. Care should be exercised in interpreting results of analysis in such cases.

The controllability of interarea modes with PSS is a complex function of many factors:

- Location of unit with PSS
- Characteristics and location of loads
- Types of exciters on other units

On some units, the PSS does not have the desired effect on the damping of interarea oscillations. Reference 24 presents results of detailed study of factors influencing PSS performance in damping interarea and interplant modes of oscillation.

Other effective means of stabilizing interarea modes of oscillation include modulation of HVDC converter controls and static var compensator controls.

Analysis of interarea oscillations requires detailed representation of the entire interconnected power system. Models for excitation system and loads, in particular should be accurate, and the same level of modelling detail should be used throughout

the system.

3 Test System Simulations

3.1 Introduction

In this Chapter, a two-area system, which is quite similar to the Kundur system, is studied with the DigSILENT PowerFactory software. According to the mode-based analysis theory presented in Chapter 2, eigenvalues and oscillation modes of the test system are calculated and identified.

Since the thesis aims at validating the effectiveness of dynamic mode decomposition algorithm in electromechanical oscillations analysis, real-time measurements are required. In this Chapter, five load events, three short-circuit events, three generator events and two switch events are applied to the tested system. Selected variables in different scenarios are extracted, thereby giving a data base for dynamic mode decomposition algorithm. An additional Matlab script is used to simulate the stochastic load deviation in real time.

3.2 Parameters of the test system

In this section, we analyze the small-signal stability of a simple two-area system as shown in Figure 3.1. Parameters of the test system is quite similar to the classic Kundur system. However, several control devices, such as PSS, governors and AVRs are applied, which would influence the dynamic behavior of the system.

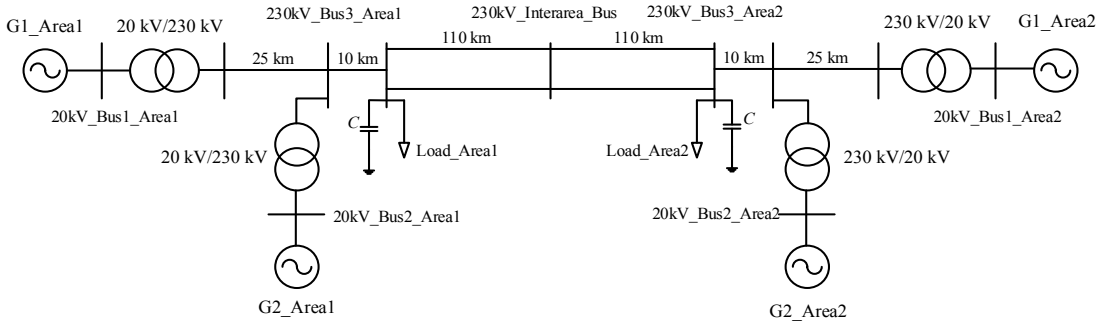

Figure 3.1 two-area system

The test system consists of two similar areas connected by two weak tie links. Each area consists of two coupled units, each having a rating power of 900MVA and a rating voltage of 20 kV. The generator parameters in per unit on the rated MVA and kV base are as follows:

Table 3.1 Parameters of synchronous machines

X_d=1.8	X_q=1.7	X_l=0.2	X'_d=0.3
X''_d=0.25	X''_q=0.25	X'_q=0.55	T'_{d0}=8.0 s
T''_{d0}=0.03 s	T'_{q0}=0.4s	T''_{q0}=0.05s	K_d=0
H=6.5 (for G1 and G2)		H=6.175 (for G3 and G4)	

Each step-up transformer with Yn/D connection, has an impedance of 0+j0.15 p.u., and an off-nominal ratio of 1.0.

The transmission system nominal voltage is 230 kV. The line lengths are identified in Figure 3.1. The parameters of lines in per unitbase are as follows:

Table 3.2 Parameters of transmission lines

r=0.0001 pu/km	x_l=0.001pu/km	b_c=0.00175 pu/km

The system is operating with area1 exporting 400MV to area2, and the generating units are loaded as follows:

Table 3.3 Generating units and load

Synchronous machine	P/(MW)	Q/(MVar)	E_t
G1_Area1:	700	185	1.03∠20.2°
G2_Area1:	700	234	1.01∠10.4°
G1_Area2:	719	176	1.03∠-6.8°
G2_Area2:	700 MW	202	1.01∠-17.0°

The load and reactive power supplied (Q_c) by the shunt capacitors at 230kV_Bus3_Area1 and 230kV_Bus3_Area1 are as follows:

Table 3.4 Load and reactive power supplied (Q_c)

Line	P_L	Q_L	Q_c
230kV_Bus3_Area1	967 MW	100 MVar	200 MVar
230kV_Bus3_Area2	1767 MW	100 MVar	350 MVar

3.3 Eigenvalues and mode shape of the test system

The eigenvalues, frequencies, and damping ratios of rotor oscillation modes are here determined when all the four generators are equipped with PSS, governors and AVRs. Moreover, the active components of loads have constant current characteristics, and the reactive components of loads have constant impedance characteristics. The results are shown in Table 3.5.

Figure 3.2 shows a plot of all eigenvalues on a complex plane. Table 3.5

summarizes the eigenvalues of the system state matrix. The first row represents the zero eigenvalue due to the redundant state variables. According to the theory [1], the zero eigenvalue is due to lack of uniqueness of absolute rotor angle (there is no infinite bus, and the rotor angles are referred to a common reference frame).

In Figure 3.2 and Table 3.6, we can see that the system is stable. To identify the critical modes of electromechanical oscillation, eigenvalues of modes with frequencies in the range of 0.1 Hz to 5 Hz are extracted. Figure 3.3 shows a plot of these eigenvalues on a complex plane. The box in the figure represents the modes of oscillation that mainly depend on $\triangle\omega$ and $\triangle\delta$ of four generators. Their mode shapes (normalized eigenvector components corresponding to rotor speeds) are shown in Figure 3.4.

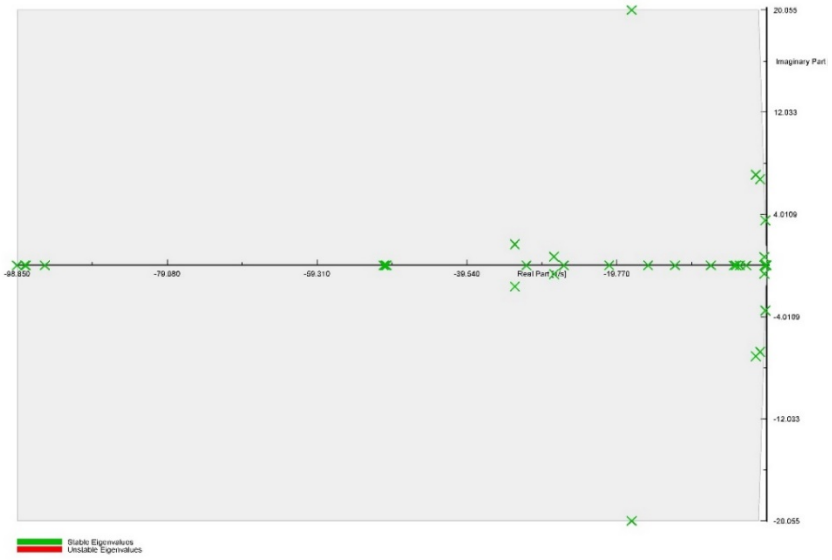

Figure 3.2 Eigenvalues of the system

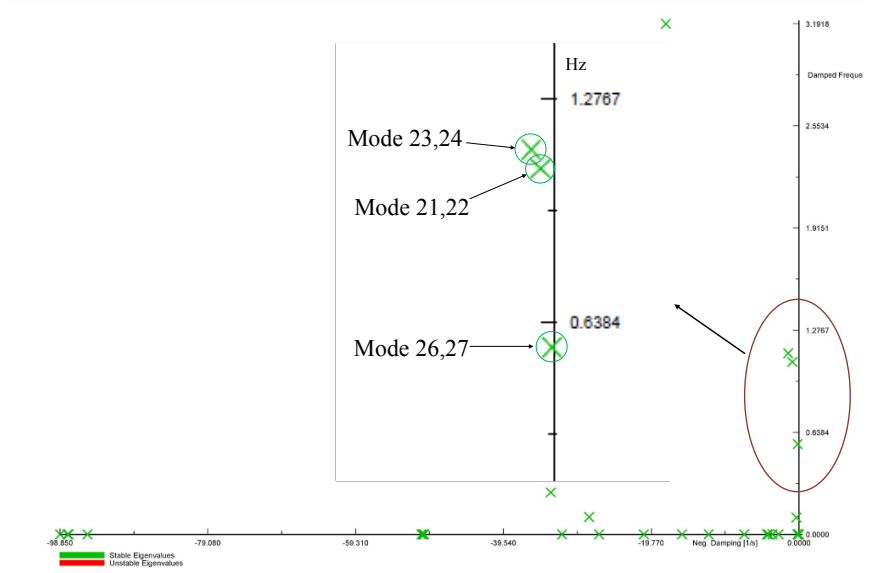

Figure 3.3 Modes of electromechanical oscillation

Table 3.5 Test system modes

Name	Eigenvalues		Frequency (Hz)	Damping Ratio
	Real part	Imaginary part		
Mode 1	0.0000	-	-	-
Mode 2	-95.1931	-	-	1.0000
Mode 3	-98.8498	-	-	1.0000
Mode 4	-97.8364	-	-	1.0000
Mode 5	-97.7063	-	-	1.0000
Mode 6	-50.5244	-	-	1.0000
Mode 7	-50.1216	-	-	1.0000
Mode 8	-50.2778	-	-	1.0000
Mode 9	-50.2260	-	-	1.0000
Mode 10,11	-17.7977	±20.0546	3.1918	0.6638
Mode 12,13	-33.2134	±1.6476	0.2622	0.9988
Mode 14	-31.6904	-	-	1.0000
Mode 15,16	-28.0529	±0.6845	0.1089	0.9997
Mode 17	-26.7544	-	-	1.0000
Mode 18	-20.7742	-	-	1.0000
Mode 19	-15.6368	-	-	1.0000
Mode 20	-12.0767	-	-	1.0000
Mode 21,22	-0.8797	±6.7700	1.0775	0.1289
Mode 23,24	-1.4478	±7.1173	1.1328	0.1993
Mode 25	-7.3389	-	-	1.0000
Mode 26,27	-0.1826	±3.5402	0.5634	0.0515
Mode 28	-4.2823	-	-	1.0000
Mode 29	-4.0563	-	-	1.0000
Mode 30	-3.5389	-	-	1.0000
Mode 31	-2.7235	-	-	1.0000
Mode 32,33	-0.3214	±0.6628	0.1055	0.4363
Mode 34	-0.0742	-	-	1.0000
Mode 35	-0.2462	-	-	1.0000
Mode 36	-0.2432	-	-	1.0000
Mode 37	-0.1014	-	-	1.0000
Mode 38	-0.1019	-	-	1.0000
Mode 39	-0.1017	-	-	1.0000
Mode 40	-0.2107	-	-	1.0000
Mode 41	-0.1939	-	-	1.0000
Mode 42	-0.1842	-	-	1.0000
Mode 43	-0.1848	-	-	1.0000
Mode 44	-0.1851	-	-	1.0000

According to the mode shapes, the 1.077 Hz mode represents an electromechanical mode in area1, with G1 swinging against G2. The second electromechanical mode, with frequency of 1.133 Hz, is a local mode in area2. Finally, the 0.563 Hz mode is an interarea mode, in which the two generators in area 1 are swinging against those in area 2.

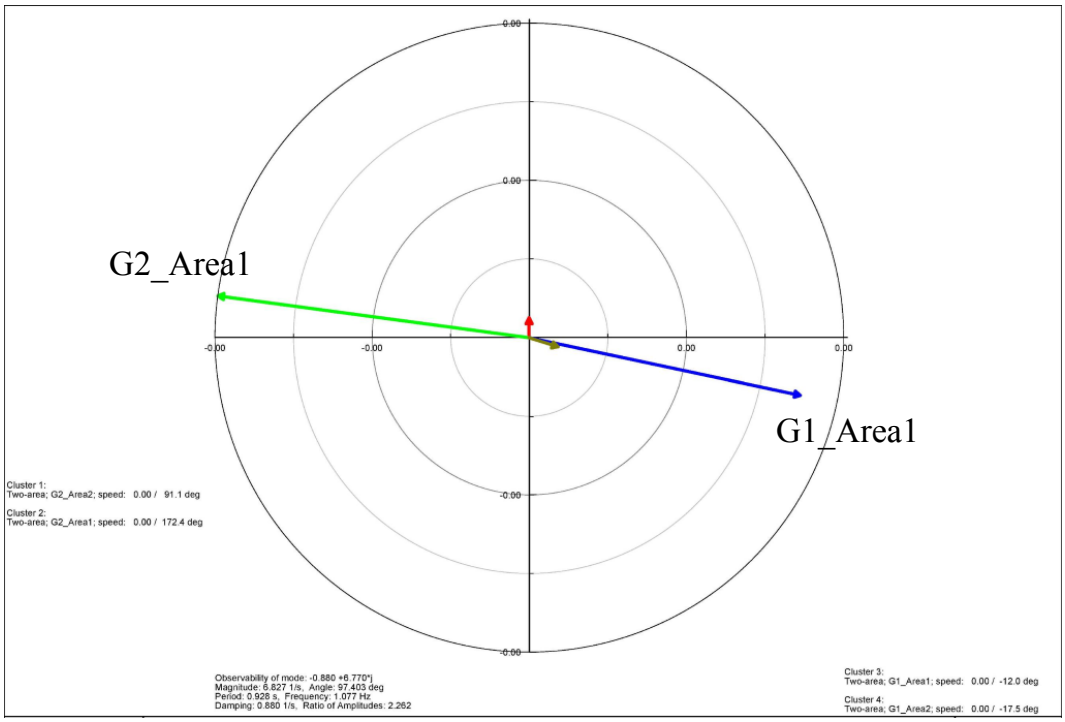

(a) Area 1 local mode f=1.077 Hz, ζ=0.1289

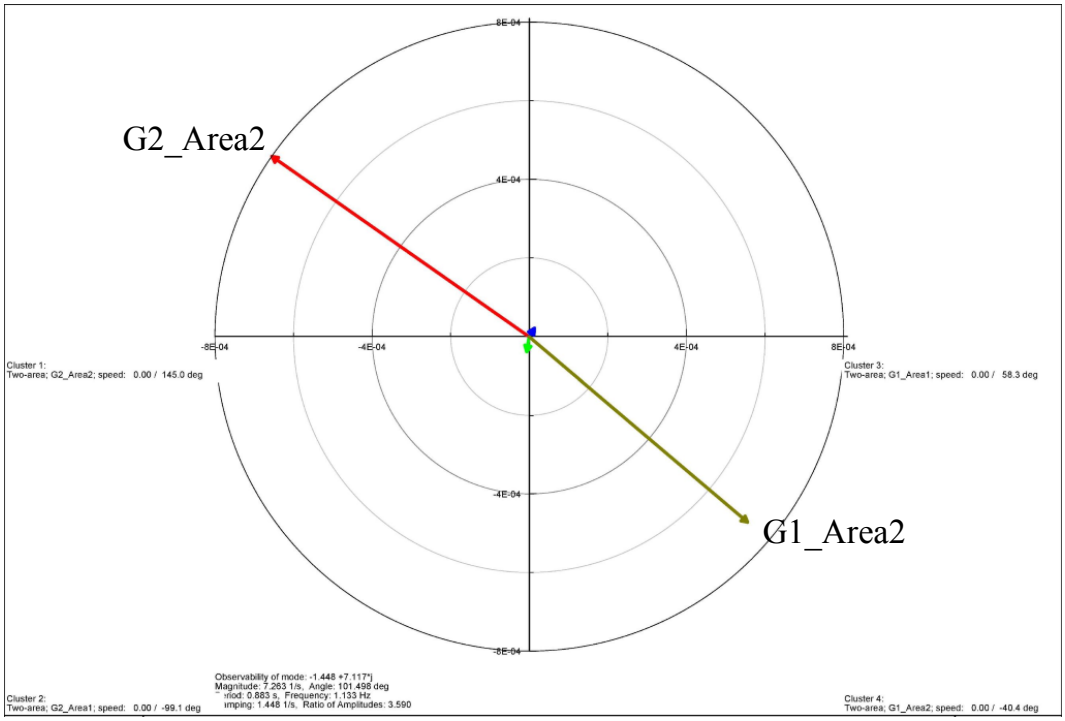

(b) Area 2 local mode f=1.133 Hz, ζ=0.1993

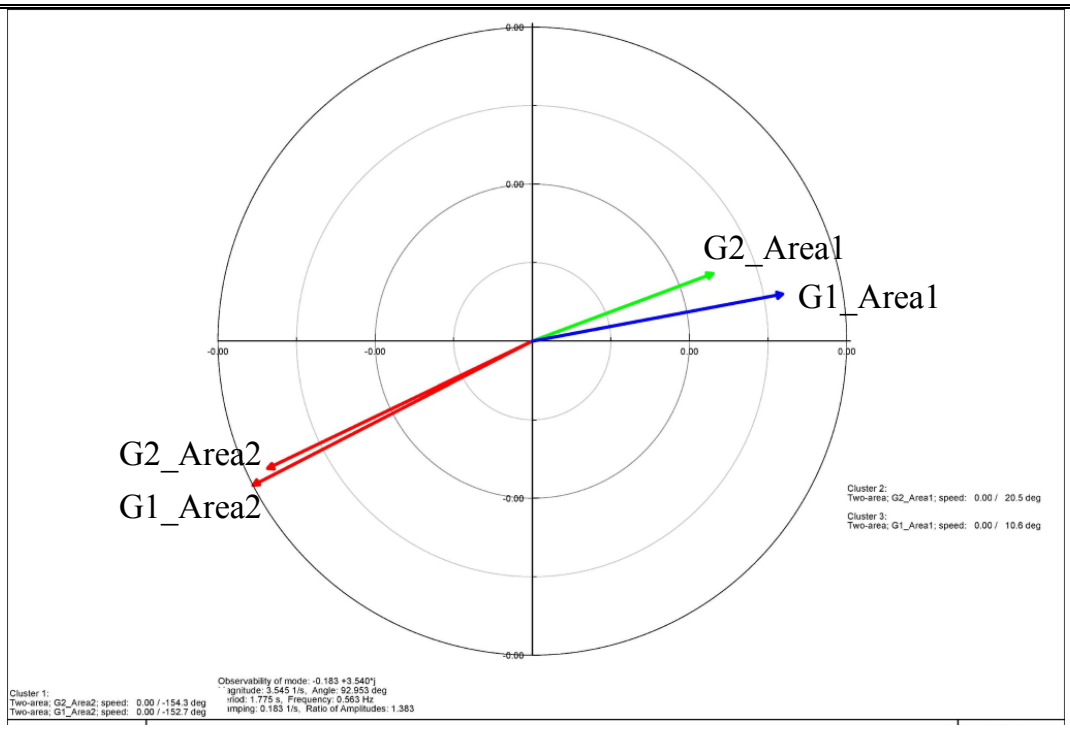

(c) Interarea mode f=0.563 Hz, ζ=0.0515

Figure 3.4 Mode shapes of rotor angle

3.4 Stochastic Load Deviation Generation

Irregular load fluctuation may cause risk for system operation, thus, it is necessary to involve the stochastic load deviation in our simulations.

Typical load curve can be decomposed into three components as shown in Equation (3-1)

$$P_L = P_{Ls} + P_{Lm} + P_{Lf} \qquad (3\text{-}1)$$

where P_{Ls} refers to the short-term load component, whose changing period is within 10s. The proportion of P_{Ls} is generally less than 1%. P_{Lm} refers to the load component with a changing period from 10s to several minutes. Its average changing range is more or less 2.5% of the peak load. P_{Lf} refers to the continuously varying load component with a long period.

We are concerned about the real-time load fluctuation, only the component of very short period is taken into consideration. Therefore, we add a stochastic load deviation of 0.5%(less than 1%) to the given load in the two-area system. Since we cannot simulate stochastic load variations with Digsilent, a Matlab script for stochastic load generation is used. The codes are given as follows:

Matlab code:

```
clear all
clc
%% Original data
%Initial loads - kundur System - Set the initial values of the load

La=967+1i*100;
Lb=1767+1i*100;

%Power Factor
phi_La=atan(imag(La)/real(La)); %inductive, lagging, +
phi_Lb=atan(imag(Lb)/real(Lb)); %inductive, lagging, +
PF_La=cos(phi_La); % by doing this, the angle will be
PF_Lb=cos(phi_Lb); % always the same

%% Stochastic profile

%Mean and deviation Stochastic load deviation: 0.5%
mu_a=real(La); sig_a=5;
mu_b=real(Lb); sig_b=10;

%Sampling time
samt=0.1; %10 samples per s
simt=1000; %simulation time in s
nums=simt/samt; %number of samples
stvec=0:samt:simt; stvec(1)=[]; stvec=stvec';

%Generating the active power load profile following gaussian distr.
% generates a random number from the normal distribution with mean parameter
% mu and standard deviation parameter sigma.
PLa=normrnd(mu_a,sig_a,[nums,1]);
PLb=normrnd(mu_b,sig_b,[nums,1]);

%Generating the reactive power load profile considering the PF constant
QLa=PLa.*tan(phi_La);
QLb=PLb.*tan(phi_Lb);

%Matrices with time
```

```
Lavec=[stvec PLa QLa];
Lbvec=[stvec PLb QLb];

%% Saving

% dlmwrite('myFile.txt',M,'delimiter','\t','precision',3) Write matrix M to a file, 'myFile.txt',
% delimited by the tab character and using a precision of x significant digits
dlmwrite('PLa.txt',Lavec,'delimiter','\t','precision',7)
dlmwrite('PLb.txt',Lbvec,'delimiter','\t','precision',7)
disp('Saved')
```

3.5 Description of scenarios generated as the data base of DMD

We use DIgSILENT PowerFactory software in order to implement and study the stability of the test system. PowerFactory is a leading power system analysis software application for the analyses of generation, transmission, distribution and industrial systems. It covers the full range of functionality from standard features to highly sophisticated and advanced applications including wind power, distributed generation, real-time simulation and performance monitoring for system testing and supervision. PowerFactory offers a complete suite of functions for studying large interconnected power systems and addressing these emerging needs. Its fast and robust simulation algorithms can be applied to any AC or DC network topology and support the simulation of new technologies such as converter-based power generation, FACTS, voltage-sourced converters (VSC), HVDC cables and overhead lines, DC breakers, filters, and various types of MW- and Mvar-controllers and virtual power plants.

3.5.1 Selected variables

To verify the ability of dynamic mode decomposition algorithm, simulated measurements in different scenarios are required. The following variables of power grid are selected to form a data base.

1) Frequency of busbars;
2) Voltage magnitudes and angles of busbars;
3) Currents on transmission lines;
4) Speeds and rotor angles of synchronous machines.

3.5.2 Working list

The two-area system is simulated in the software as shown in Figure3.5

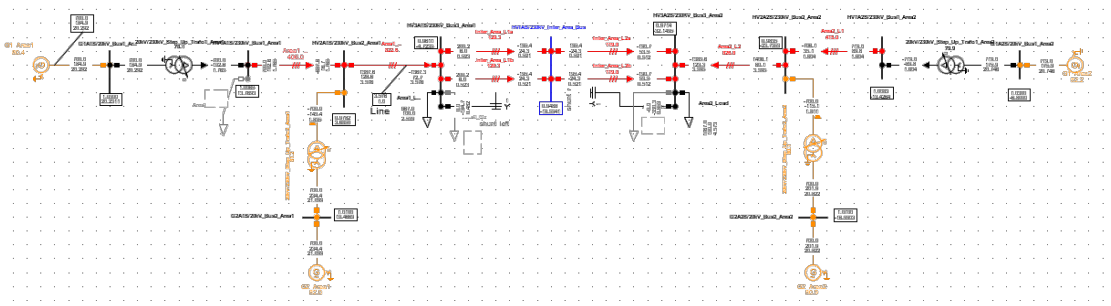

Figure 3.5 Test case in Power Factory:

The simulation step size is set a 10ms for a total duration of 100s. Stochastic load deviations are selected as 0.5% of rated loads' power. As listed in Table 3.6, five load events, three short-circuit events, three generator events and two switch events are applied to generate the data base.

Table 3.6 Working list:

Case	No.	Description
Load Event	1	Increase Area1_Load for 10% every 10s for three times;
	2	Decrease Area1_Load for 10% every 10s for three times;
	3	Increase Area2_Load for 10% every 10s for three times;
	4	Decrease Area2_Load for 10% every 10s for three times;
	5	Increase Area1_Load and Area2_Load both for 10%
Short-circuit Event	1	3 phase short-circuit event on InterArea_L1a at 10s, clear the fault after 20ms
	2	3 phase short-circuit event on InterArea_L2a at 10s, clear the fault after 20ms
	3	3 phase short-circuit on Area1_G1 at 5s, after 20ms clear the fault. 3 phase short-circuit on Area1_G2 at 25s, after 20ms clear the fault. 3 phase short-circuit on Area2_G2 at 45s, after 20ms clear the fault. 3 phase short-circuit on Area2_G1 at 65s, after 20ms clear the fault.
Generator Event	1	Decrease Area1_G2 for 100MW and increase Area2_G2 for 100MW at the same time (t=10s). Back to the initial condition at t=40s.
	2	Decrease Area1_G2 for 300MW and increase Area2_G2 for 300MW at the same time (t=10s). Back to the initial condition at t=40s.
	3	Decrease Area1_G1 for 600MW and increase Area1_G2 for 600MW at the same time(t=10s). Keep for 30s, then remove Area1_G1 at t=40s.
Switch Event	1	Open the switch on line Inter_Area_L1a at 10s
	2	Open the switch on line Inter_Area_L2a at 10s

3.6 Simulation results

3.6.1 Element as Reference

Taking a single-machine infinite system as an example, if the generator uses the classical second-order model, ignoring the dynamic process of the prime mover, the governor, and the excitation system [28].

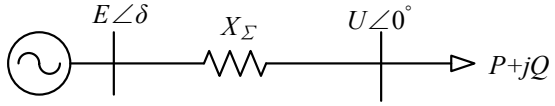

Figure 3.6 Single-machine infinite system

The complete mathematical model of the system can be described as

$$\begin{cases} M\dfrac{d\omega}{dt} = P_m - P_e \\ \dfrac{d\delta}{dt} = \omega \end{cases} \tag{3-2}$$

where, ω refers to the deviation between rotor speed and synchronous speed; δ refers the rotor angle; P_m=const. refers to the mechanical power; $P_e = \dfrac{EU}{X_\Sigma}\sin\delta$ refers to the electromagnetic power; X_Σ is the total reactance of the system between $E\angle\delta$ the internal potential of the generator) and $U\angle 0^\circ$ (the voltage of infinite system), whereas the resistance is assumed zero. E and U are constant, M is the inertia time constant (T_J) of the generator.

The Kinetic energy of the system V_k can be define as (note that ω is the deviation from the synchronous speed, in steady state V_k=0)

$$V_k = \frac{1}{2}M\omega^2 \tag{3-3}$$

Now, let us consider the energy function of a multi-machine system. Each generator is still described as a classical second-order model, ignoring the dynamic process of the prime mover, the governor, and the excitation system. A constant impedance model is used to represent the load, assuming that the load impedance and the generator impedance X'_d are included into the node admittance array. In the system node admittance matrix, the load nodes and the network nodes are eliminated, only the inner nodes of the generators (the internal electromotive force nodes) are retained in the matrix. As shown in the figure below, for a n-machine system, the i-th generator can be

described as

$$\begin{cases} M_i \dfrac{d\omega_i}{dt} = P_{mi} - P_{ei} \\ \dfrac{d\delta_i}{dt} = \omega_i \end{cases} \quad (i = 1, 2, \cdots n) \qquad (3\text{-}4)$$

where P_{mi}=const., M, ω, δ, P_m, P_e have the same definition as in Formula (3-2), and

$$P_{ei} = \mathrm{Re}\left(\dot{E}_i \quad \overset{*}{I}_i \right) = \mathrm{Re}\left(\dot{E}_i \quad \sum_{j=1}^{n} \overset{*}{Y}_{ij} \overset{*}{E}_j \right) = E_i^2 G_{ii} + \sum_{\substack{j=1 \\ j \neq i}}^{n} \left(E_i E_j B_{ij} \sin\delta_{ij} + E_i E_j G_{ij} \cos\delta_{ij} \right)$$

$$\dot{E}_i = E_i \angle \delta_i, \delta_{ij} = \delta_i - \delta_j, G_{ij} + jB_{ij} = Y_{ij}$$

are the elements of the admittance matrix[28].

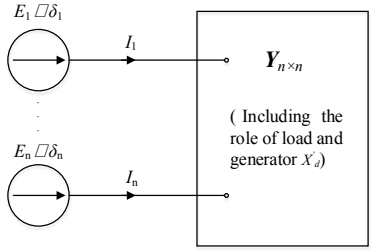

Figure 3.7 Multi-machine system schematic

If we define that E_iE_j=C_{ij}, $E_iE_jG_{ij}$=D_{ij}, and C_{ij}=C_{ji}, D_{ij}=Dji, P_{ei} in (3-4) can be described as

$$P_{ei} = E_i^2 G_{ii} + \sum_{\substack{j=1 \\ j \neq i}}^{n} \left(C_{ij} \sin\delta_{ij} + D_{ij} \sin\delta_{ij} \right) \qquad (3\text{-}5)$$

Formula (3-4) and (3-5) form a complete dynamic model for the system. Similar to a single-machine infinite system, the kinetic energy can be defined as

$$V_k = \sum_{i=1}^{n} \frac{1}{2} M_i \omega_i^2 \qquad (3\text{-}6)$$

If a system is stably operating at a frequency which is higher than the synchronous speed after the disturbance, the kinetic energy $\sum_{i=1}^{n} \frac{1}{2} M_i \omega_i^2$ of the system is still not zero, even that the system has reach a new steady state.

In fact, the kinetic energy does not result in the power system losing synchronization. That means, in the synchronous coordinates, the transient energy contains some components that would not contribute to drop-out of step. If included in energy processing and analysis, it will inevitably affect the accuracy of stability analysis [28].

3.6.2 Center of Inertia (COI) as Reference

The center of inertia (COI) coordinates are widely used in actual analysis [28]. The equivalent rotor angle δ_{COI} of COI is defined as the weighted average of all the rotor angles in the system. The weighted coefficient M_i is the inertia time constant of each generator, that is

$$\delta_{COI} = \frac{1}{M_T}\sum_{i=1}^{n} M_i \delta_i \tag{3-7}$$

where

$$M_T = \sum_{i=1}^{n} M_i \tag{3-8}$$

Similarly, the equivalent speed of COI ω_{COI} is

$$\omega_{COI} = \frac{1}{M_T}\sum_{i=1}^{n} M_i \omega_i \tag{3-9}$$

where, ω_i is the deviation from synchronous speed.

Obviously,

$$\frac{d\delta_{COI}}{dt} = \omega_{COI} \tag{3-10}$$

The definitions of rotor angle and rotor speed in COI coordinate are given as follows:

$$\begin{cases} \theta_t = \delta_i - \delta_{COI} \\ \tilde{\omega}_i = \omega_i - \omega_{COI} \end{cases} \tag{3-11}$$

It's easy to prove by the definition that

$$\sum_{i=1}^{n} M_i \theta_i = 0 \quad \sum_{i=1}^{n} M_i \tilde{\omega}_i = 0 \ \text{ and } \ \frac{d\theta_i}{dt} = \tilde{\omega}_i \tag{3-12}$$

Based on the abovementioned definitions, the inertia center motion equation can be derived as

$$\begin{cases} M_T \dfrac{d\omega_{COI}}{dt} = \sum_{i=1}^{n} \left(P_{mi} - P_{ei}\right) \overset{\text{def}}{=} P_{COI} \\ \dfrac{d\delta_{COI}}{dt} = \omega_{COI} \end{cases} \tag{3-13}$$

Formula (3-13) is the motion equations of COI, where P_{COI} refers to the

accelerating power.

The motion equations of each machine (for example, the *i*-th machine) in COI coordinates are to be derived. Substituting $\omega_i = \tilde{\omega}_i + \omega_{COI}$ into Formula (3-4) and according to Formula (3-13), we can get

$$M_i \frac{d\tilde{\omega}_i}{dt} = P_{mi} - P_{ei} - \frac{M_i}{M_T} P_{COI} \qquad (3\text{-}14)$$

where $P_{COI} = \sum_{i=1}^{n} \left(P_{mi} - P_{ei} \right)$

According to (3-12),

$$\frac{d\theta_i}{dt} = \tilde{\omega}_i \qquad (3\text{-}15)$$

The following equation can be derived from Formula (3-5) and Formula (3-11)

$$P_{ei} = E_i^2 G_{ii} + \sum_{\substack{j=1 \\ j \neq i}}^{n} \left(C_{ij} \sin \delta_{ij} + D_{ij} \sin \delta_{ij} \right) \qquad (3\text{-}16)$$

where $\theta_{ij} = \theta_i - \theta_j$.

Formulas (3-14), (3-15) and (3-16) are the motion equations for the *i*-th machine in COI coordinates.

With the definitions in COI coordinates, we can get

$$\sum_{i=1}^{n} \frac{1}{2} M_i \omega_i^2 - \sum_{i=1}^{n} \frac{1}{2} M_i \tilde{\omega}_i^2 = \frac{1}{2} M_T \omega_{COI}^2 \qquad (3\text{-}17)$$

That is to say, in the COI coordinates, the kinetic energy of the system is $\frac{1}{2} M_T \omega_{COI}^2$ less than that in synchronous coordinates [28], which is precisely the kinetic energy that does not contribute to loss of synchronization. The use of COI coordinates can improve the accuracy of the stability analysis than synchronous coordinates.

In the following section, simulation results in synchronous coordinates and in COI coordinates are simultaneously given for comparison.

3.6.3 Simulation results of load events

Figures from 3.8 to 3.12 display the simulation results of five load events.

In Figure 3.8, we find that the bus voltages will drop and gradually transit to a new steady state, if Load_Area1 increases suddenly. It should be noted that new steady-state voltages of some busbars are larger than the initial ones. As the load increases in Load_Area1, the system frequency decreases. Currents inside each area increase,

nevertheless currents on the transmission lines interconnect the two areas decrease. In synchronous coordinates, the rotor angle of G1_Area2 is the reference of the system. The rotor angles of generators in Area1 change rapidly while those in Area2 remain basically unchanged. In the COI coordinates, the rotor angles of all the four generators change apparently.

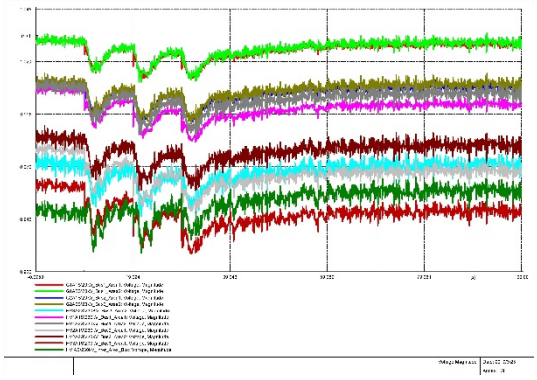

(a)Voltage magnitude under reference element

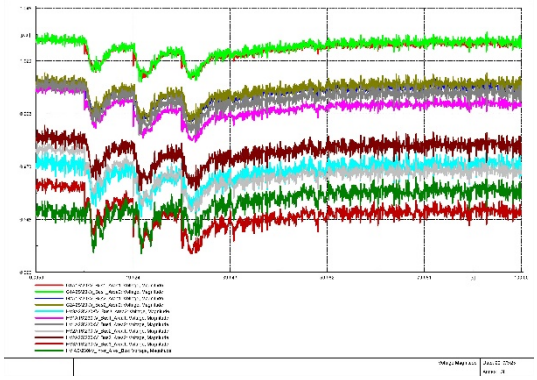

(b)Voltage magnitude under reference COI

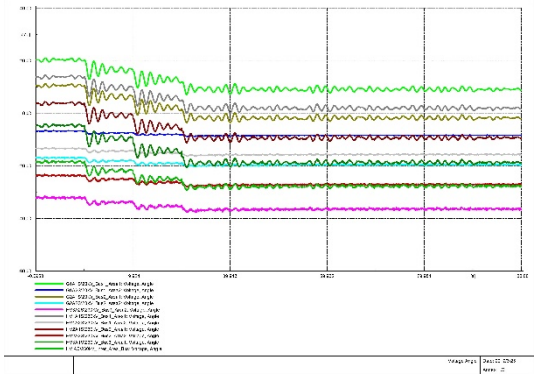

(c)Voltage angle under reference element

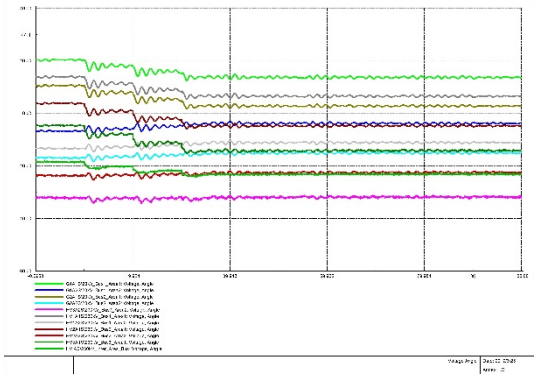

(d)Voltage angle under reference COI

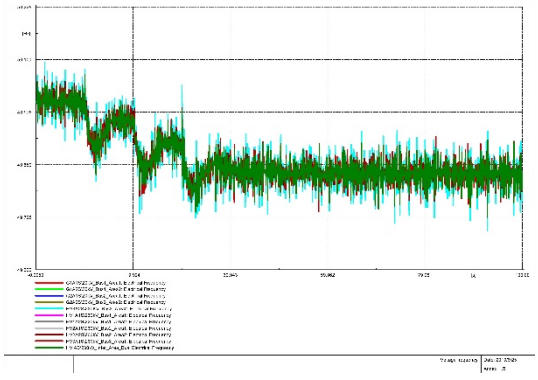

(e)Frequency under reference element

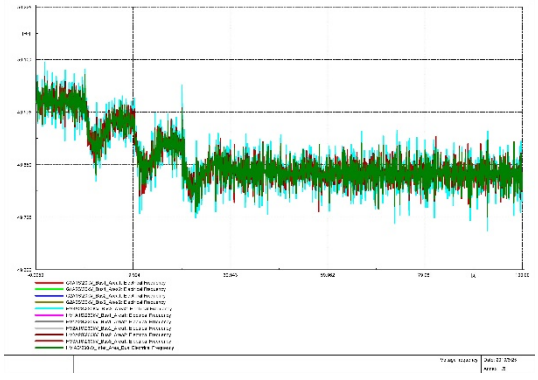

(f)Frequency under reference COI

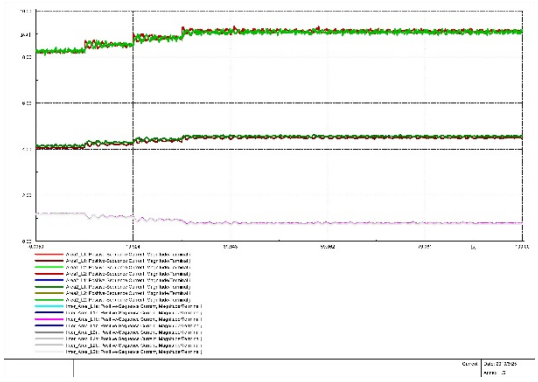

(g)Line current under reference element

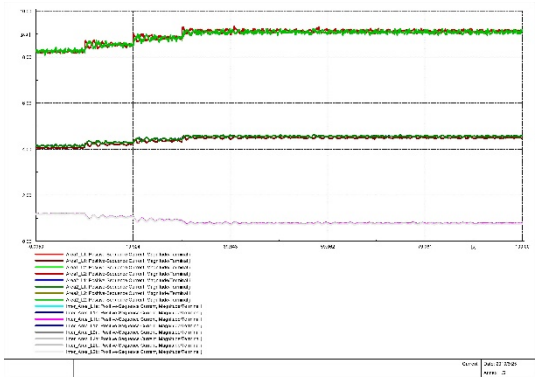

(h)Line current under reference COI

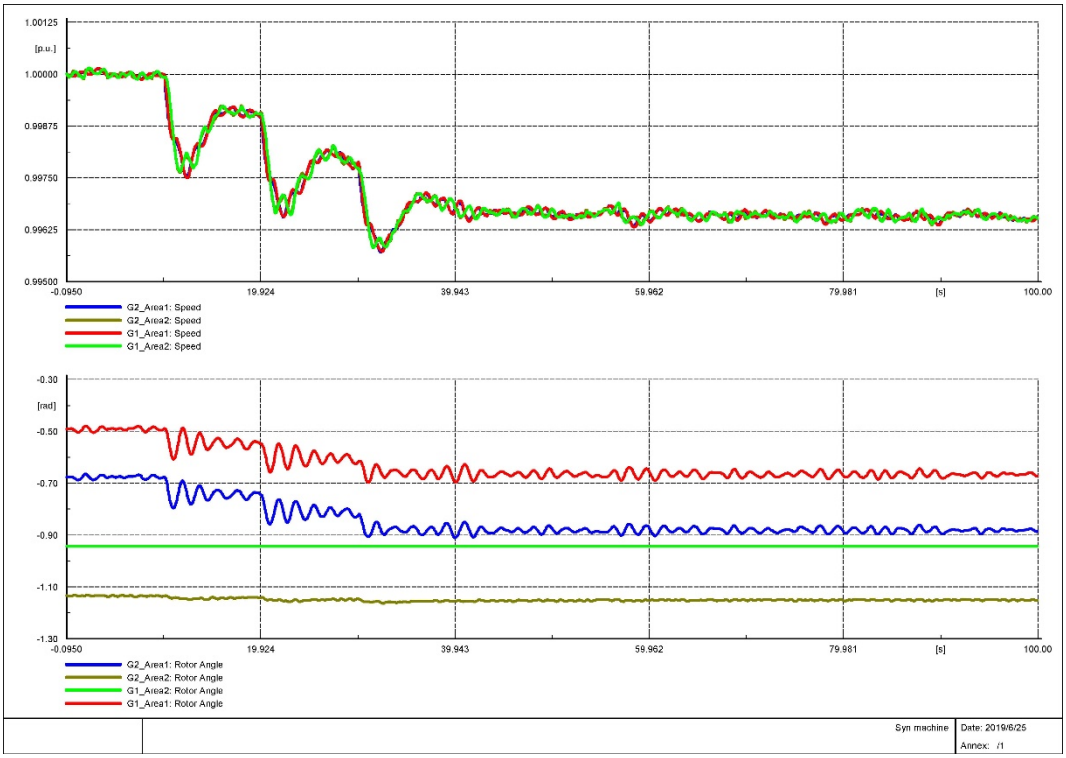

(i) rotor angle and speed of synchronous machines under reference element

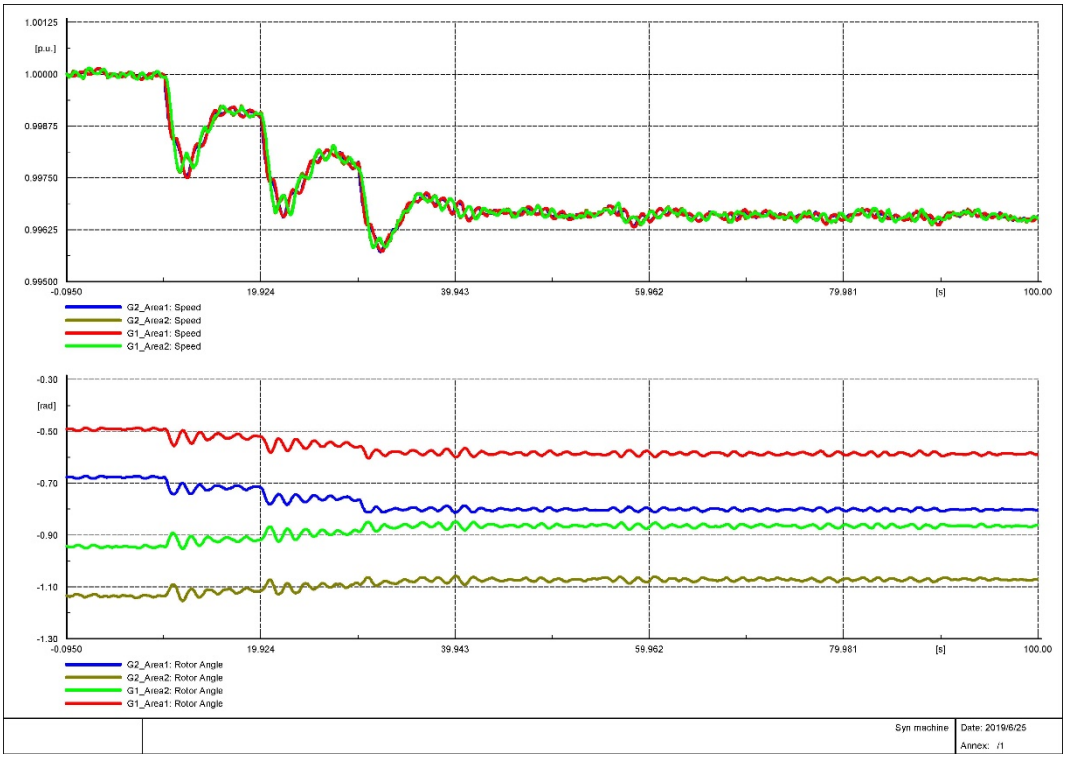

(j) rotor angle and speed of synchronous machines under reference COI

Figure 3.8 Simulation results of load event 1

According to Figure 3.9, voltages of the busbars will increase, if Load_Area1 suddenly decreases. For some busbars, after the transient process of the load event, the steady-state voltages are lower than the initial values. When the load decreases, the system frequency increases, currents in each area decreases, and currents on the tie lines increases. The new steady-state frequency is higher than the initial value.

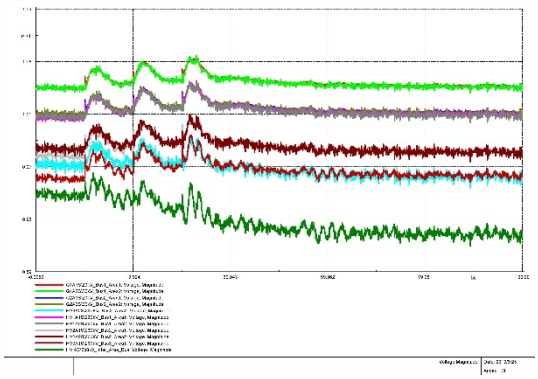

(a)Voltage magnitude under reference element

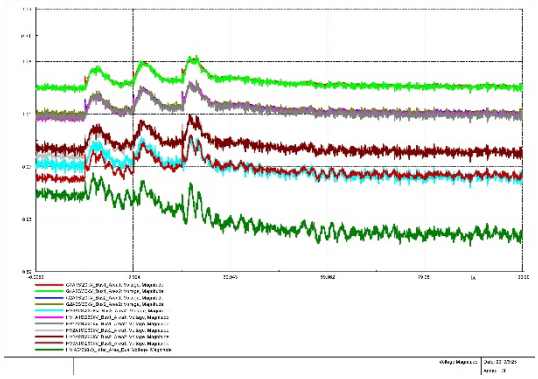

(b)Voltage magnitude under reference COI

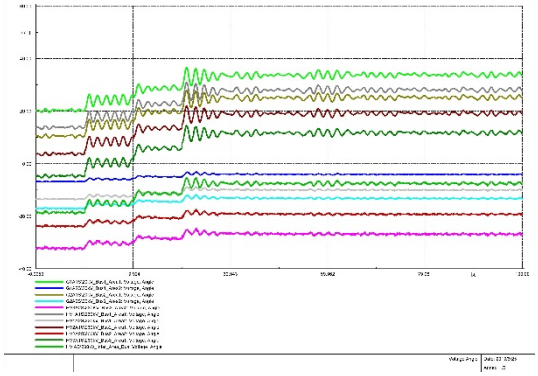

(c)Voltage angle under reference element

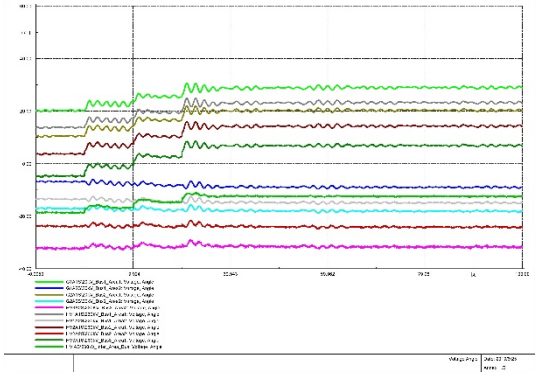

(d)Voltage angle under reference COI

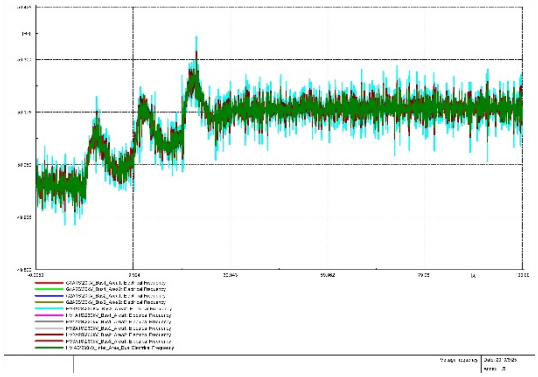

(e)Frequency under reference element

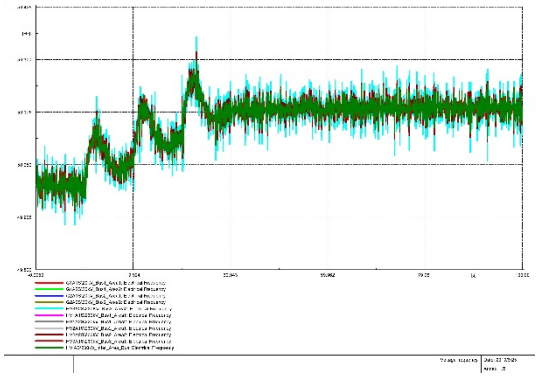

(f)Frequency under reference COI

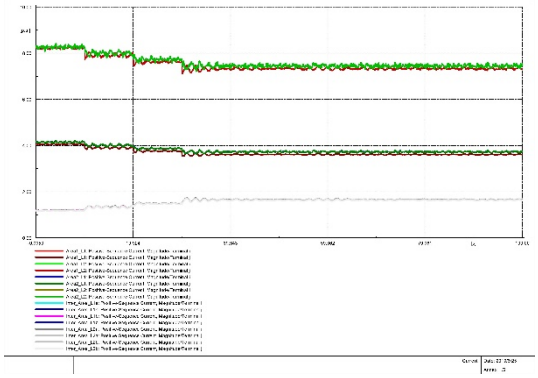

(g)Line current under reference element

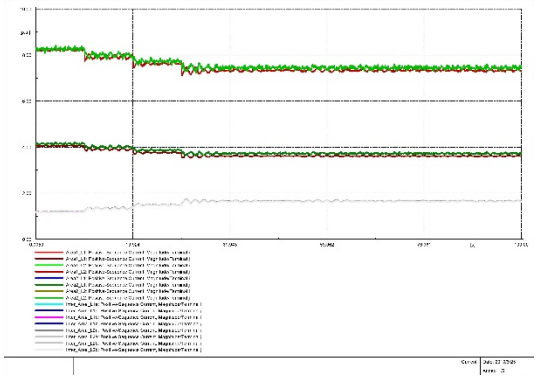

(h)Line current under reference COI

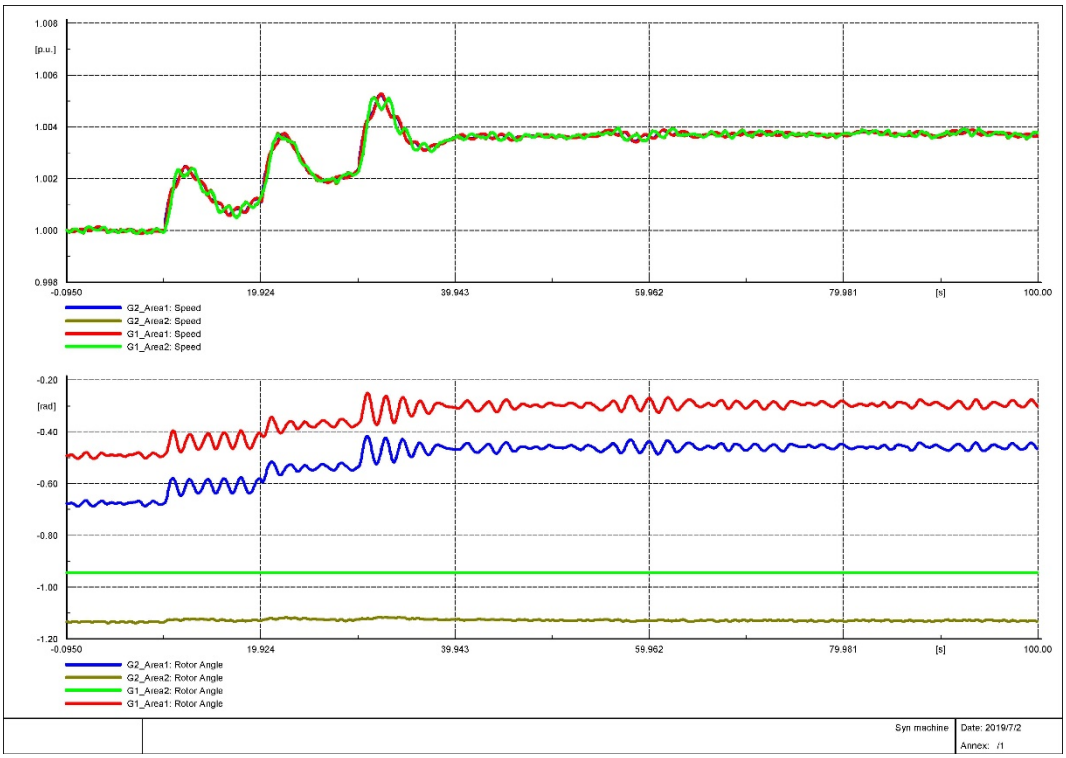

(i) rotor angle and speed of synchronous machines under reference element

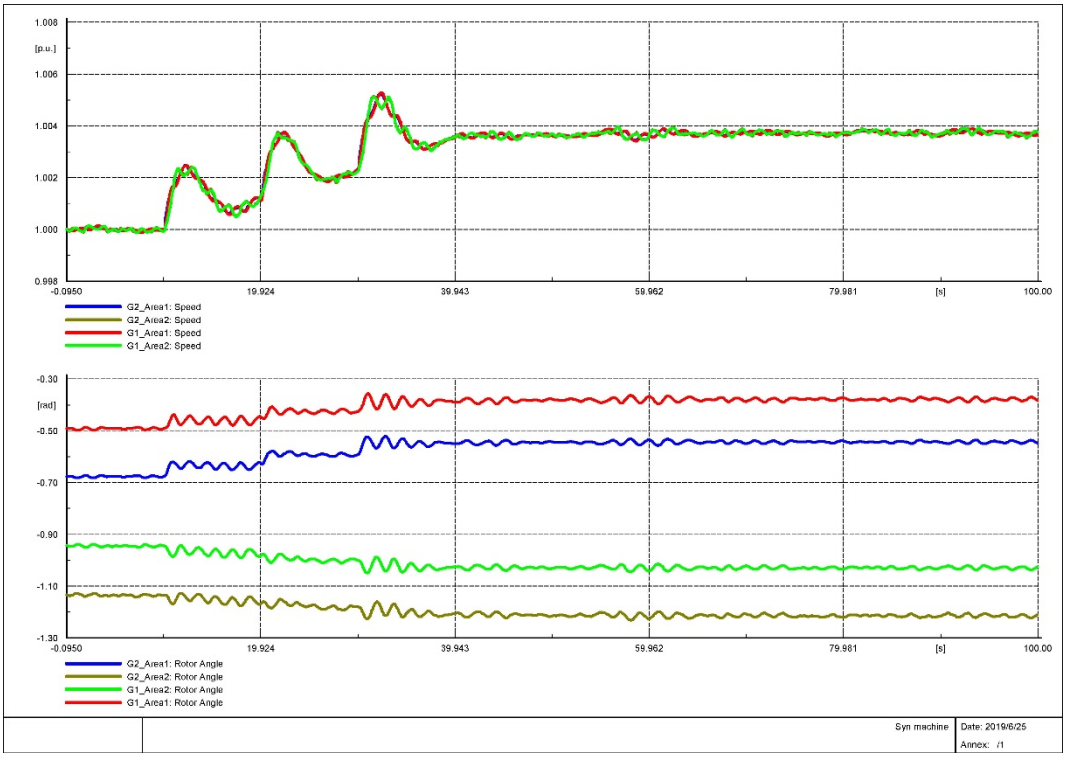

(j) rotor angle and speed of synchronous machines under reference COI

Fig 3.9 Simulation results of load event 2

In Figure 3.10, voltages of the busbars will decrease, if Load_Area2 suddenly

increases. As the load in area2 increases, the system frequency decreases, and currents on the transmission line increase. G1_Area2 is the balanced generator of the system. In this case, the output of G1_Area2 increases obviously to make up the power shortage, and the rotor speed changes rapidly. In the synchronous coordinates, with G1_Area2 as a reference, rotor angles of the two generators in Area1 also change greatly.

According to the figures, the system is obviously oscillating after load_Area2 is increased for three times. The operating status of the system is changed due to the severe overloading on the tie links.

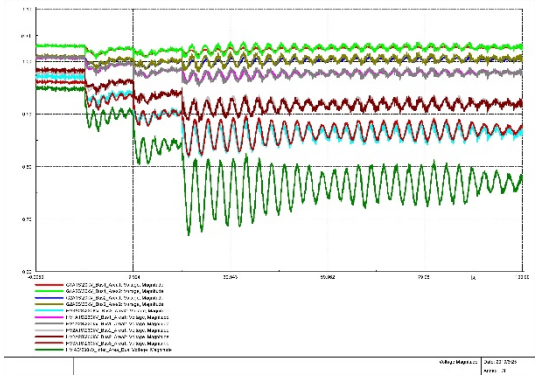

(a)Voltage magnitude under reference element

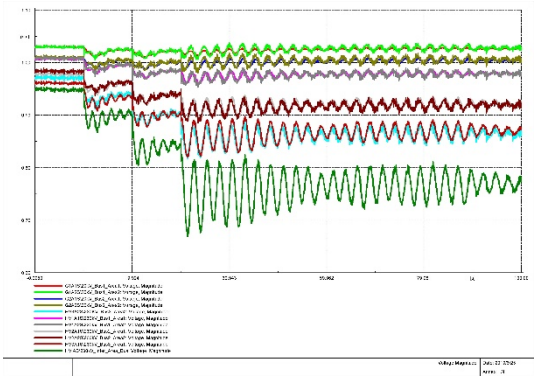

(b)Voltage magnitude under reference COI

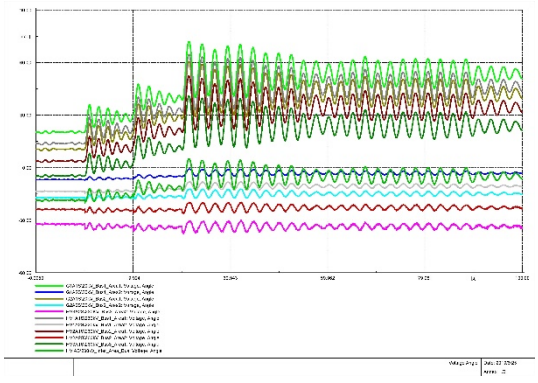

(c)Voltage angle under reference element

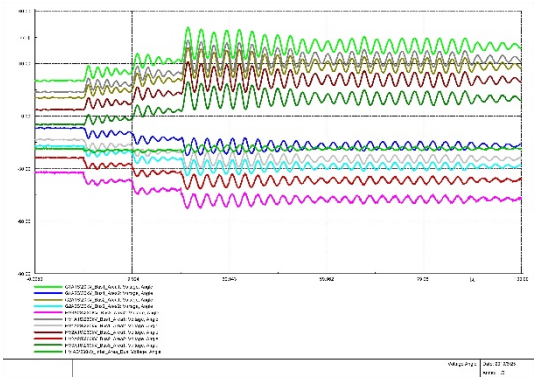

(d)Voltage angle under reference COI

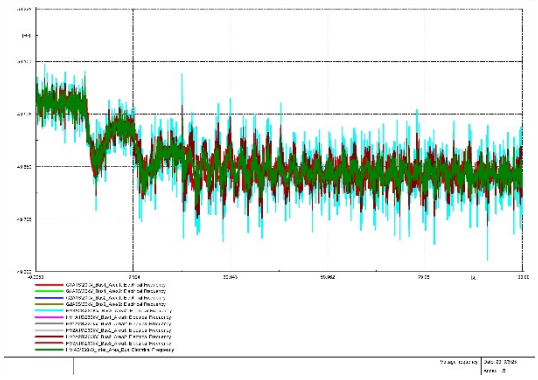

(e)Frequency under reference element

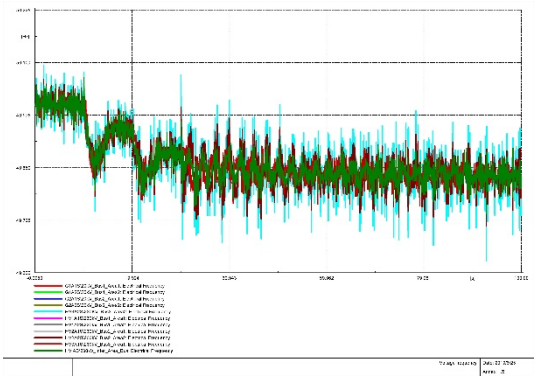

(f)Frequency under reference COI

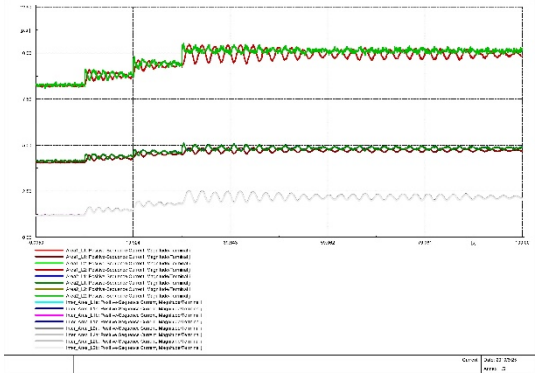

(g)Line current under reference element

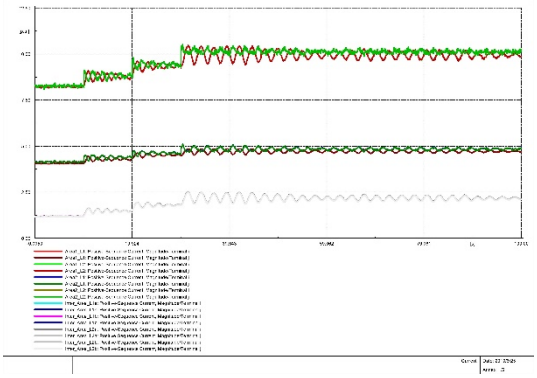

(h)Line current under reference COI

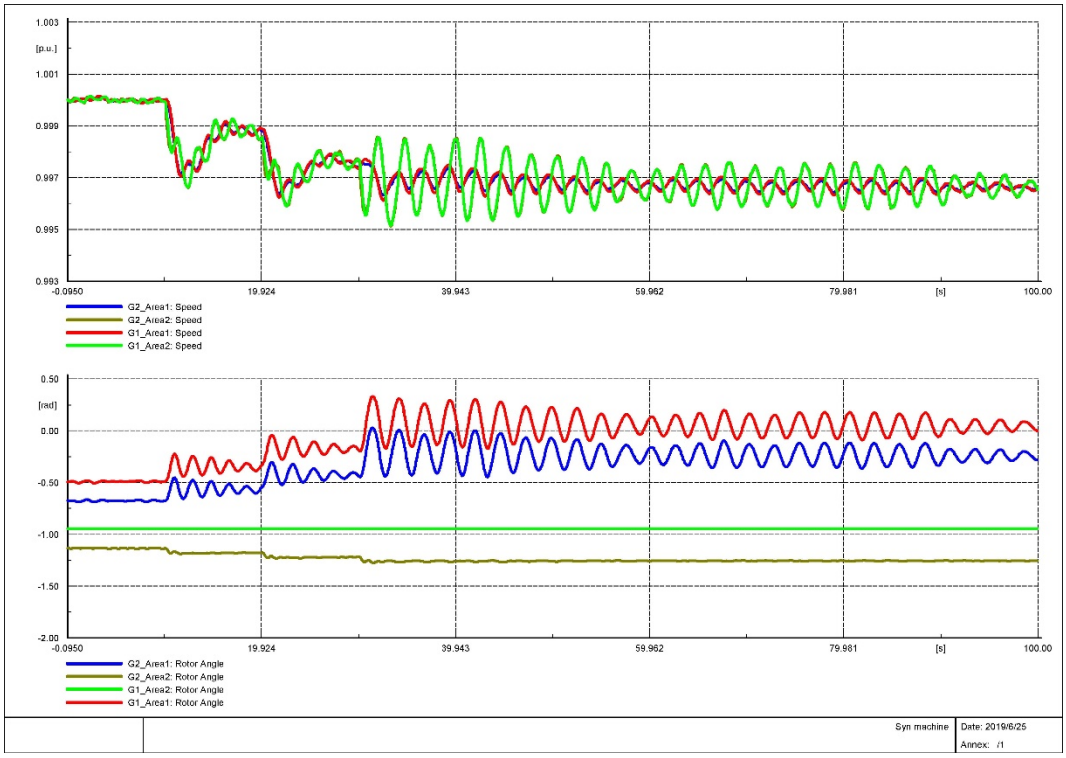

(i) rotor angle and speed of synchronous machines under reference element

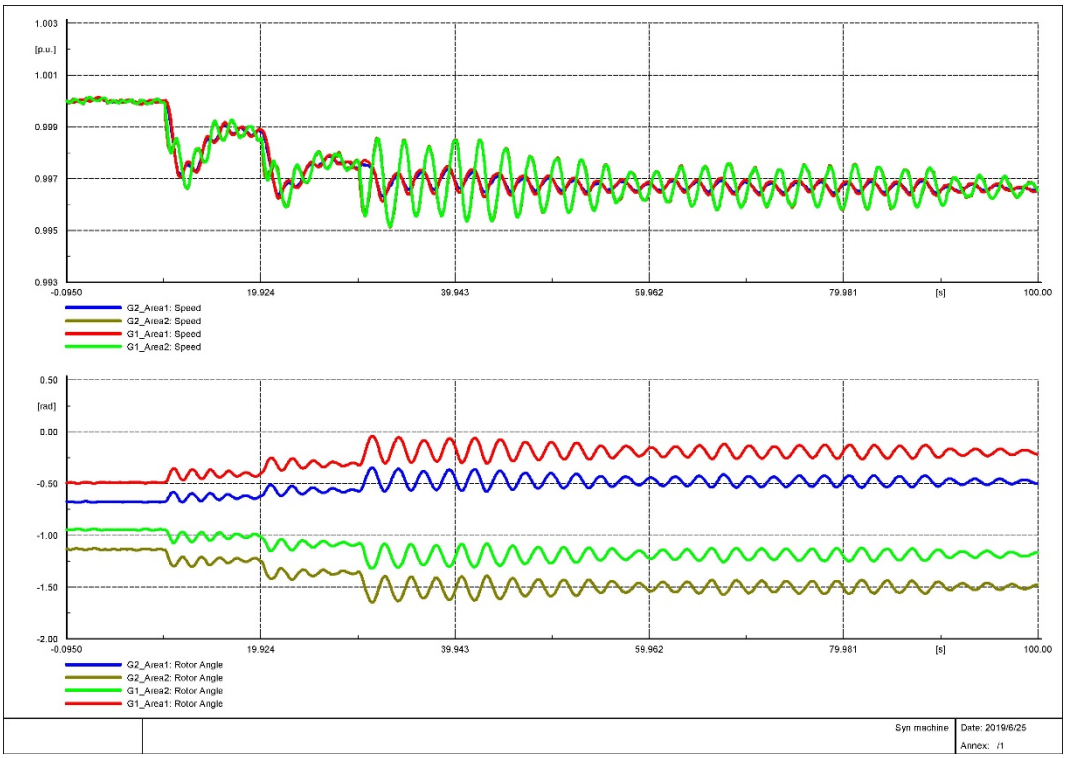

(j) rotor angle and speed of synchronous machines under reference COI

Figure 3.10 Simulation results of load event 3

In Figure 3.11, we can see that voltages of the busbars increase when Load_Area2 suddenly decreases. The system frequency rises, and the transmission line currents decrease. The frequency in the new steady state is higher than the initial value.

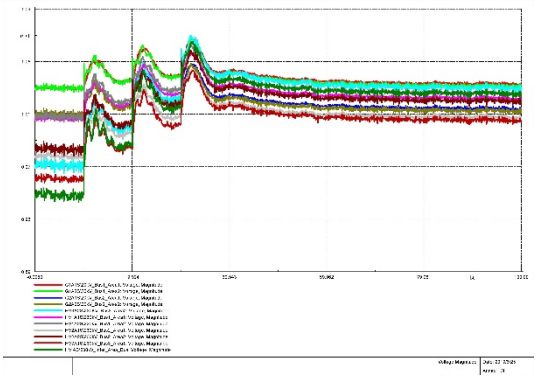

(a)Voltage magnitude under reference element

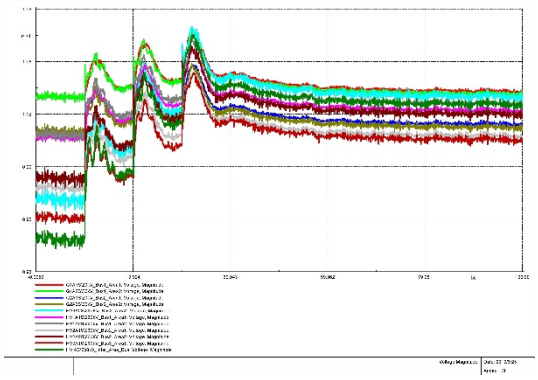

(b)Voltage magnitude under reference COI

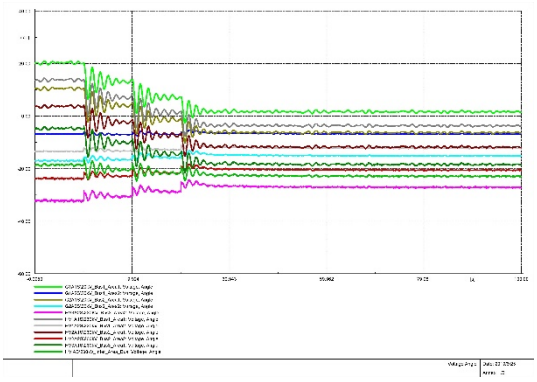

(c)Voltage angle under reference element

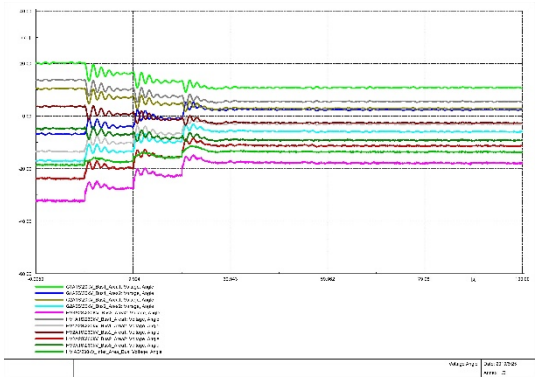

(d)Voltage angle under reference COI

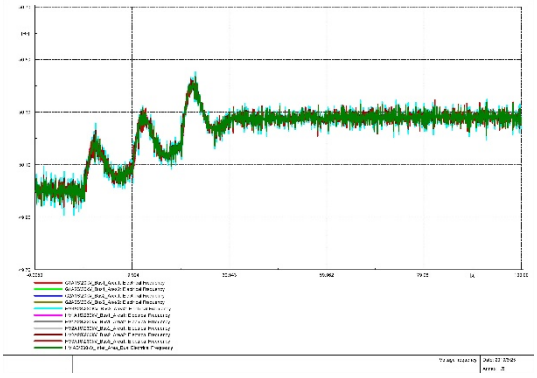

(e)Frequency under reference element

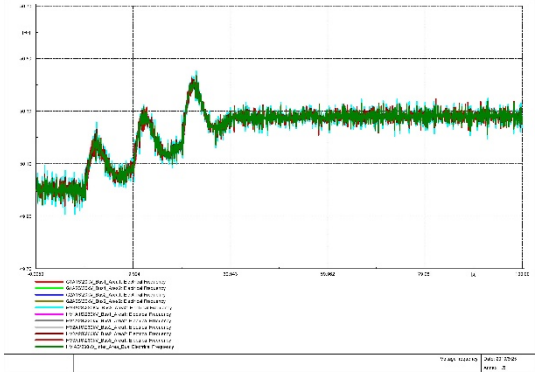

(f)Frequency under reference COI

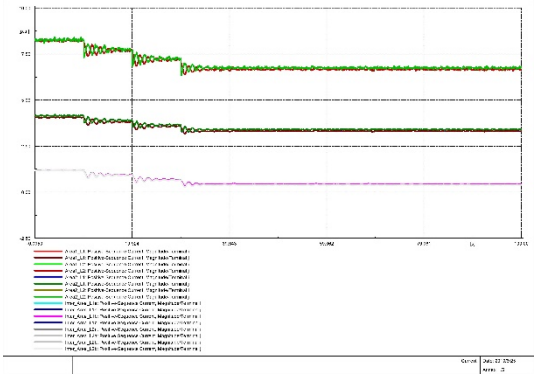

(g)Line current under reference element

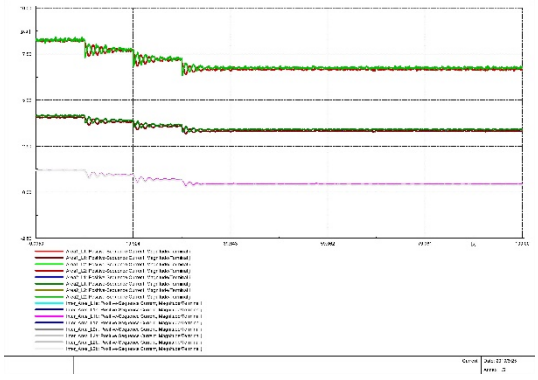

(h)Line current under reference COI

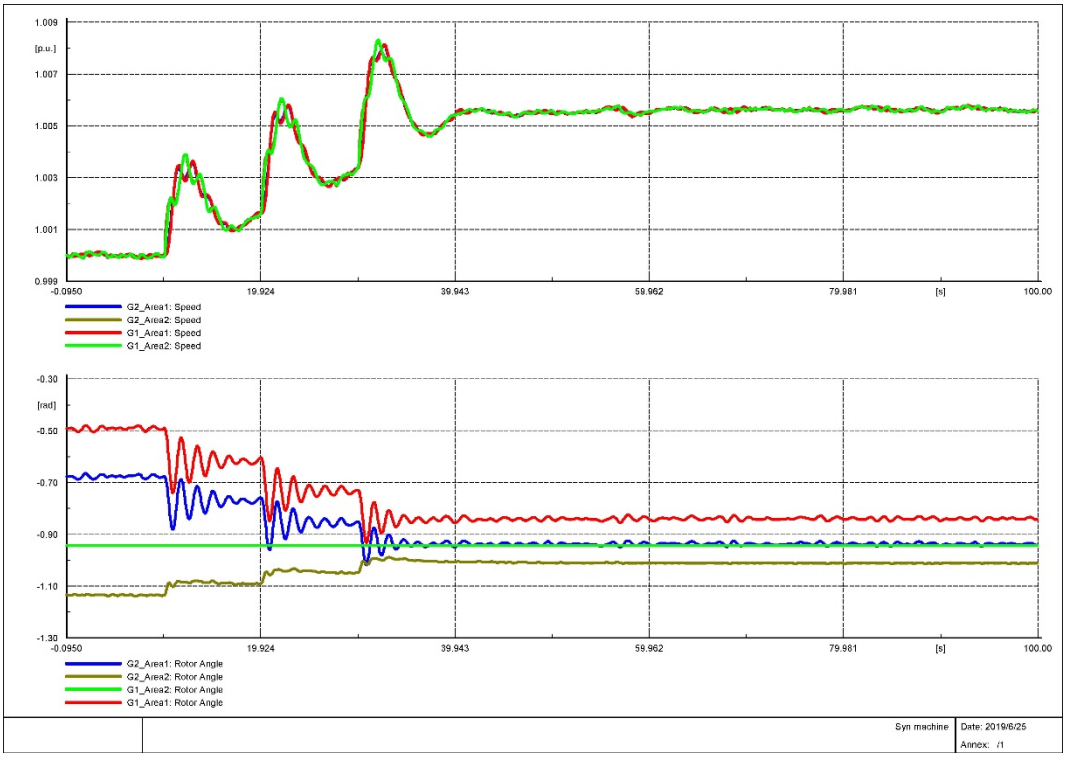

(i) rotor angle and speed of synchronous machines under reference element

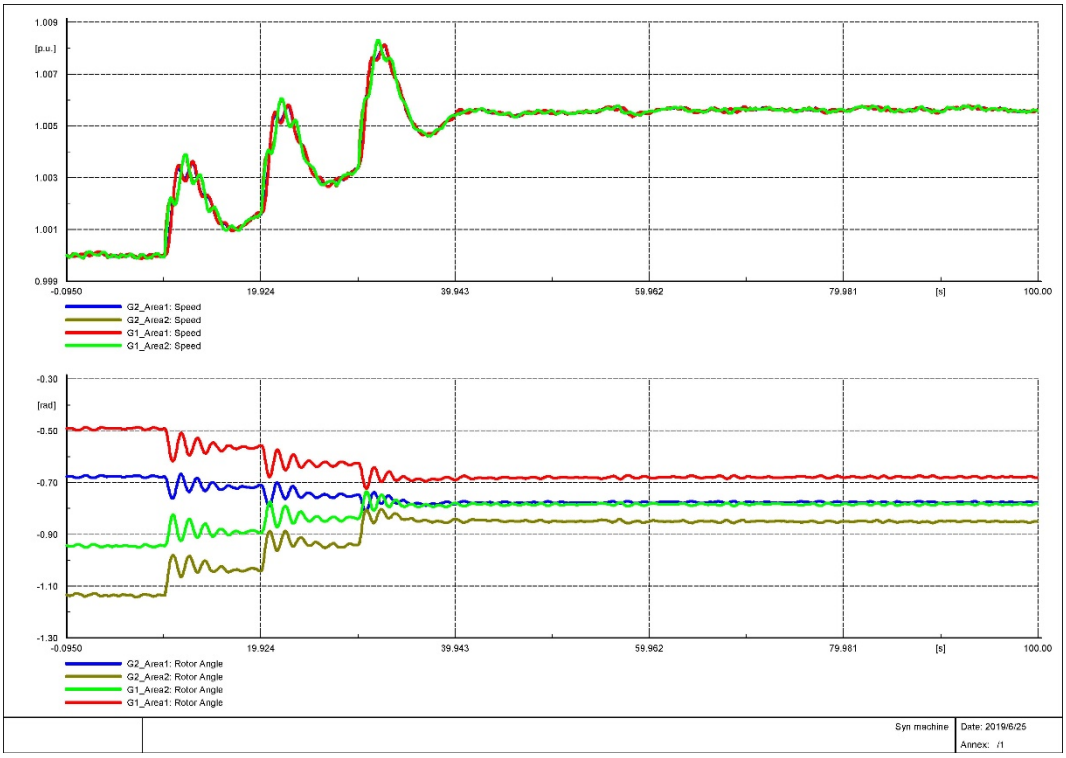

(j) rotor angle and speed of synchronous machines under reference COI

Figure 3.11 Simulation results of load event 4

If Load_Area1 and Load_Area2 are increased by 10% at the same time, as shown in Figure 3.12, the changes of selected variables are similar to those in load event 3. Since Load_Area2 is much larger than Load_Area1, the simulation results are closer to the results of load event in area 2.

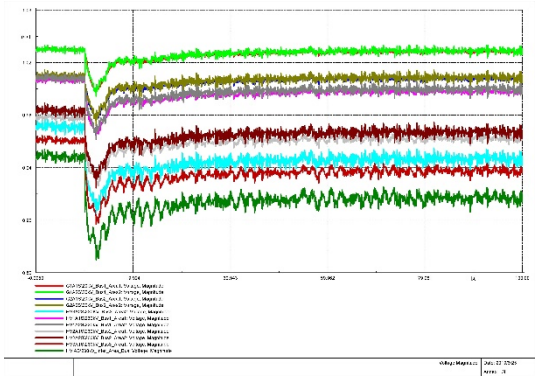

(a)Voltage magnitude under reference element

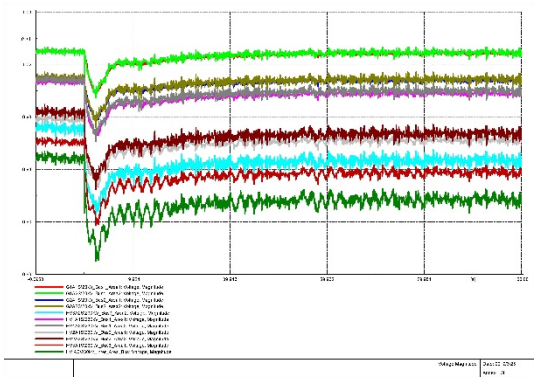

(b)Voltage magnitude under reference COI

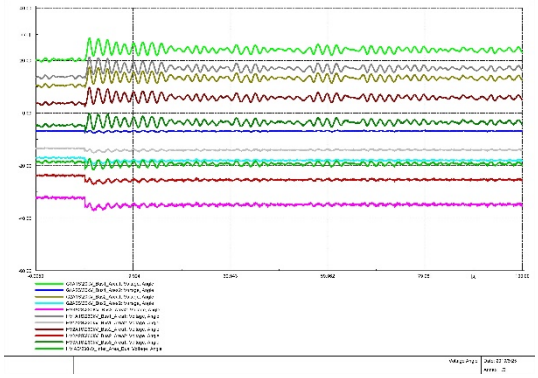

(c)Voltage angle under reference element

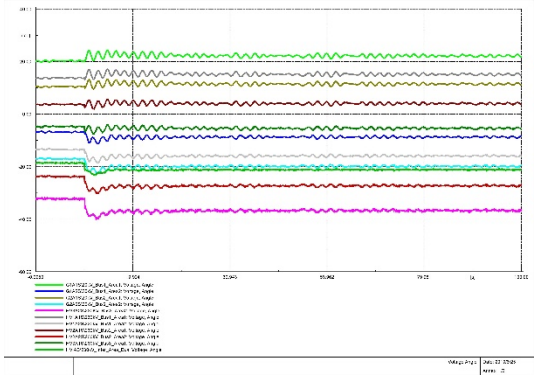

(d)Voltage angle under reference COI

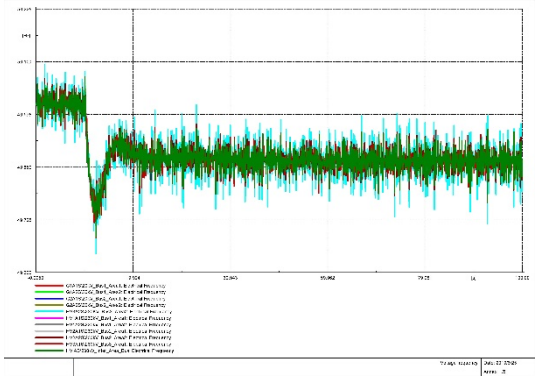

(e)Frequency under reference element

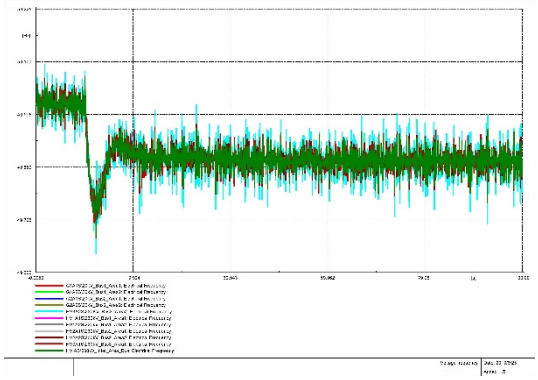

(f)Frequency under reference COI

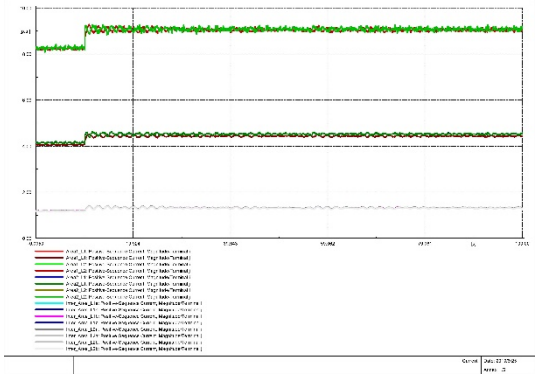

(g)Line current under reference element

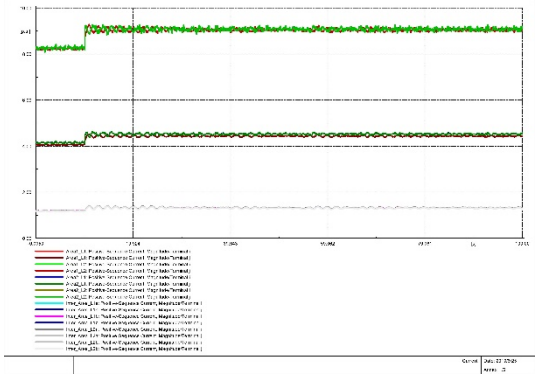

(h)Line current under reference COI

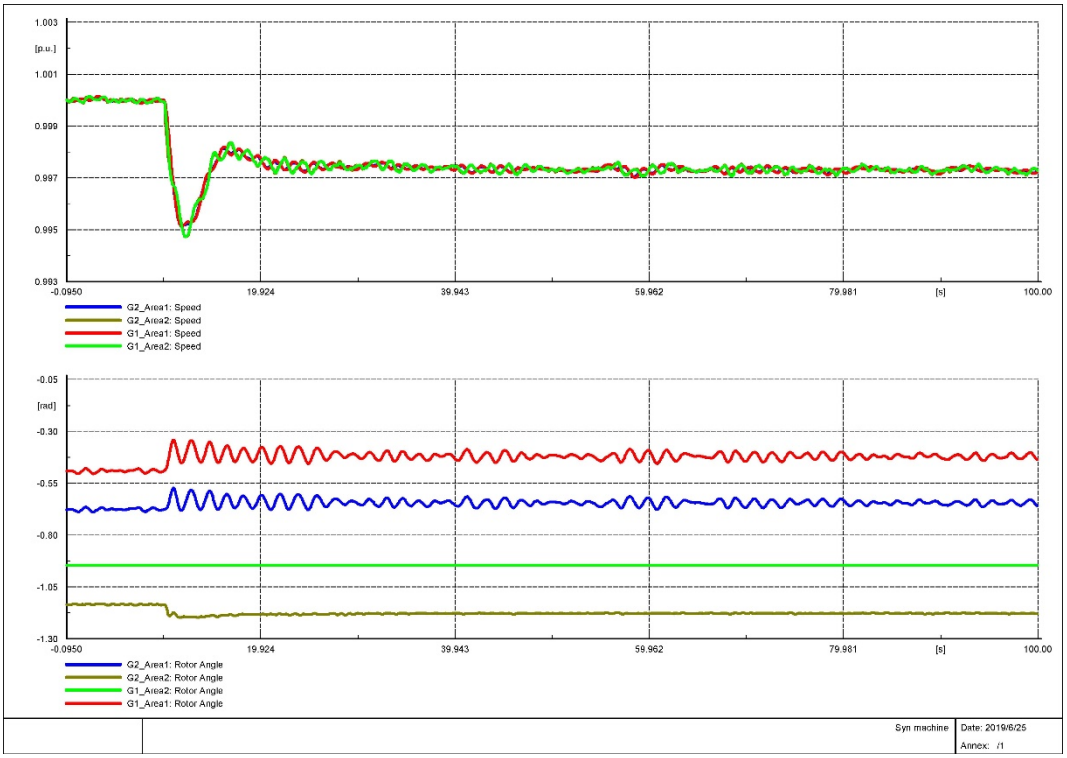

(i) rotor angle and speed of synchronous machines under reference element

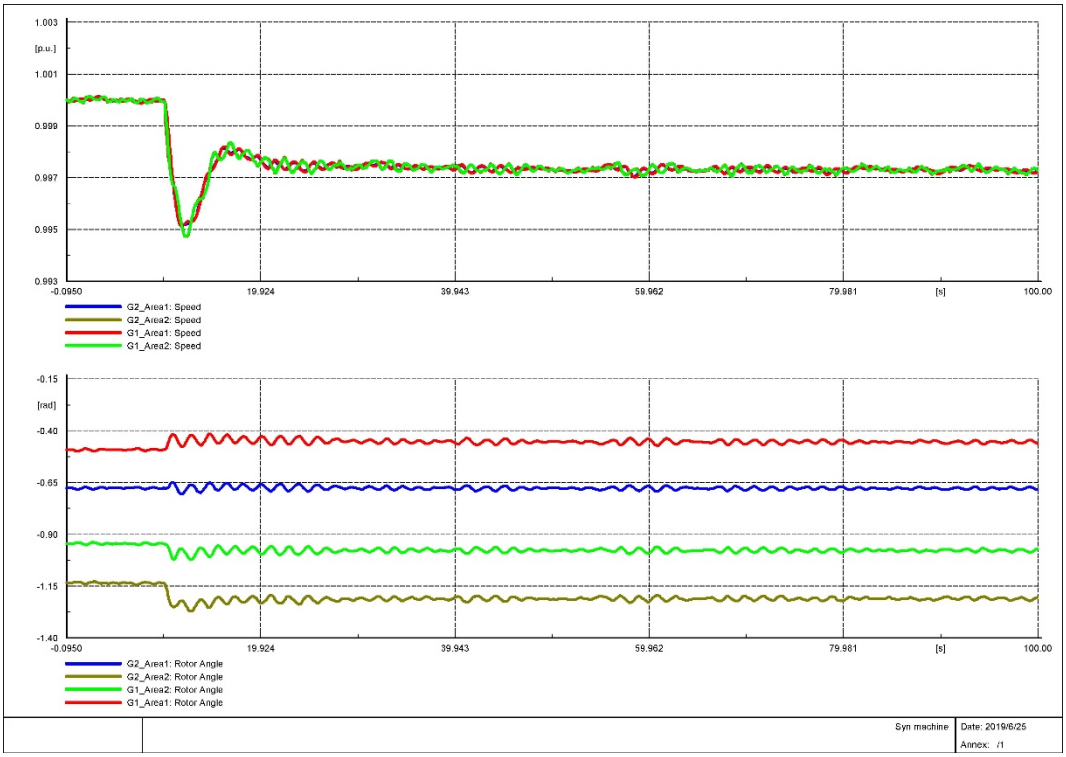

(j) rotor angle and speed of synchronous machines under reference COI

Figure 3.12 Simulation results of load event 5

3.6.4 Simulation results of short-circuit events

Figure 3.13 to Figure 3.15 display the simulation results of three short-circuit events. According to Figure 3.13 and Figure 3.14, when a three-phase short-circuit fault occurs at one of the interarea lines, voltages of the corresponding busbars drop to zero immediately, the frequency and currents on the transmission lines increase rapidly. The fault is removed at the zero crossing after a power frequency cycle (after more or less 0.02s), and the system resumes steady-state operation after a short-term oscillation.

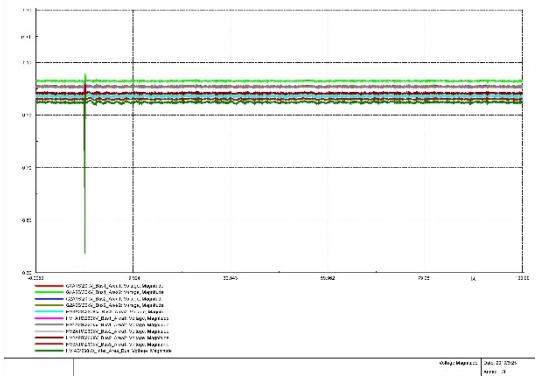

(a)Voltage magnitude under reference element

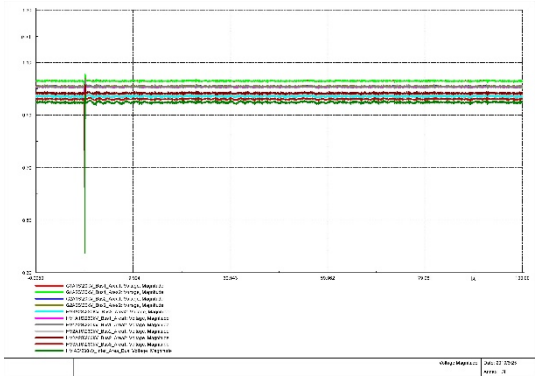

(b)Voltage magnitude under reference COI

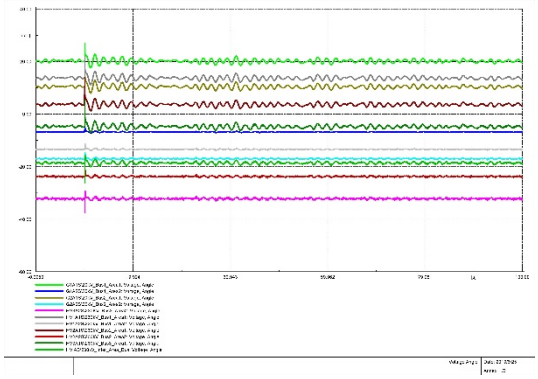

(c)Voltage angle under reference element

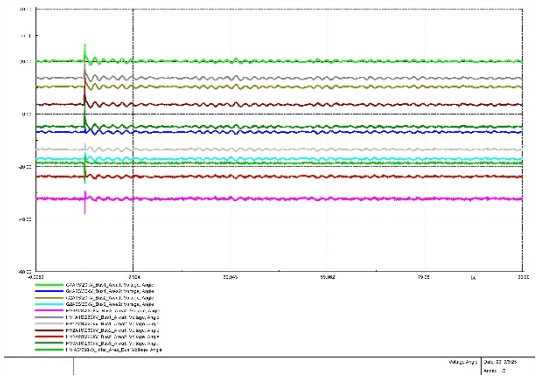

(d)Voltage angle under reference COI

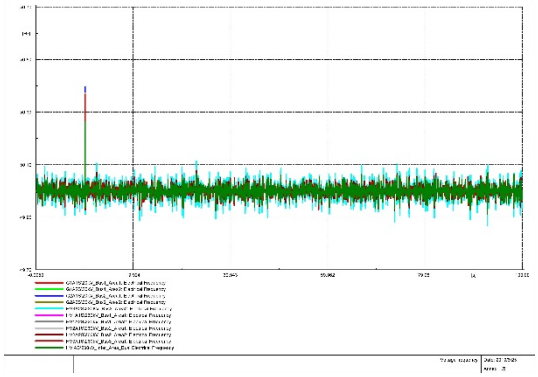

(e)Frequency under reference element

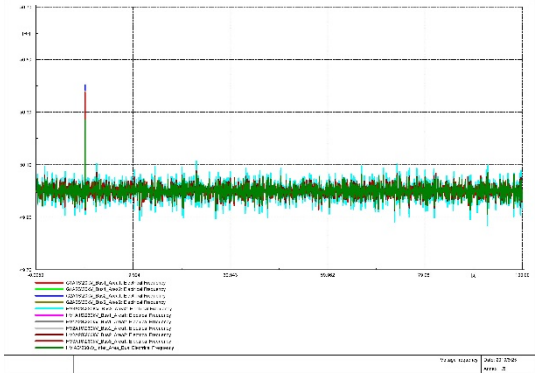

(f)Frequency under reference COI

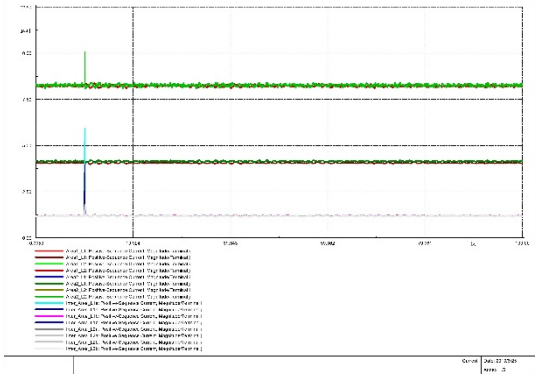

(g)Line current under reference element

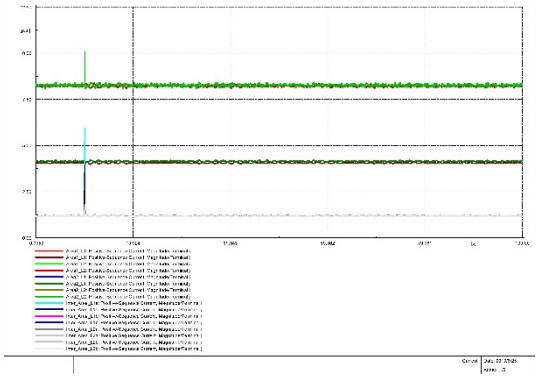

(h)Line current under reference COI

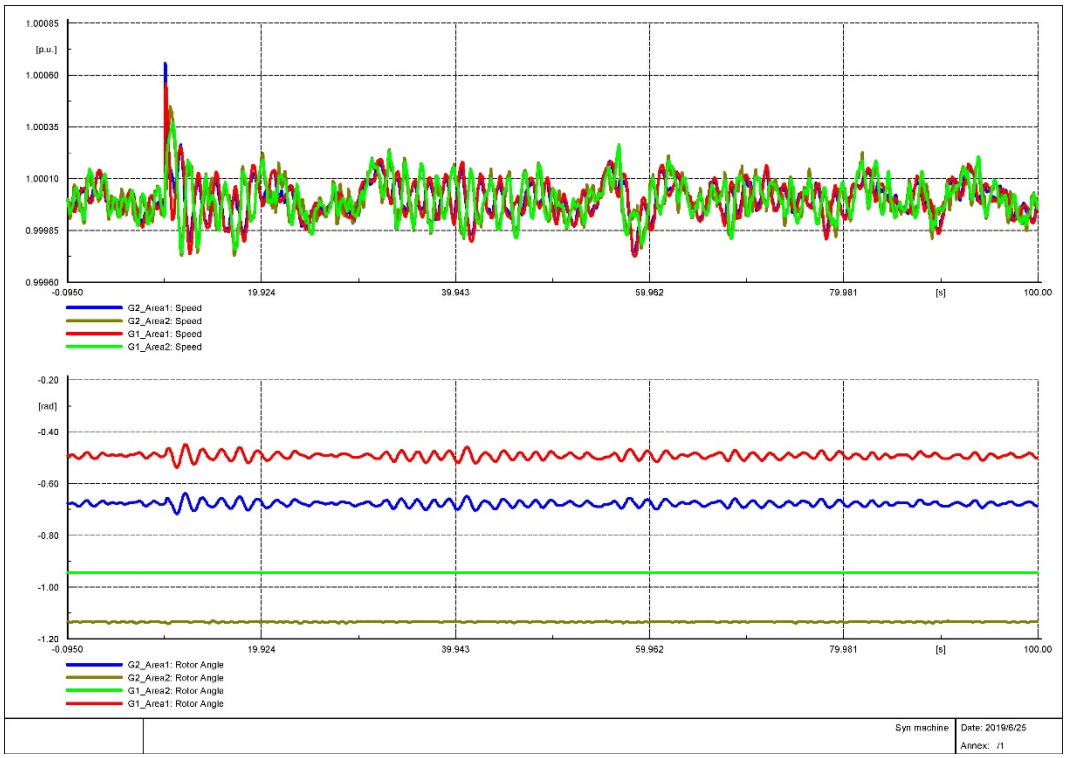

(i) rotor angle and speed of synchronous machines under reference element

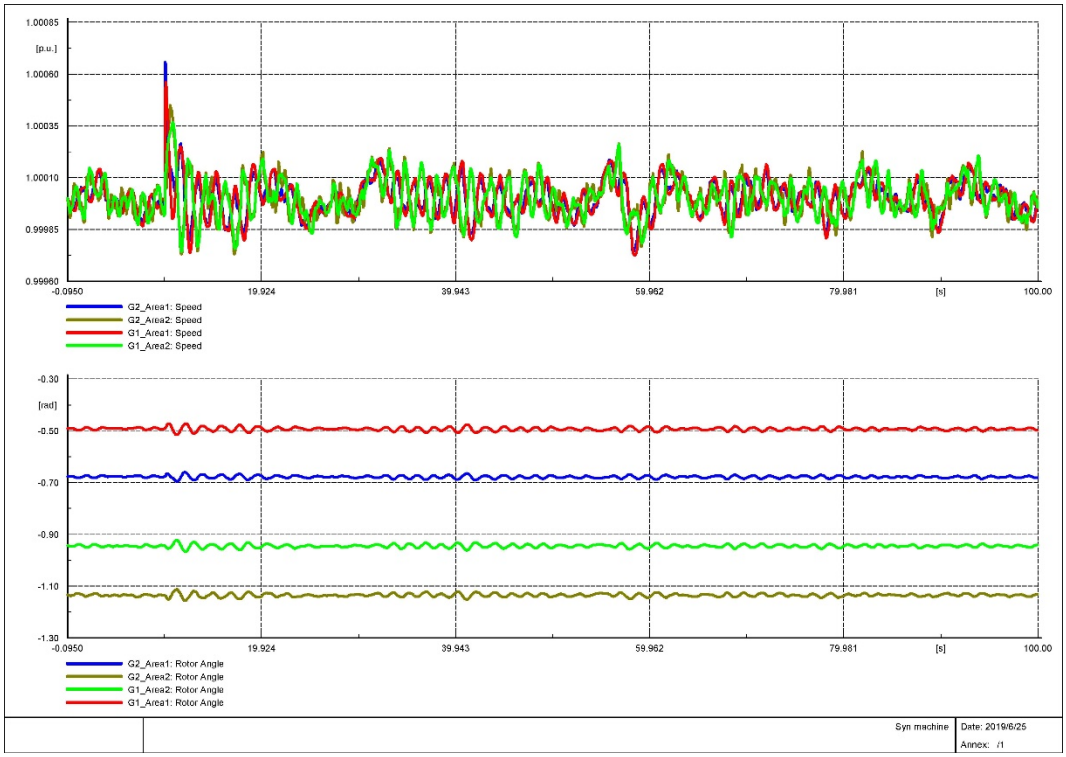

(j) rotor angle and speed of synchronous machines under reference COI

Figure 3-12 Simulation results of short circuit event 1

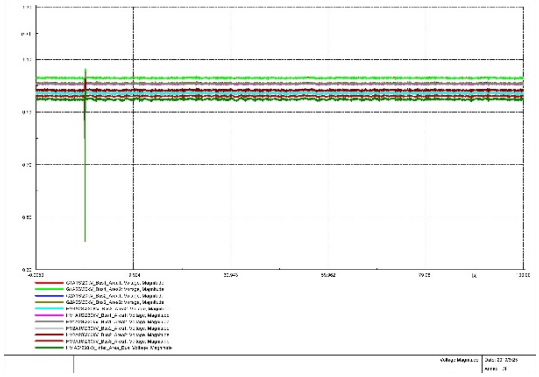

(a)Voltage magnitude under reference

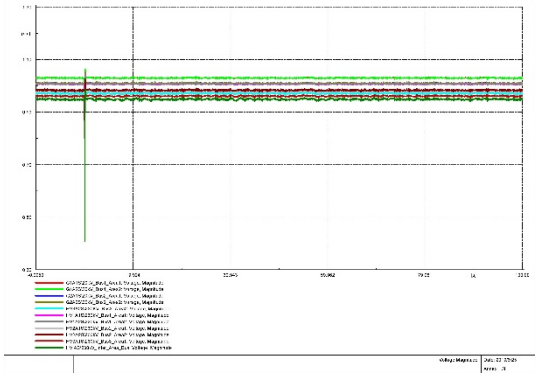

(b)Voltage magnitude under reference COI

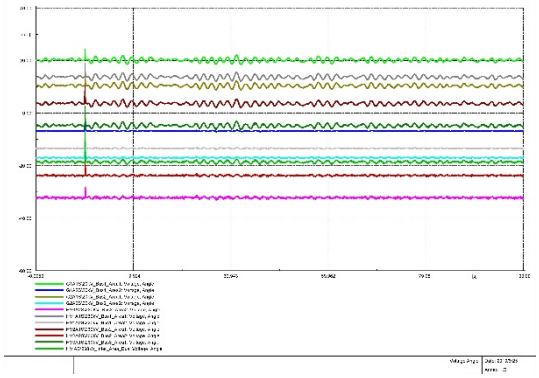

(c)Voltage angle under reference element

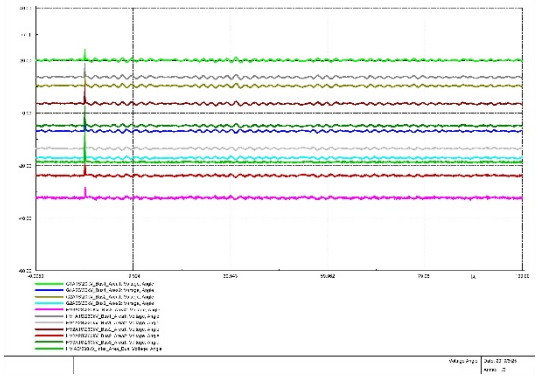

(d)Voltage angle under reference COI

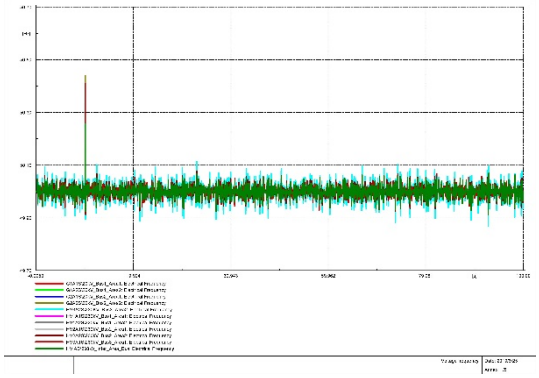

(e)Frequency under reference element

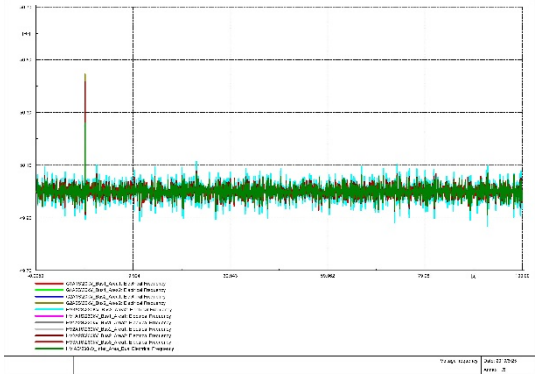

(f)Frequency under reference COI

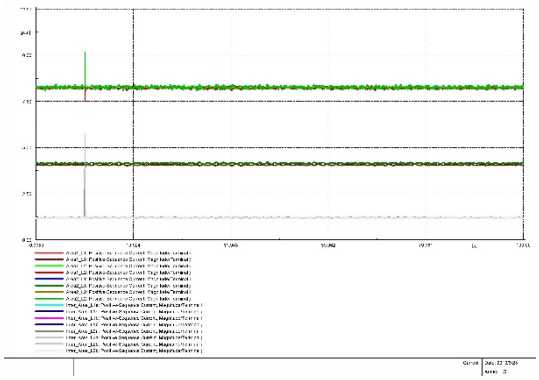

(g)Line current under reference element

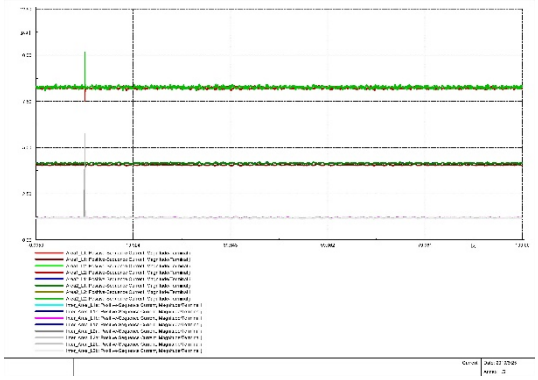

(h)Line current under reference COI

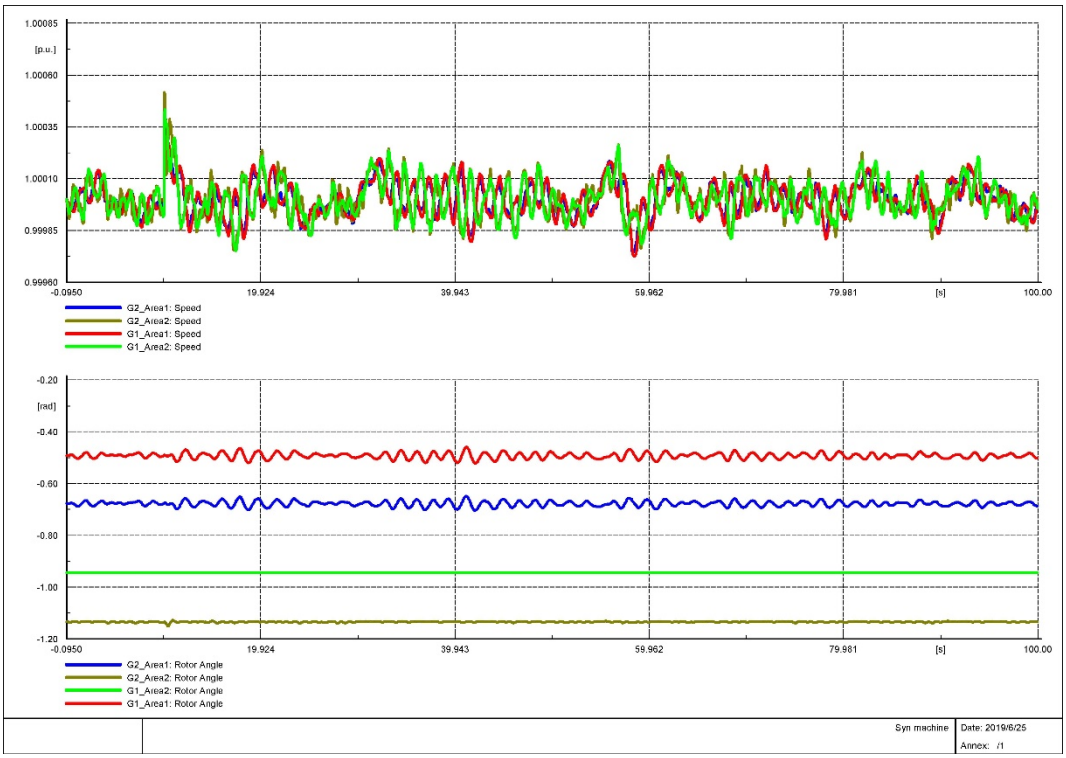

(i) rotor angle and speed of synchronous machines under reference element

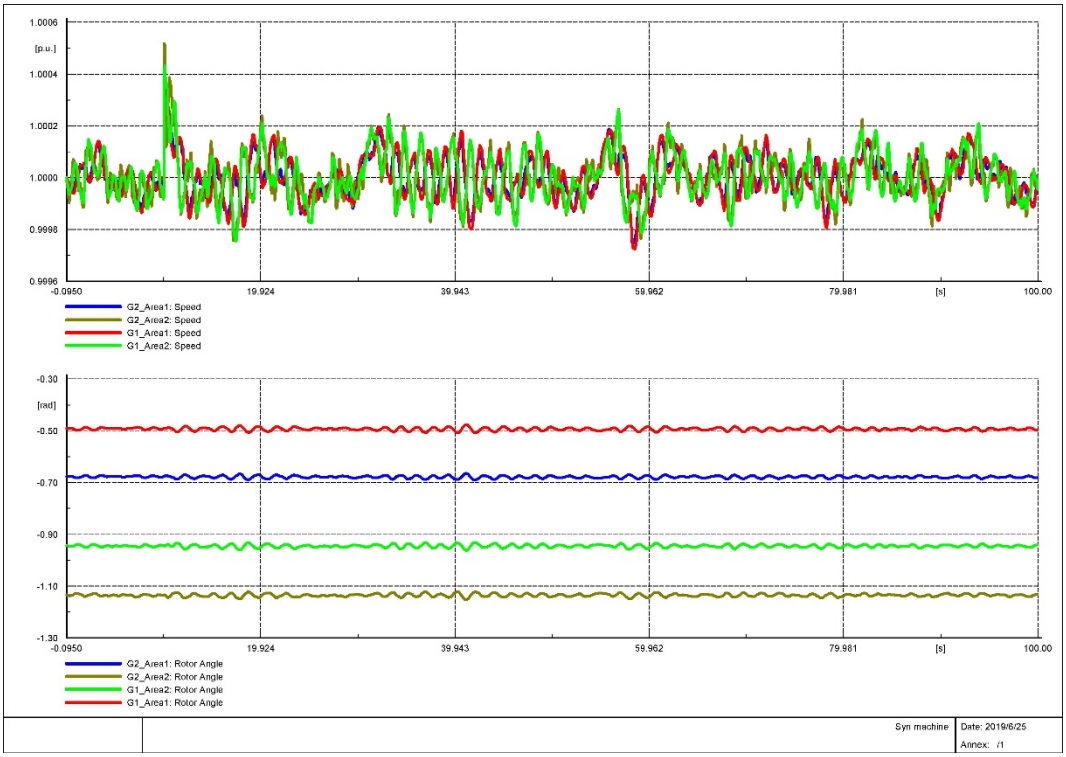

(j) rotor angle and speed of synchronous machines under reference COI

Figure 3.14 Simulation results of short circuit event 2

As shown in Figure 3.15, compared with transmission line short-circuit events, the system will experience a longer oscillation process if a three-phase short circuit occurs at a generator busbar. The fluctuations of voltages, frequency and currents are also larger.

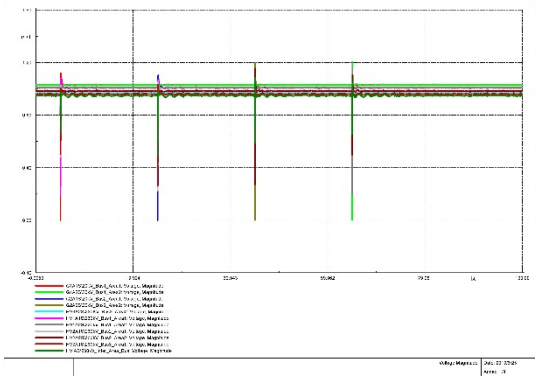

(a)Voltage magnitude under reference element

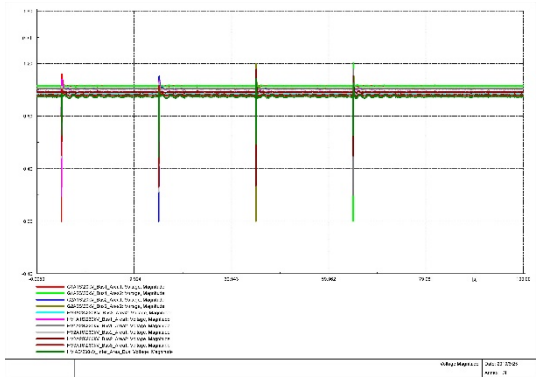

(b)Voltage magnitude under reference COI

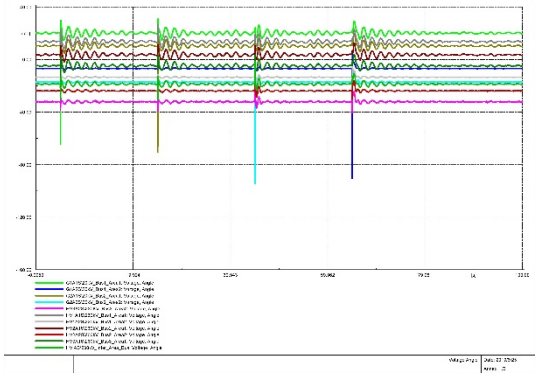

(c)Voltage angle under reference element

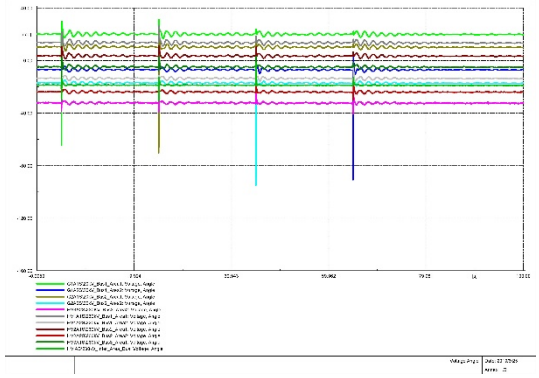

(d)Voltage angle under reference COI

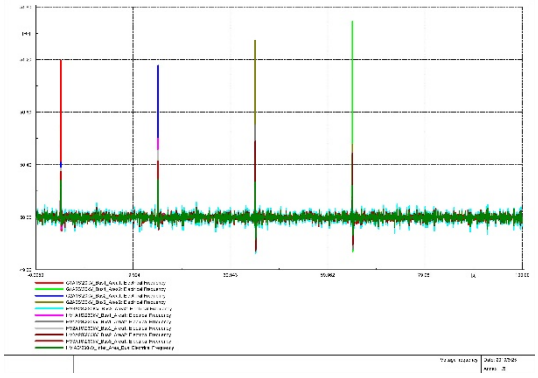

(e)Frequency under reference element

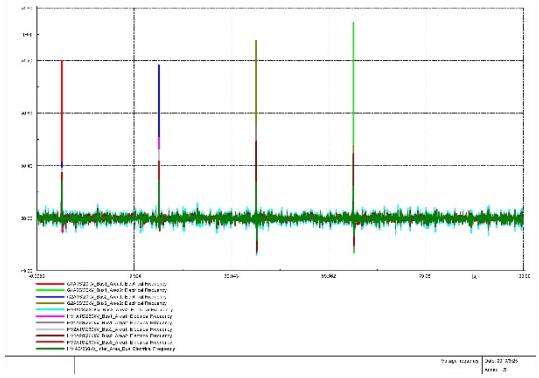

(f)Frequency under reference COI

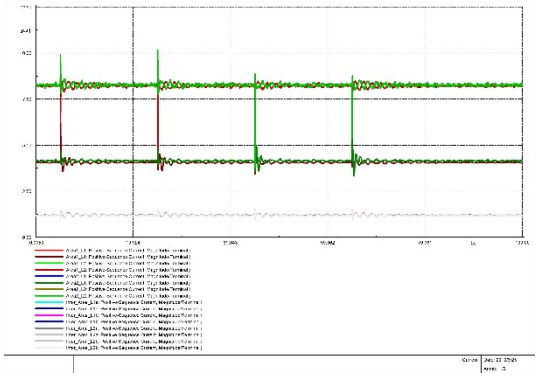

(g)Line current under reference element

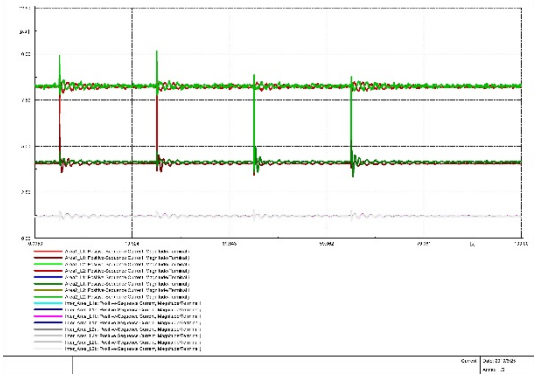

(h)Line current under reference COI

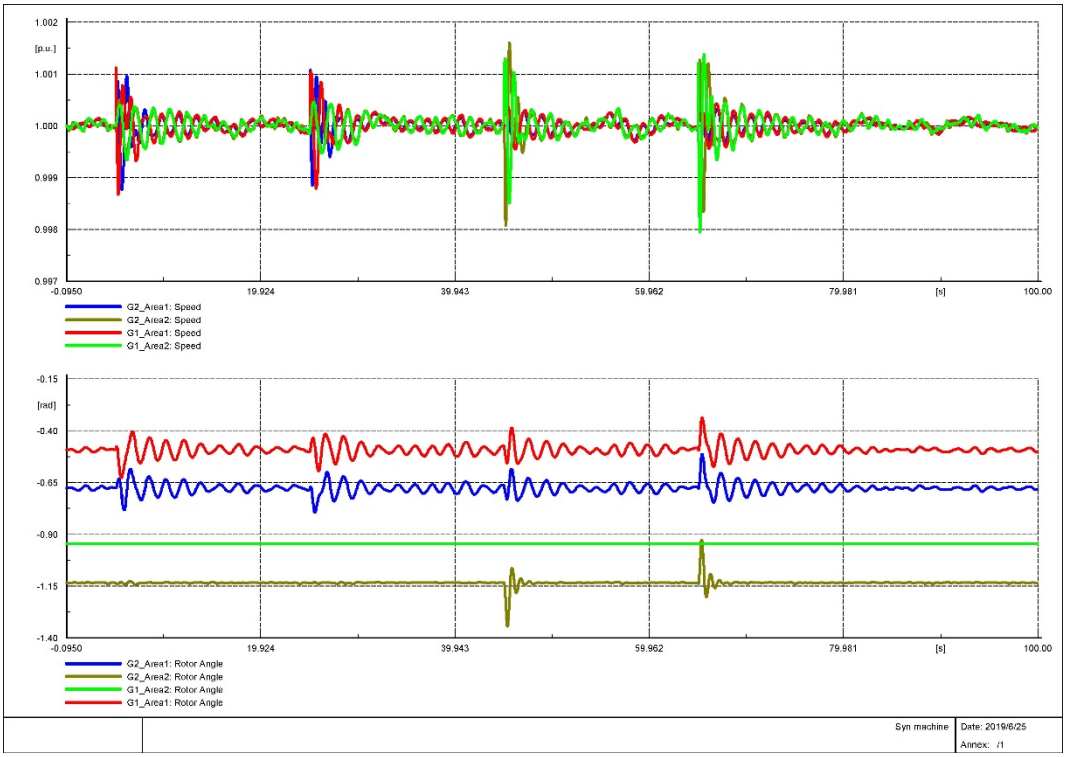

(i) rotor angle and speed of synchronous machines under reference element

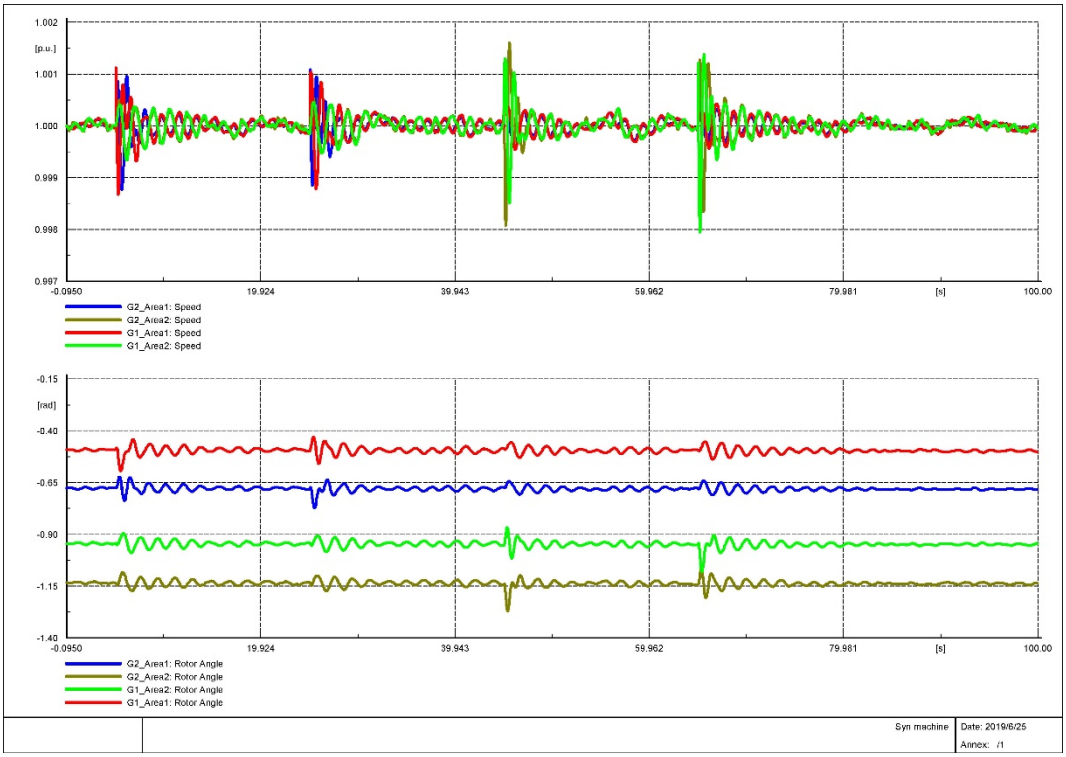

(j) rotor angle and speed of synchronous machines under reference COI

Figure 3.15 Simulation results of short circuit event 3

3.6.5 Simulation results of generator events

Figure 3.16 to Figure 3.18 represent the simulation results of three generator events.

It can be seen from Figure 3.16 and Figure 3.17 that decreasing the output power of G2 in area 1, meanwhile increasing the output power of G2 in area2 has little effect on the frequency. The currents on the transmission lines that directly connected to G2_Area1 and G2_Area 2 change in the same trends with the output power. The voltage magnitudes of interarea busbars increase obviously.

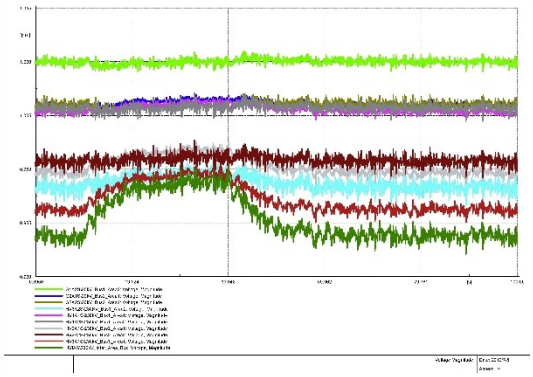

(a)Voltage magnitude under reference element

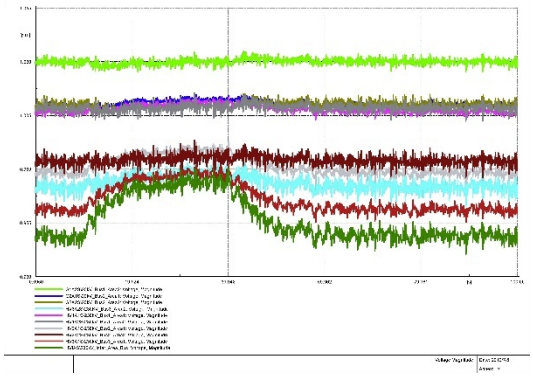

(b)Voltage magnitude under reference COI

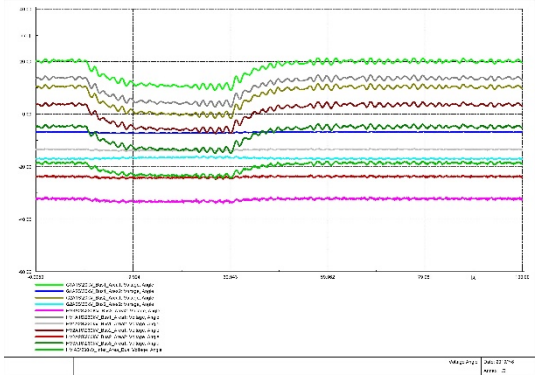

(c)Voltage angle under reference element

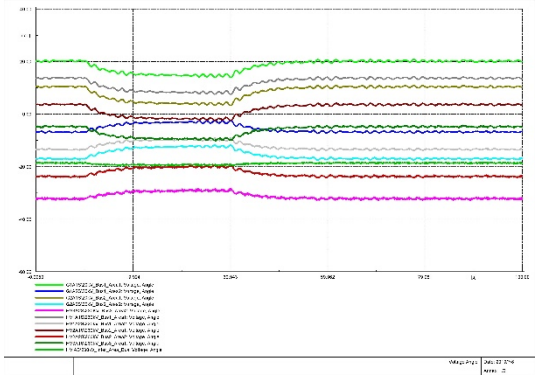

(d)Voltage angle under reference COI

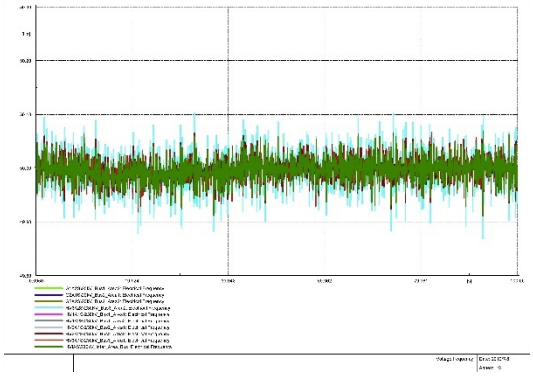

(e)Frequency under reference element

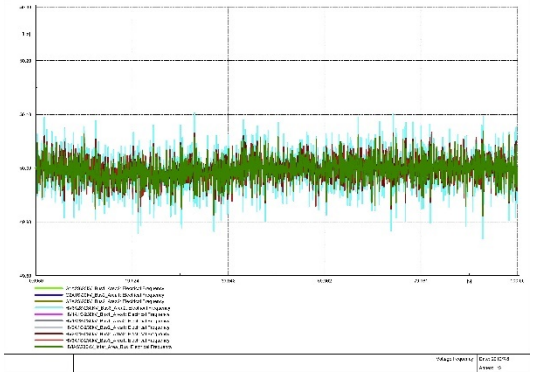

(f)Frequency under reference COI

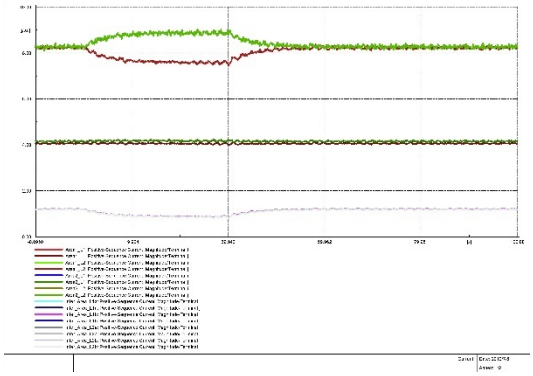

(g)Line current under reference element

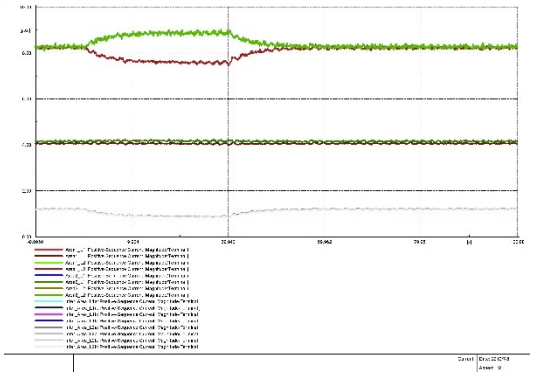

(h)Line current under reference COI

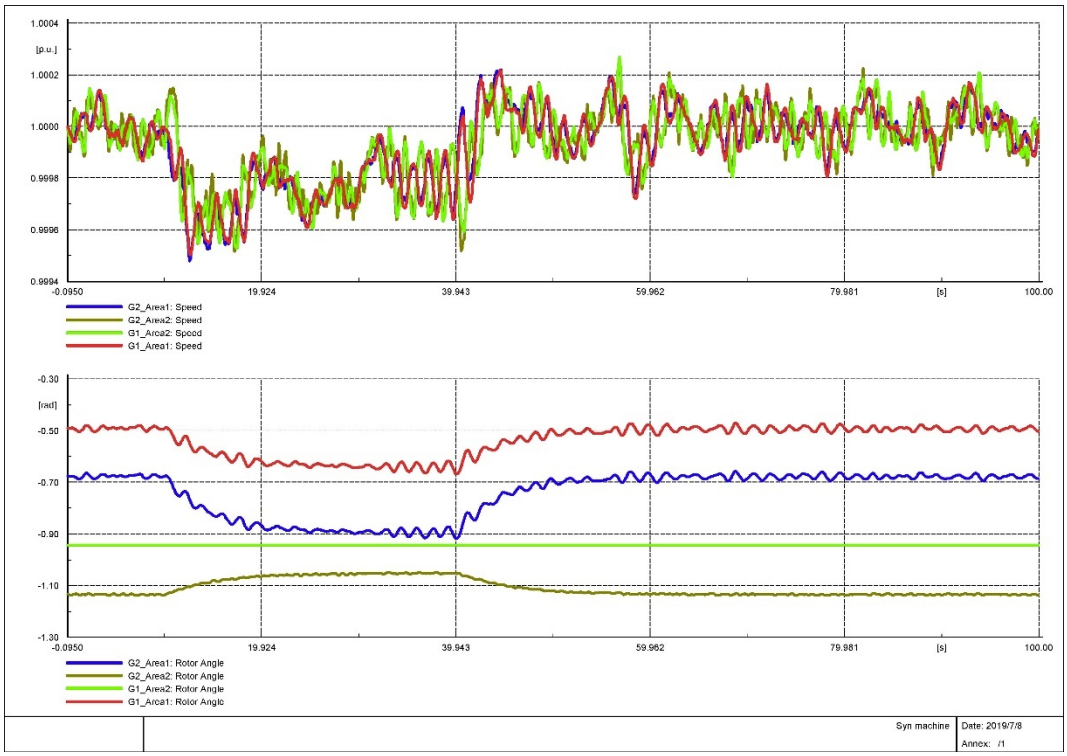

(i) rotor angle and speed of synchronous machines under reference element

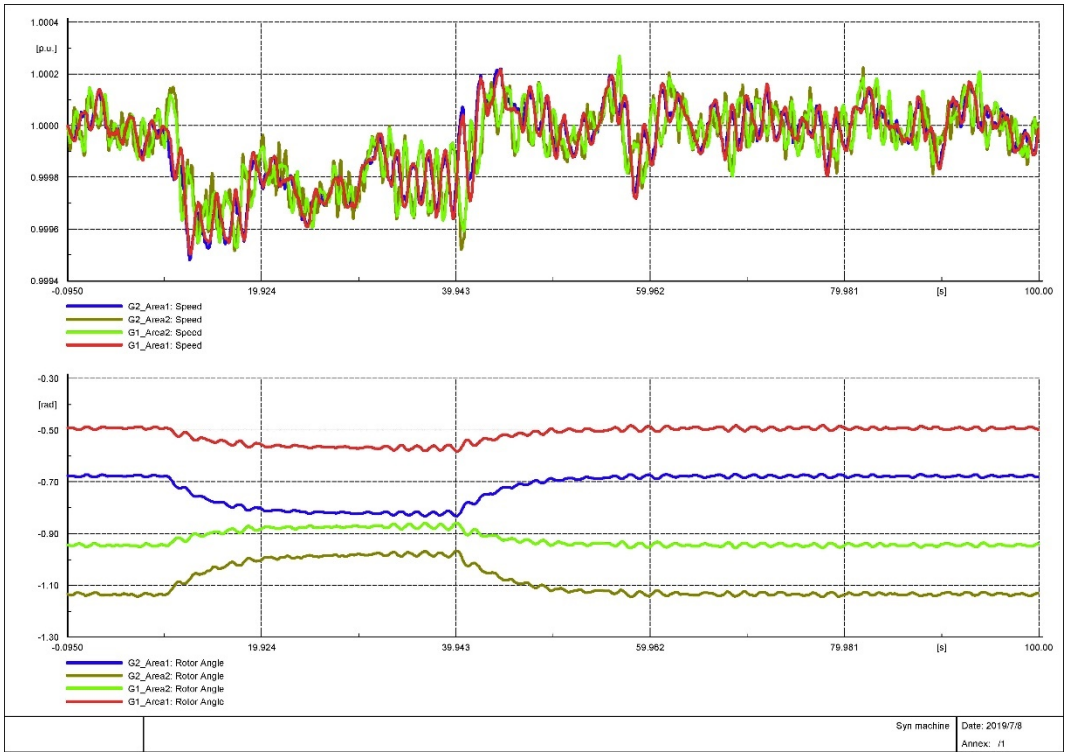

(j) rotor angle and speed of synchronous machines under reference COI

Figure 3.16 Simulation results of generator event 1

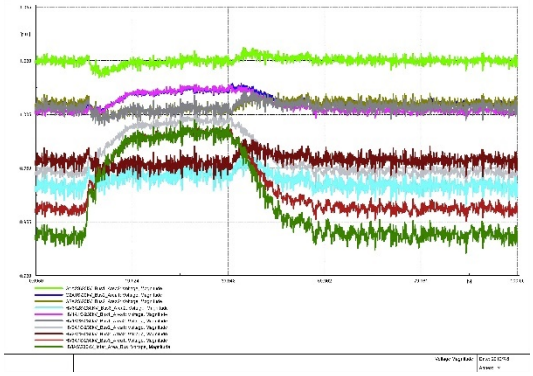

(a)Voltage magnitude under reference element

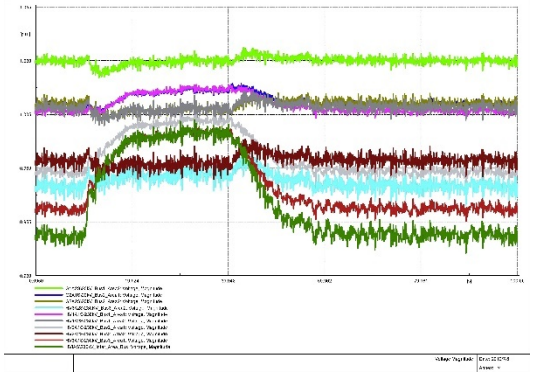

(b)Voltage magnitude under reference COI

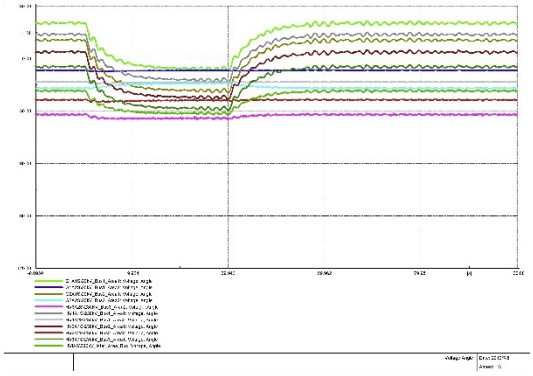

(c)Voltage angle under reference element

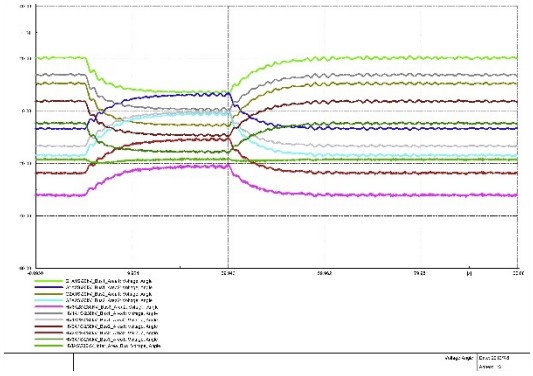

(d)Voltage angle under reference COI

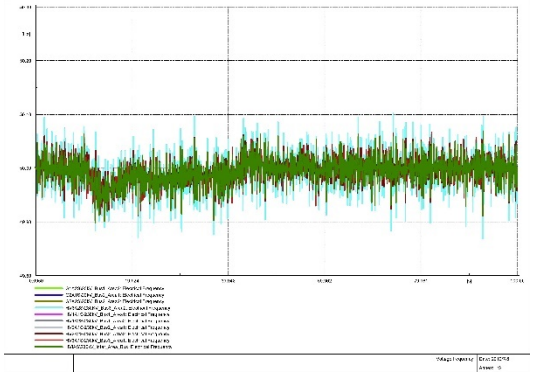

(e)Frequency under reference element

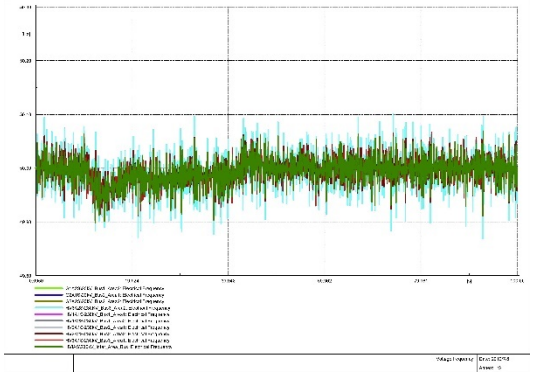

(f)Frequency under reference COI

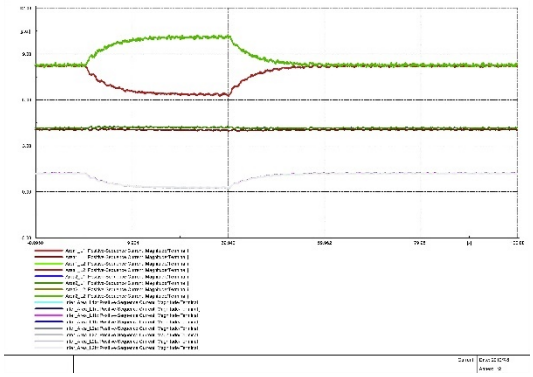

(g)Line current under reference element

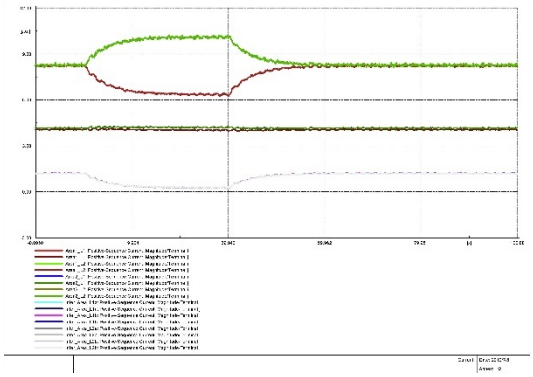

(h)Line current under reference COI

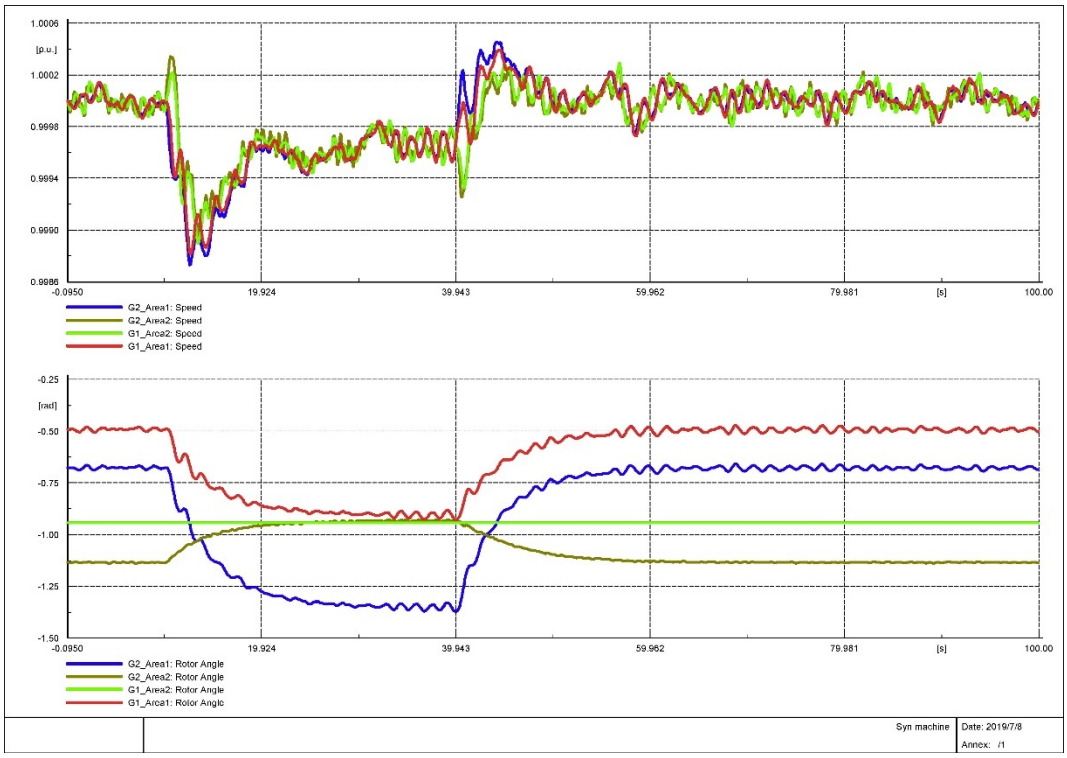

(i) rotor angle and speed of synchronous machines under reference element

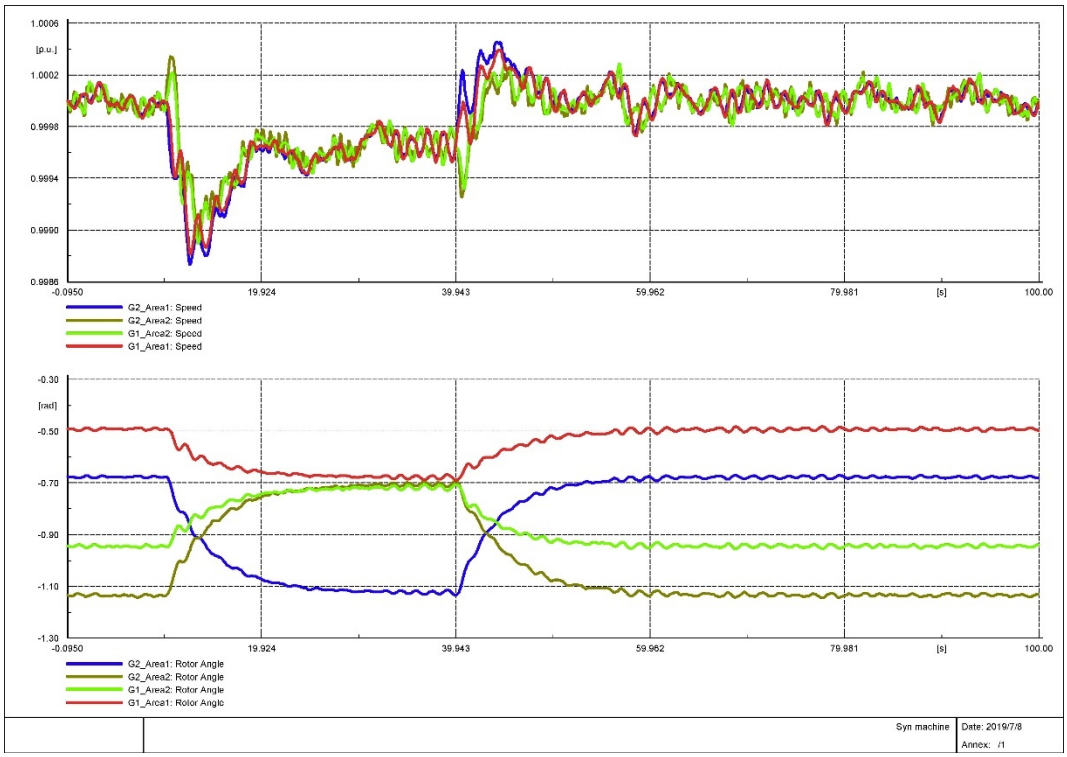

(j) rotor angle and speed of synchronous machines under reference COI

Figure 3.17 Simulation results of generator event 2

In the third generator event, 600 MW active power is transferred from G1_Area1 to G2_Area1 at t=10s. At this time, the output power of G1 and G2 are 100MW and 1300MW respectively. After the system reaches a new operating state, G1_Area1 is cut off. Simulation results are shown in the Figure 3.18.

After the removal of G1_Area1，the rotor speed of G1_Area1decreases to zero. The whole system runs out of step. The voltages of the busbars, the rotor angles and the currents on the transmission lines are oscillating. In the synchronous coordinates，the rotor angle of G1_Area2 is regarded as reference. The oscillation magnitude of the rotor angle of G2_Area2 is smaller than that of G2_Area1. In the COI coordinates, due to the resection of G1_Area1, the symmetry of the network and the center of inertia are changed. The remaining generators display apparent oscillations.

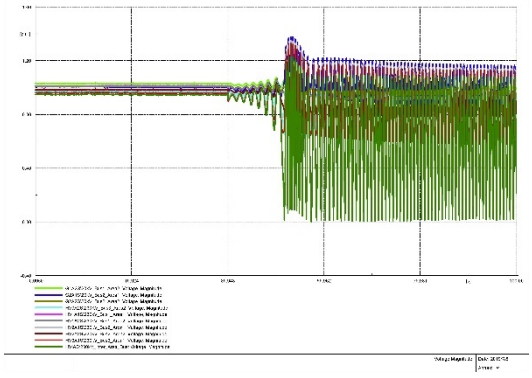

(a)Voltage magnitude under reference element

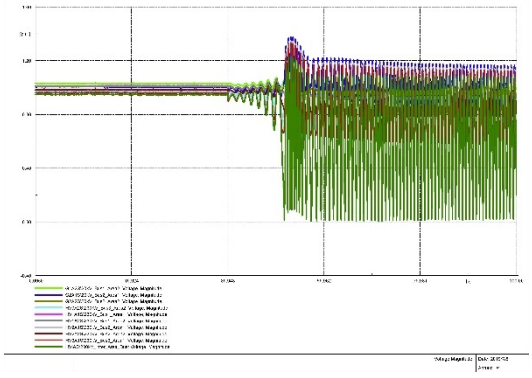

(b)Voltage magnitude under reference COI

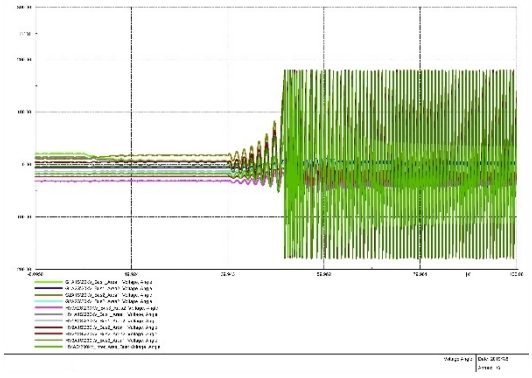

(c)Voltage angle under reference element

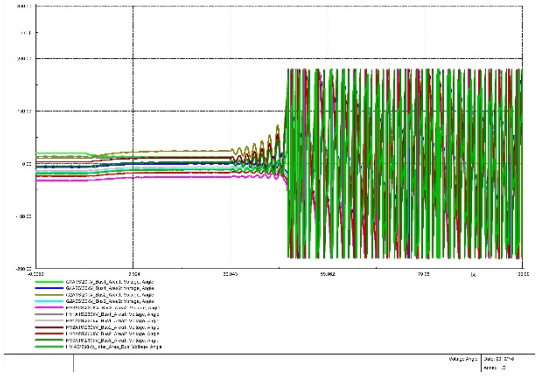

(d)Voltage angle under reference COI

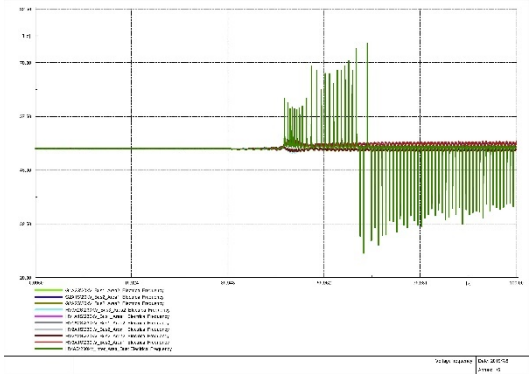

(e)Frequency under reference element

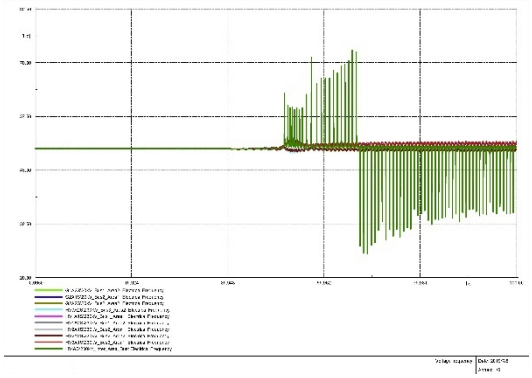

(f)Frequency under reference COI

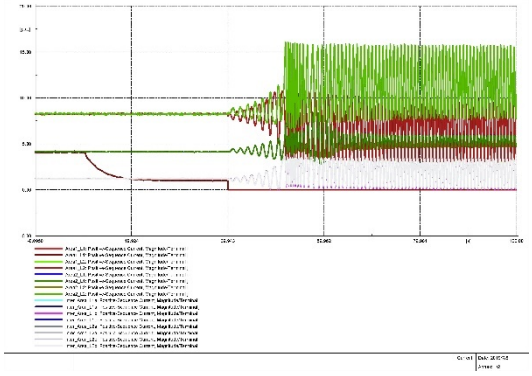

(g)Line current under reference element

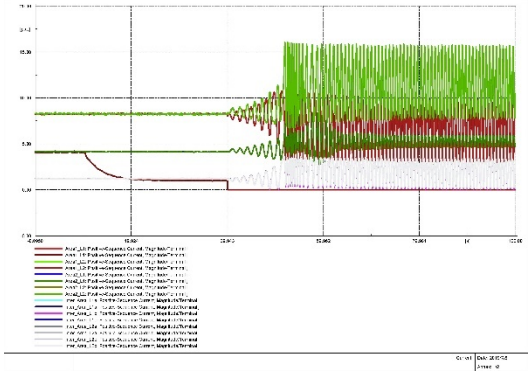

(h)Line current under reference COI

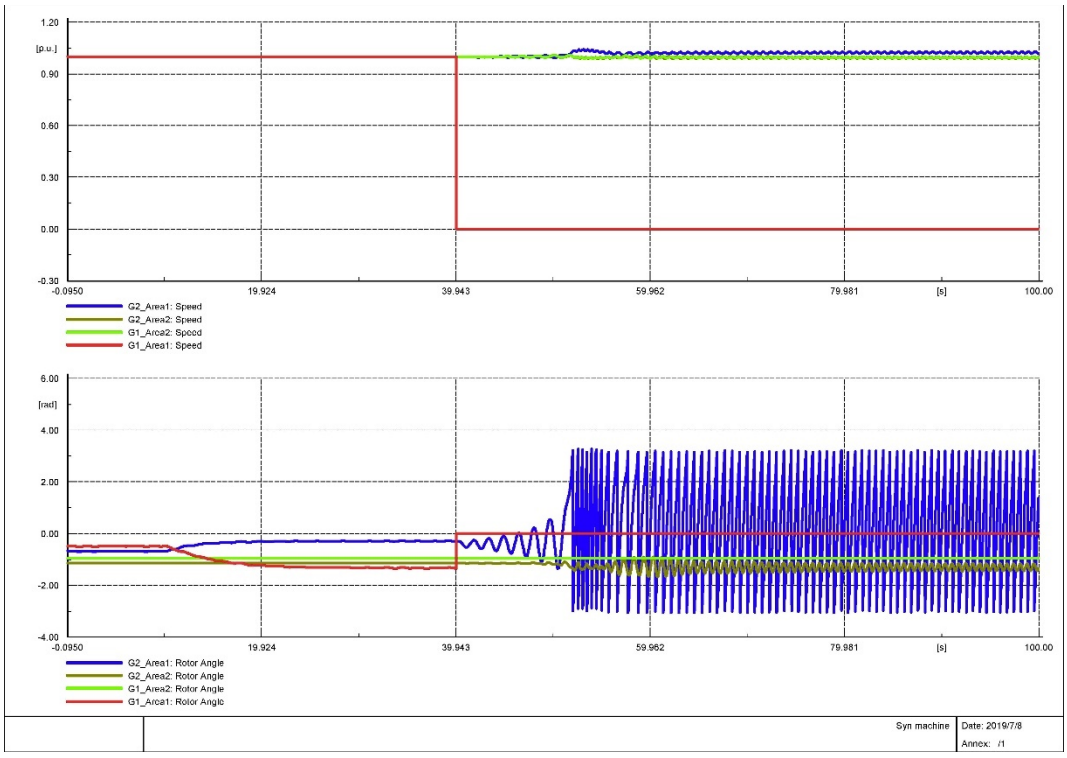

(i) rotor angle and speed of synchronous machines under reference element

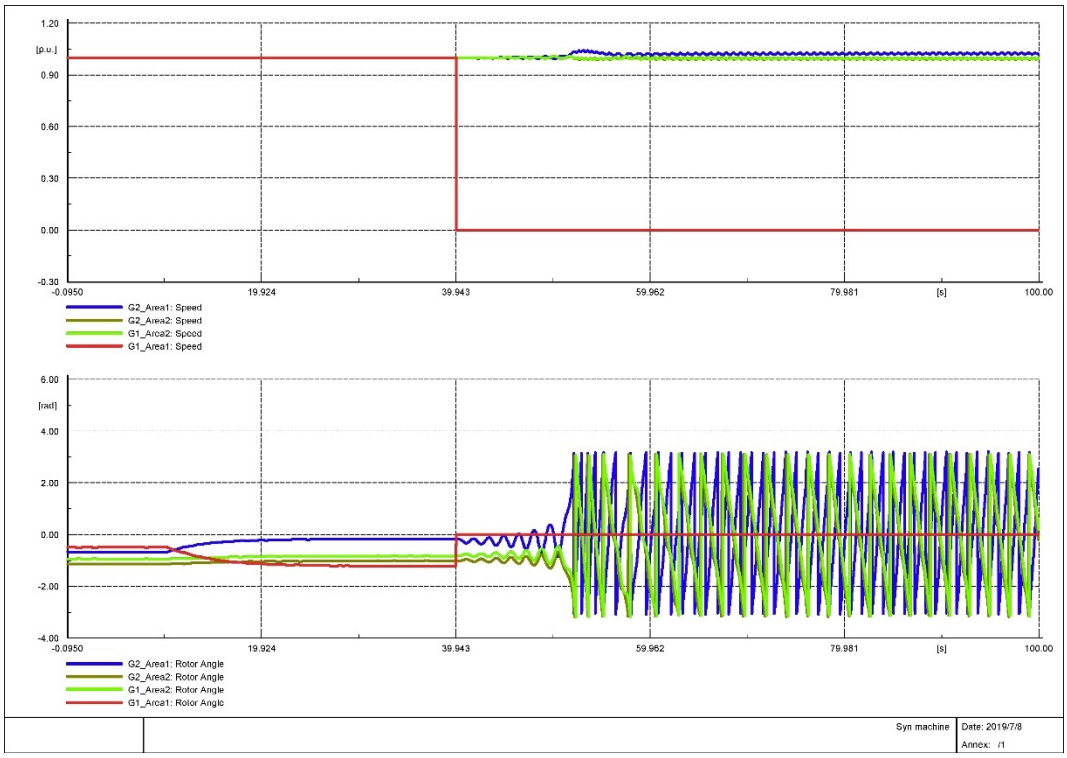

(j) rotor angle and speed of synchronous machines under reference COI

Figure 3.18 Simulation results of generator event 3

3.6.6 Simulation results of switch events

Figure 3.19 and Figure 3.20 represent the simulation results of two switch events. Due to the symmetry of the test system, simulation results of the removal of line Inter_area_L1a and line Inter_area_L2a are quite similar. All the selected variables are damped oscillating to reach a new steady state.

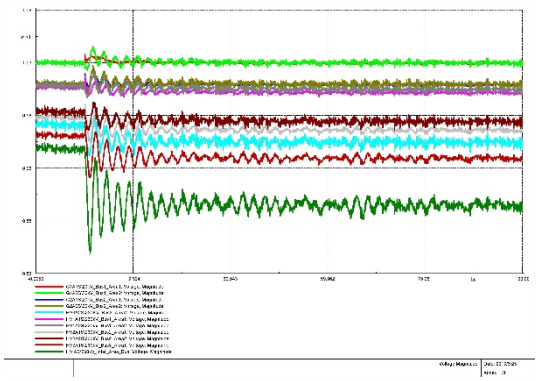

(a)Voltage magnitude under reference element

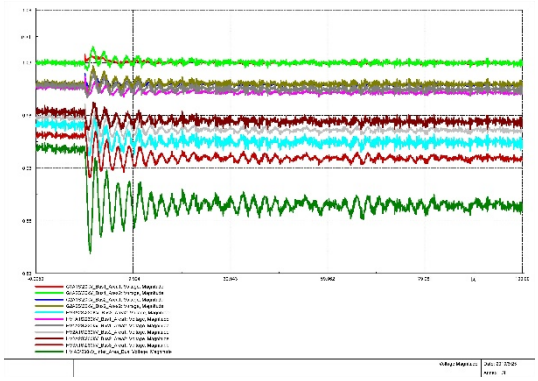

(b)Voltage magnitude under reference COI

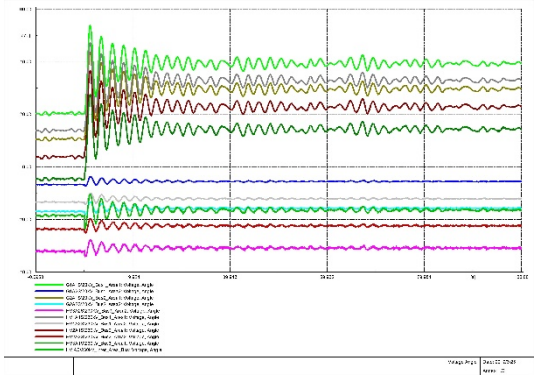

(c)Voltage angle under reference element

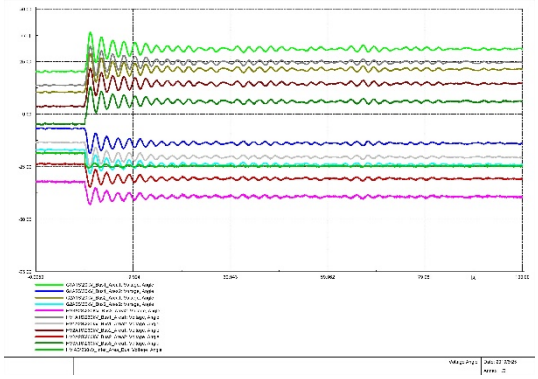

(d)Voltage angle under reference COI

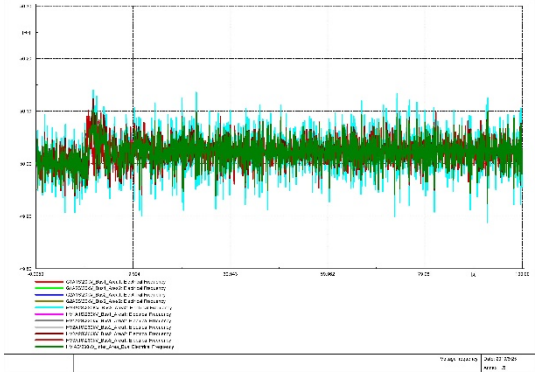

(e)Frequency under reference element

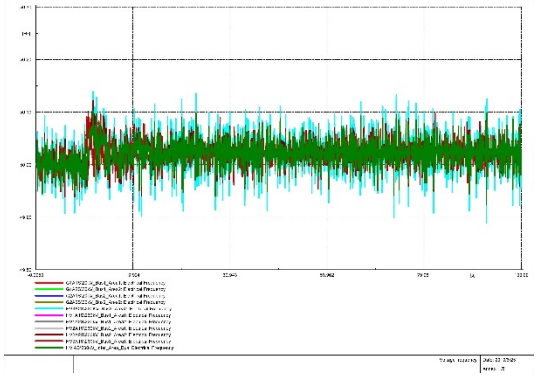

(f)Frequency under reference COI

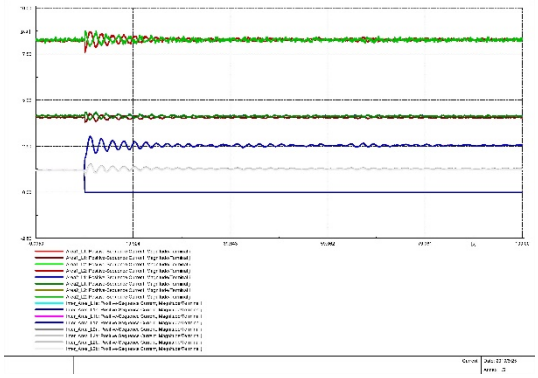

(g)Line current under reference element

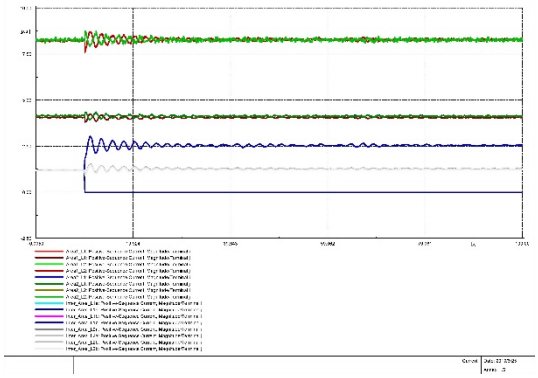

(h)Line current under reference COI

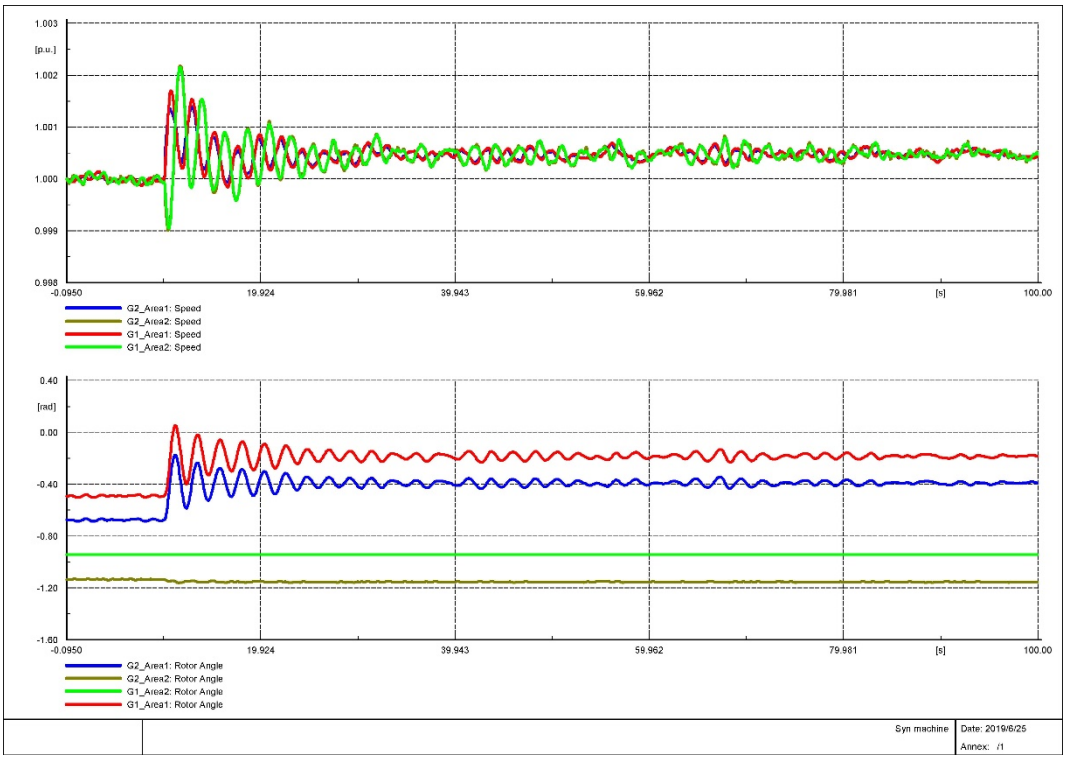

(i) rotor angle and speed of synchronous machines under reference element

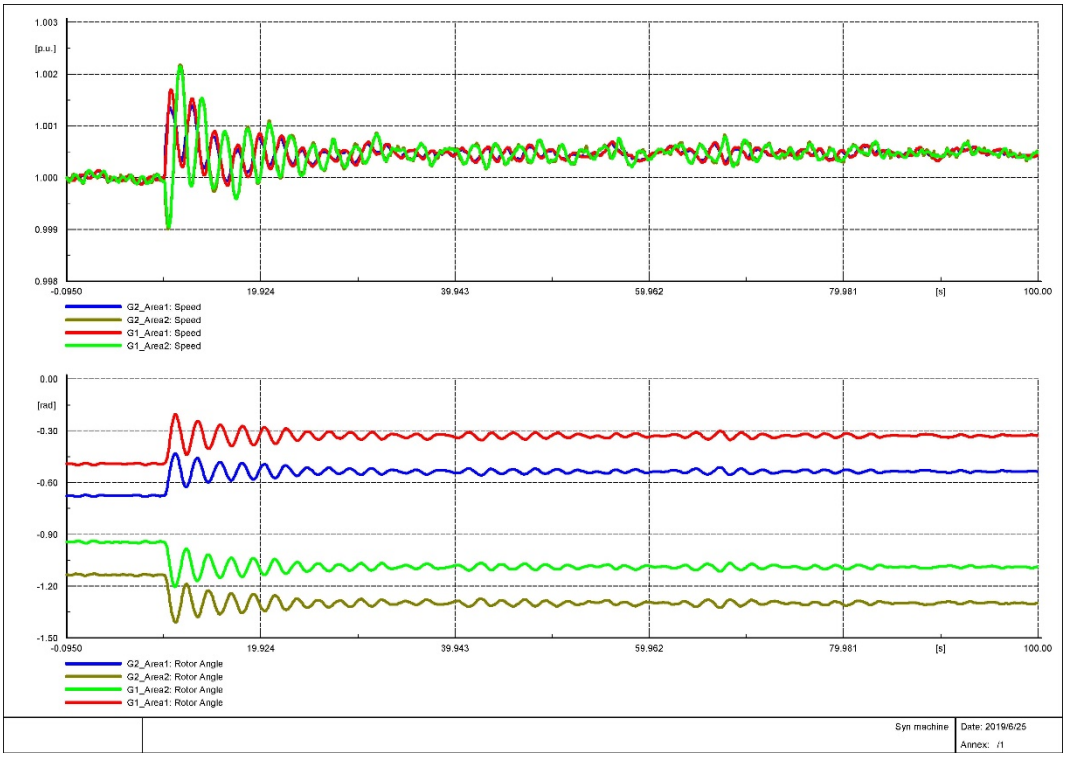

(j) rotor angle and speed of synchronous machines under reference COI

Figure 3.19 Simulation results of switch event 1

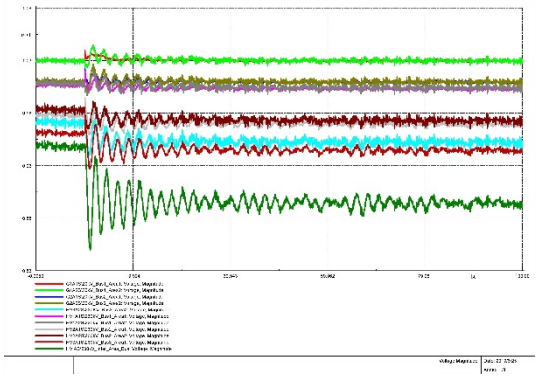

(a)Voltage magnitude under reference element

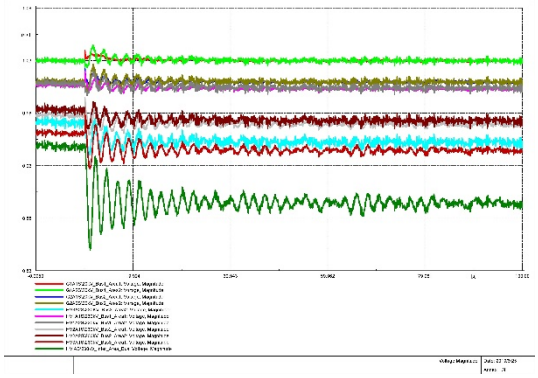

(b)Voltage magnitude under reference COI

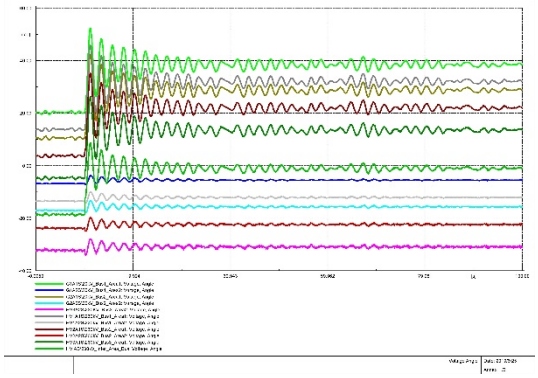

(c)Voltage angle under reference element

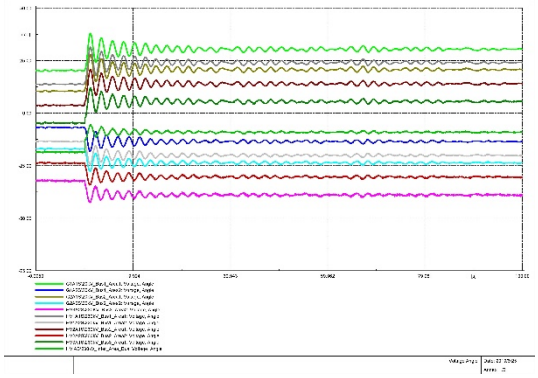

(d)Voltage angle under reference COI

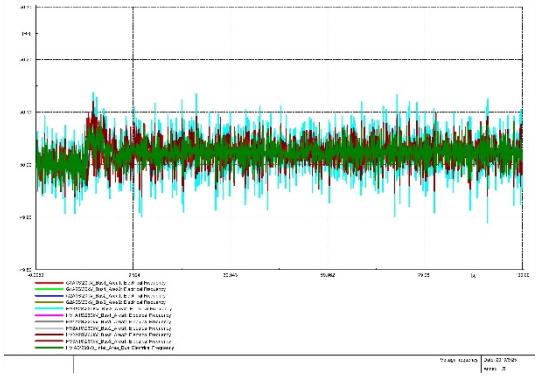

(e)Frequency under reference element

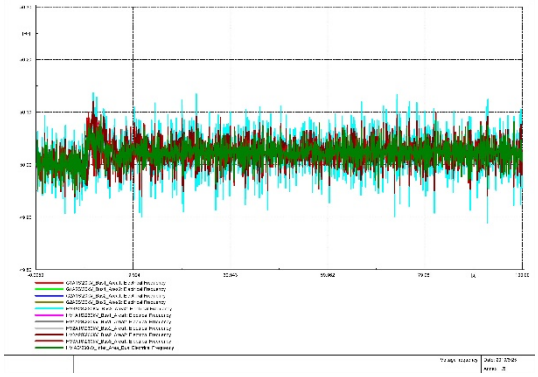

(f)Frequency under reference COI

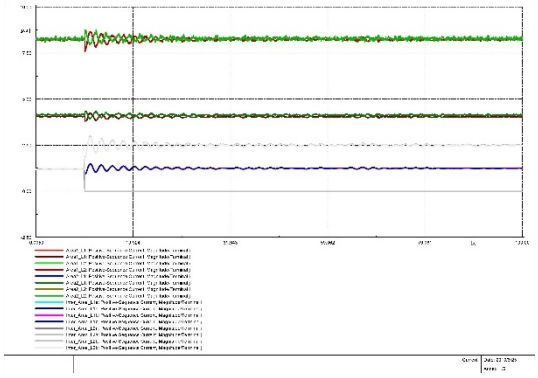

(g)Line current under reference element

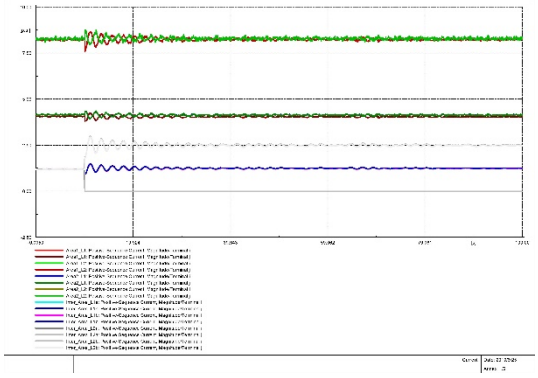

(h)Line current under reference COI

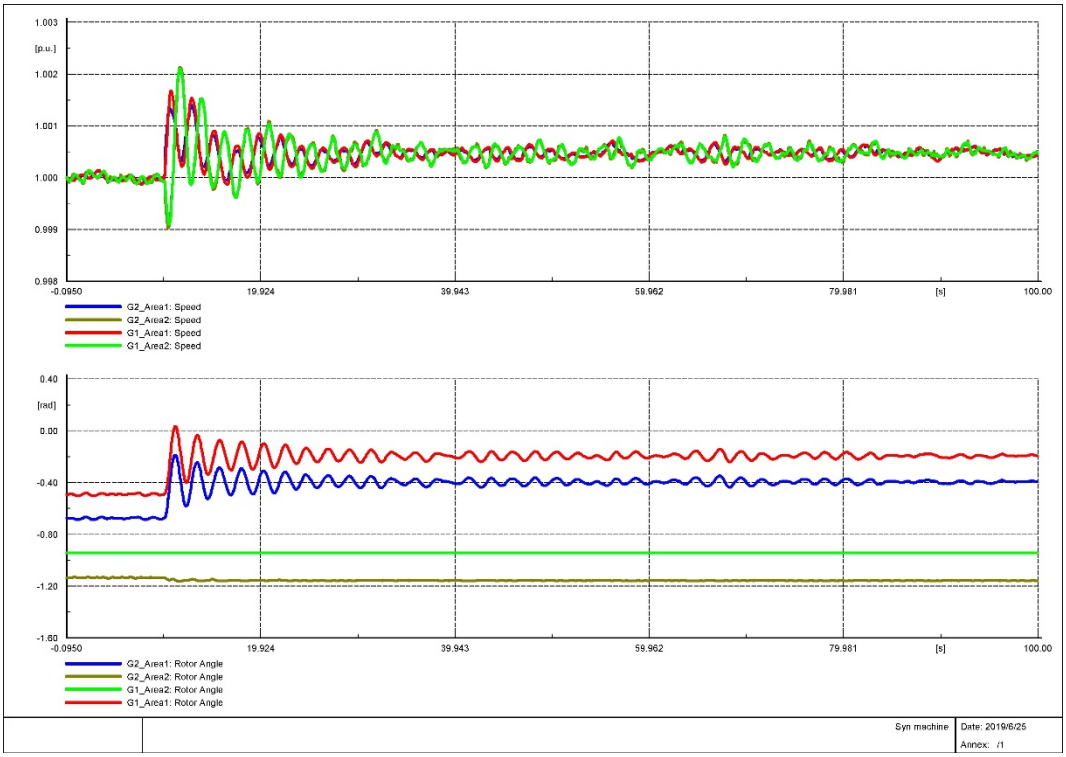

(i) rotor angle and speed of synchronous machines under reference element

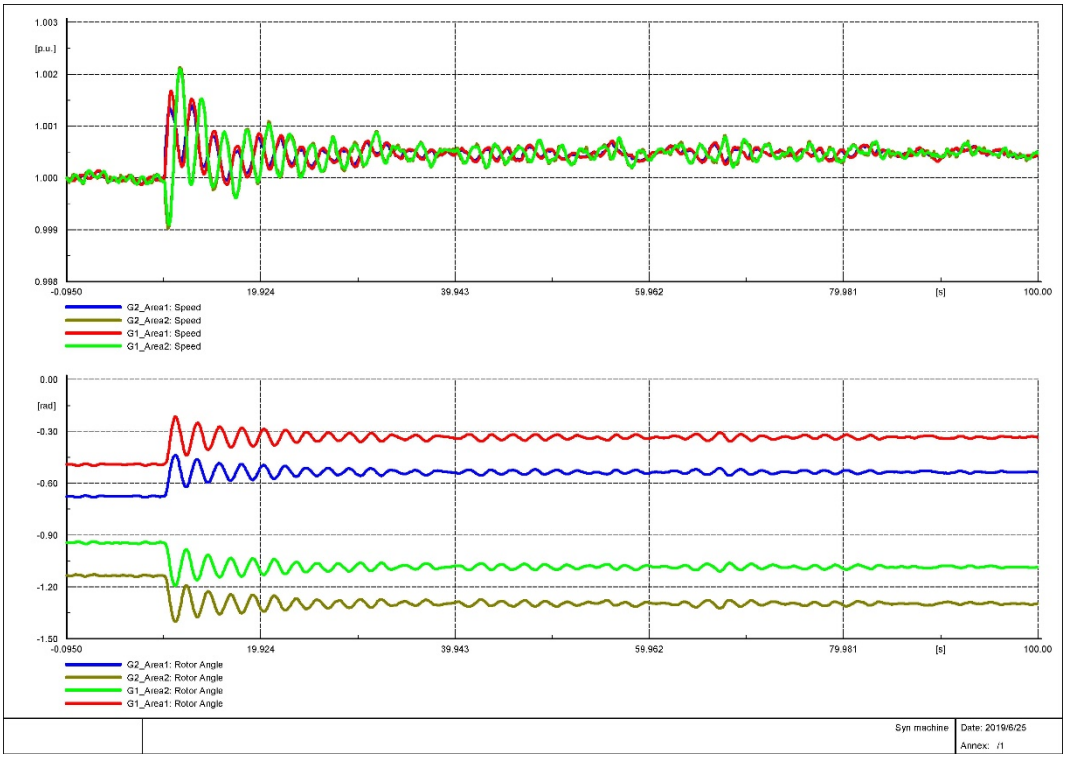

(j) rotor angle and speed of synchronous machines under reference COI

Figure 3.20 Simulation results of switch event 2

4 Validation of DMD algorithm

4.1 Introduction

Dynamic mode decomposition (DMD), a mathematical method that aims at finding a low dimensional approximate matrix of the system, is here presented. According to DMD theory, the electromechanical oscillation modes of the power system could be extracted from observational data.

In this chapter, DMD algorithm is applied to identify oscillation modes in two typical events, on the basis of real-time measurement generated in Chapter 3. Comparisons between the results obtained by DMD algorithm and conventional mode-based method validate the effectiveness of DMD algorithm in electromechanical oscillation modes identification.

4.2 DMD Algorithm

4.2.1 Background

In recent years, the dynamic feature parameters extraction method based on multi-channel dataset has been gradually developed. In order to determine the oscillation modes of the system, it is necessary to analyze the dynamic behaviors of the generator from a global perspective.

Dynamic mode decomposition (DMD) algorithm was proposed by Schmid, using a linear finite-dimensional system to approximate the nonlinear finite-dimensional system. DMD algorithm is a low-dimensional approximation technique developed on the basis of Koopman operator theory [16].

The measurement dataset of actual systems is very large, resulting in a high-dimensional system matrix that is difficult to analyze. Researchers hope to approximate the eigenvalues of the system matrix A using the eigenvalues of a low-dimensional approximation matrix. That is, the dynamic characteristics of the system can be studied by analyzing the low-dimensional approximation matrix, even if the precise matrix A is unknown. Specific steps of the dynamic mode decomposition algorithm is described below.

Assume that $x\left(v_j, t_i\right), j=1,\ldots,m, i=1,\ldots,N$ denotes an element of observation, where v_j is the j-th grid or measurement point, and t_i is the time at which the observations are made. To introduce the proposed method, define the data matrix $\boldsymbol{X}_1^N$,

as

$$\boldsymbol{X}_1^N = \begin{bmatrix} \overbrace{x(v_1,t_1)}^{\boldsymbol{x}_1} & \cdots & \overbrace{x(v_1,t_l)}^{\boldsymbol{x}_l} & \cdots & \overbrace{x(v_1,t_N)}^{\boldsymbol{x}_N} \\ x(v_m,t_1) & \cdots & x(v_m,t_l) & \cdots & x(v_m,t_N) \end{bmatrix} \in {}^{m\times N} \qquad (4\text{-}1)$$

Whose *l*-th column is the observation sequence $\boldsymbol{x}_l$.

Let now, $\hat{\boldsymbol{\Phi}} = \begin{bmatrix} \hat{\varphi}_1 & \hat{\varphi}_2 & \cdots & \hat{\varphi}_N \end{bmatrix}$ be a set of functions obtained from the data itself.

Dynamic mode decomposition (DMD) is a global multiscale method that can approximate a few Koopman functions φ_j using two sets of time ordered sequences of data snapshots. More precisely, the method assumes that the data sequences or snapshots, x_i in equation (4-1) are generated by a discrete-time linear dynamical system whose evolution is governed by the linear mapping[14]:

$$\boldsymbol{x}_{i+1} = \boldsymbol{A}\boldsymbol{x}_i + n_i, i = 1,\cdots,N-1 \qquad (4\text{-}2)$$

where $\boldsymbol{A}$ is an unknown (time-independent) operator matrix of dimension $m\times m$ that captures the dynamics inherent in the data matrix and $\boldsymbol{\eta_i}$ is some noise process. This is a local approximation to system dynamics with a linear system: the eigenvalues and eigenvectors of $\boldsymbol{A}$ determine dynamic behavior of the mapping.

Practical algorithms to estimate the linear operator $\boldsymbol{A}$ and its associated relevant eigenvalues and eigenvectors that do not require explicit knowledge of the mapping matrix are discussed below.

In the noise-free case, use of formula (4-2) in (4-11) yields the Krylow sequences:

$$\boldsymbol{X}_1^N = \begin{bmatrix} \boldsymbol{x}_1 & \boldsymbol{A}\boldsymbol{x}_1 & \boldsymbol{A}^2\boldsymbol{x}_1 & \cdots & \boldsymbol{A}^{N-1}\boldsymbol{x}_1 \end{bmatrix} = \begin{bmatrix} \boldsymbol{x}_1 & \cdots & \boldsymbol{x}_N \end{bmatrix} \qquad (4\text{-}3a)$$

$$\boldsymbol{X}_1^{N\text{-}1} = \begin{bmatrix} \boldsymbol{x}_1 & \boldsymbol{A}\boldsymbol{x}_1 & \boldsymbol{A}^2\boldsymbol{x}_1 & \cdots & \boldsymbol{A}^{N-2}\boldsymbol{x}_1 \end{bmatrix} = \begin{bmatrix} \boldsymbol{x}_1 & \cdots & \boldsymbol{x}_{N\text{-}1} \end{bmatrix} \qquad (4\text{-}3b)$$

$$\boldsymbol{X}_2^N = \begin{bmatrix} \boldsymbol{A}\boldsymbol{x}_1 & \boldsymbol{A}^2\boldsymbol{x}_1 & \cdots & \boldsymbol{A}^{N-1}\boldsymbol{x}_1 \end{bmatrix} = \begin{bmatrix} \boldsymbol{x}_2 & \cdots & \boldsymbol{x}_N \end{bmatrix} \qquad (4\text{-}3c)$$

It can be proved that as more vectors $\boldsymbol{x}_{l+1}=\boldsymbol{A}^l\boldsymbol{x}_1$, l=0, are appended, the rank of the Krylov sequences increases until it reaches a maximal value [17]. For a sufficiently large number of snapshots, it can be assumed that the N^{th} snapshot can be expressed as a linear combination of the previous measurements, i.e.,

$$\boldsymbol{x}_N = c_1\boldsymbol{x}_1 + c_2\boldsymbol{x}_2 + \cdots c_{N-1}\boldsymbol{x}_{N-1} + \boldsymbol{r} \qquad (4\text{-}4)$$

where the c_i's are unknown expansion coefficients, $r \in$ $^{m\times 1}$ is a vector of residuals.

Equation (4-4) can be rewritten in a more useful form as

$$\boldsymbol{x}_N = c_1\boldsymbol{x}_1 + c_2\boldsymbol{x}_2 + \cdots c_{N-1}\boldsymbol{x}_{N-1} + \boldsymbol{r} = \boldsymbol{X}_1^{N\text{-}1}\boldsymbol{c} + \boldsymbol{r}$$

in which $\boldsymbol{c}=[c_1\ c_2\ c_3\ \ldots\ c_{N\text{-}1}]^{\boldsymbol{T}}$ is a vector of unknown coefficients.

Multiplying (4-3b) $\boldsymbol{A}$ yields

$$\boldsymbol{A}\boldsymbol{X}_1^{N-1} = \boldsymbol{X}_2^N \tag{4-5}$$

It can be easy to show that the data sequence $\boldsymbol{X}_2^N$ can be expressed as

$$\boldsymbol{X}_2^N = \left[\boldsymbol{x}_2 \quad \boldsymbol{x}_3 \quad \boldsymbol{x}_4 \quad \cdots \quad \left(\boldsymbol{X}_1^{N-1}\boldsymbol{c}\right)\right] + \boldsymbol{r}\boldsymbol{e}_{N-1} \tag{4-6}$$

where $\boldsymbol{e}_{N\text{-}1}=[0\ 0\ 0\ \ldots\ 1]\in$ $^{1\times N-1}$ and use has been made of (4-4).

Further in matrix form, formula (4-5) in connection with formula (4-6) can be written as

$$\boldsymbol{X}_2^N = \boldsymbol{A}\boldsymbol{X}_1^{N-1} = \boldsymbol{X}_1^{N-1}\boldsymbol{S} + \boldsymbol{r}\boldsymbol{e}_{N-1} \in \ ^{m\times N-1} \tag{4-7}$$

where

$$S = \begin{bmatrix} 0 & & & & c_1 \\ 1 & 0 & & & c_2 \\ & & & & \\ & & 1 & 0 & c_{N\text{-}2} \\ & & & 1 & c_{N-1} \end{bmatrix} \in \ ^{N-1\times N-1} \tag{4-8}$$

is a companion (or Frobenius) matrix associated with the DMD method.

In light of this, the unknown matrix $\boldsymbol{S}$ can be determined by minimizing the residual $\boldsymbol{r}$

$$\boldsymbol{S} = \underbrace{\min}_{\boldsymbol{S}} \left\| \boldsymbol{X}_2^N - \boldsymbol{X}_1^{N-1}\boldsymbol{S} \right\| \tag{4-9}$$

A solution to the optimization problem is given by $S=\left(\boldsymbol{X}_1^{N-1}\right)\dagger\,\boldsymbol{X}_2^N$, where the notation $\left(\cdot\right)\dagger$ denotes the Moore-Pen-rose pseudo-inverse. Once matrix $\boldsymbol{S}$ is determined, the DMD modes and eigenvalues are obtained by solving the eigenvalue problem $\boldsymbol{S}\varphi_i = \lambda_i\varphi_i, i = 1,\cdots N-1$. The quality of the estimation can then be computed from equation (4-4) and equation (4-7) as

$$\left\|\boldsymbol{r}\right\| = \left\|\boldsymbol{x}_N - \boldsymbol{X}_1^{N-1}\boldsymbol{c}\right\| \tag{4-10}$$

With m being the number of sensors. DMD can be used to obtain low-dimensional spatial decomposition of a high-dimensional transient processes. Let m be the true rank of the data matrix $\boldsymbol{X}_1^{N-1}$. In analogy with POD analysis, the singular value decomposition (SVD) of matrix $\boldsymbol{X}_1^{N-1}$ is given by[17]

$$\boldsymbol{X}_1^{N-1} = \boldsymbol{U}\sum\boldsymbol{W}^T = \left[\boldsymbol{U}\right]\left[\sum_m 0\right]\begin{bmatrix}\boldsymbol{W}_m^T \\ \boldsymbol{W}_S^T\end{bmatrix}, m \ll N \qquad (4\text{-}11)$$

where $\boldsymbol{U}$ is an $m\times m$ orthonormal matrix containing the left singular vectors, the columns of $\boldsymbol{U}$ are the eigenmodes; $\sum$ is an $m\times N$ matrix containing the singular values, σ, and $\boldsymbol{W}$ is an $N\times N$ matrix containing the right singular vectors.

$$\sum_m = \begin{bmatrix}\sigma_1 & \cdots & 0 \\ \vdots & \ddots & \vdots \\ 0 & \cdots & \sigma_m\end{bmatrix}, \sigma_1 \geq \sigma_2 \geq \cdots \geq \sigma_m > 0$$

A truncated basis can be found by substituting formula (4-10) into formula (4-7). This yield a reduced model that approximates the original model equation (4-8) constructed by projecting onto $\tilde{S}$ the vector field:

$$\tilde{\boldsymbol{X}}_2^N \approx \boldsymbol{A}\boldsymbol{U}\sum_m \boldsymbol{W}_m^T \qquad (4\text{-}12)$$

Multiplying equation (4-11) by $\boldsymbol{U}^T$ from the left and by $W_m\sum_m^{-1}$ (from the right), a representation of $\boldsymbol{A}$ in the basis spanned by POD modes of $\tilde{\boldsymbol{X}}_2^N$ is obtained as equation (4-6) and equation (4-7),

$$\tilde{\boldsymbol{S}} \overset{\Delta}{=} \boldsymbol{U}^T\boldsymbol{A}\boldsymbol{U} = \boldsymbol{U}^T\tilde{\boldsymbol{X}}_2^N\boldsymbol{W}_m\sum_m^{-1} \in \quad ^{m\times m} \qquad (4\text{-}13)$$

Formula (4-12) constitutes the reduced companion matrix. Compared to equation (4-8), matrix $\tilde{\boldsymbol{S}}$ is of dimension $m\times m$, (m<<N-1) and holds information of the modal spatial ($\boldsymbol{U}$) and temporal structures ($\boldsymbol{W}_m\sum_m^{-1}$) as discussed below.

4.2.2 Modal Decomposition

An interesting interpretation of system dynamic behavior can be obtained from the eigen-decomposition of the low-dimensional system matrix, $\tilde{\boldsymbol{S}}$.

Suppose that matrix $\tilde{\boldsymbol{S}}$ is diagonalizable with eigenvalue decomposition

$$\tilde{\boldsymbol{S}}=\boldsymbol{Y}\Lambda\boldsymbol{Y}^{-1} \qquad (4\text{-}14)$$

where $\Lambda=diag\begin{bmatrix} \lambda_1 & \lambda_2 & \cdots & \lambda_m \end{bmatrix}\in\mathbb{C}^{m\times m}$ is a diagonal matrix consisting of empirical Ritz eigenvalues λ_j, and $\boldsymbol{Y}=\begin{bmatrix} \boldsymbol{y}_1 & \boldsymbol{y}_2 & \cdots & \boldsymbol{y}_m \end{bmatrix}\in\mathbb{C}^{m\times m}$ is the matrix of right eigenvectors, respectively.

As discussed above, equation (4-14) determines a low-dimensional representation of the mapping $\boldsymbol{A}$ on the subspace spanned by the POD modes of $\boldsymbol{X}_2^N$. Substituting equation (4-14) into equation (4-13) yields

$$\boldsymbol{U}^T\tilde{\boldsymbol{X}}_2^N\boldsymbol{W}_m\sum\nolimits_m^{-1}=\boldsymbol{Y}\Lambda\boldsymbol{Y}^{-1} \tag{4-15}$$

From equation (4-15), it is straightforward to show that $\tilde{\boldsymbol{X}}_2^N$ can be approximated using a linear combination of the DMD modes. Multiplying equation (4-15) from the left by $\boldsymbol{U}$ and from the right by $\sum_m\boldsymbol{W}_m^T$, yields

$$\tilde{\boldsymbol{X}}_2^N\approx\boldsymbol{U}\boldsymbol{Y}\Lambda\boldsymbol{Y}^{-1}\sum\nolimits_m\boldsymbol{W}_M^T \tag{4-16}$$

Equation (4-16) constitutes a reduced-order modal approximation of dimension $m\times N$. Based on this idea, two distinct notions of this decomposition are established.

A first useful interpretation is obtained by inserting equation (4-14) in equation (4-16):

$$\tilde{\boldsymbol{X}}_2^N\approx\boldsymbol{U}\tilde{\boldsymbol{S}}\sum\nolimits_m\boldsymbol{W}_M^T\approx\boldsymbol{U}\tilde{\boldsymbol{S}}\Gamma_m(t) \tag{4-17}$$

or

$$\tilde{\boldsymbol{X}}_2^N\approx\begin{bmatrix} \vdots & \vdots & \vdots & \vdots \\ \boldsymbol{u}_1 & \boldsymbol{u}_2 & \cdots & \boldsymbol{u}_m \\ \vdots & \vdots & \vdots & \vdots \end{bmatrix}\begin{bmatrix} \tilde{s}_{11} & \tilde{s}_{12} & \cdots & \tilde{s}_{1m} \\ \tilde{s}_{21} & \tilde{s}_{22} & \cdots & \tilde{s}_{2m} \\ \vdots & \vdots & \ddots & \vdots \\ \tilde{s}_{m1} & \tilde{s}_{m2} & \cdots & \tilde{s}_{mm} \end{bmatrix}\begin{bmatrix} \boldsymbol{a}_1(t) \\ \boldsymbol{a}_2(t) \\ \vdots \\ \boldsymbol{a}_n(t) \end{bmatrix}$$

where matrix $\tilde{\boldsymbol{S}}$ is asymmetric with rank (m,N), of upper triangular structure and contains a subset of the eigenvalues of $\boldsymbol{A}$.

The following properties can easily be verified:

1) The vectors $\boldsymbol{u}_i$ in matrix $\boldsymbol{U}$ are mutually orthogonal.
2) The m row vector of $\Gamma_m(t)$ are orthogonal, i.e., $\boldsymbol{a}_i(t)\boldsymbol{a}_i^T(t)=\gamma,\boldsymbol{a}_i(t)\boldsymbol{a}_j^T(t)=0$.
3) In analogy with 2), the temporal vectors $\boldsymbol{a}_i(t)$ are ranked in descending order of energy, i.e., $E_1>E_2>\ldots E_m$, where $E_j=\left\|\boldsymbol{a}_j(t)\right\|=\sum_{j=1}^m\sigma_j^2$.

4) When matrix $\tilde{\boldsymbol{S}}$ is an m^{th}-order identity matrix, the DMD method reduces to the conventional POD-SVD method [15].

5) The coefficients of matrix $\tilde{\boldsymbol{S}}$ can be interpreted as weights that calibrate the importance of the temporal structures in determining the system response.

This information is used in this research to determine various measures mode-state participations.

A second interpretation is now obtained in terms of the SVD of the data matrix. Define

$$\Phi \in \quad ^{m\times m} = \boldsymbol{UY} = \left[\phi_1 \phi_2 \quad \phi_m\right]$$

$$\Lambda \in \quad ^{m\times m} = \begin{bmatrix} \lambda_1 & \cdots & 0 \\ \ddots & \vdots & \\ 0 & \cdots & \lambda_m \end{bmatrix}$$

$$\tilde{\Gamma}_m(t) \in \quad ^{m\times N-1} = \boldsymbol{Y^{-1}} \sum\nolimits_m \boldsymbol{W}_m^T = \begin{bmatrix} \sum_{k=1}^{\boldsymbol{m}} \hat{\boldsymbol{Y}}_{1k} a_k(t) \\ \vdots \\ \sum_{k=1}^{\boldsymbol{m}} \hat{\boldsymbol{Y}}_{mk} a_k(t) \end{bmatrix} = \begin{bmatrix} \tilde{\boldsymbol{a}}_1(t) \\ \\ \tilde{\boldsymbol{a}}_m(t) \end{bmatrix}$$

From the previous discussion, it follows that the estimated data sequence, $\tilde{\boldsymbol{X}}_2^N$, can be expressed as

$$\tilde{\boldsymbol{X}}_2^N \approx \underbrace{\boldsymbol{UY}}_{\substack{\text{spatial} \\ \text{structure}}} \Lambda \underbrace{\boldsymbol{Y}^{-1} \cdot \sum\nolimits_m \cdot \boldsymbol{W}_m^T}_{\substack{\text{temporal} \\ \text{structure}}} = \Phi\Lambda\tilde{\Gamma}_m(t) \qquad (4\text{-}18)$$

The data matrix $\tilde{\boldsymbol{X}}_2^N$ can be now expanded in a linear combination of modal components as

$$\tilde{\boldsymbol{X}}_2^N \approx \sum_{j=1}^{m} \phi_j \lambda_j \tilde{\boldsymbol{a}}_j(t) \qquad (4\text{-}19)$$

where the $\tilde{\boldsymbol{a}}_j'$s are the temporal amplitudes, the ϕ_j's are the dynamic or spatial modes (DMD modes), and the λ_j's are the associated frequencies, with

$$\begin{cases} \rho_j = \Re\boldsymbol{e}\left\{\log\left(\lambda_j\right)\right\}/\Delta t \\ f_j = \Im\boldsymbol{e}\left\{\log\left(\lambda_j\right)\right\}/\Delta t / 2\pi \end{cases} \quad j = 1,2,\cdots m \qquad (4\text{-}20)$$

It then follows that the importance of mode *j* at time t_0 is given by $\left\|\phi_j\right\|$, while the phase (mode shape) is given by its phase, $\angle\phi_j$.

Several remarks are in order:

- *Remark 1*: Compared to POD, the modal expansion in equation (4-19) decomposes the measured data into a combination of spatiotemporal functions weighted by the corresponding Ritz eigenvalues. Compared to the Koopman modal expansions, the DMD modal expansions are of dimension $m<<N$
- *Remark 2*: As seen above, the dynamical modes, $\phi_j=\boldsymbol{U}\boldsymbol{y}_j$ corresponding to λ_j, provide the spatial coherent structure (spatial mode shape) of the corresponding oscillatory mode.

4.3 Dynamic Mode Decomposition Analysis

In this section, two typical events are selected from the database. Dynamic mode decomposition was performed on the transient stability data giving a set of modes that fully characterize system behavior. The subsequent analysis examines the ability of DMD to assess mode shapes of the system. Comparisons of the performance are made between conventional mode-based method and DMD analysis.

4.3.1 Case 1: load event 3

- Area2_Load is increased by 10% every 10s for three times, using COI as reference.

In this case, the interarea transmission lines are overloaded, resulting in changes of system behavior. Oscillation modes are re-identified using mode-based method under this new operating state. Results show that one of oscillation modes is an inter-area mode with a frequency of 0.407 Hz and damping ratio of 0.0184. It represents the swinging between generators in area 1 and area 2, as shown in Figure 4.1.

For the DMD analysis, the frequency, the voltage angles of busbars and the generator speeds are selected as input data, in a specific time window. The extracted modes are sorting in a descending order of energy, as shown in Table 4.1, among which the dominant one is exactly the inter-area mode with a frequency of 0.39 Hz and a damping ratio of -0.0078. The mode damping is negative, which means the oscillations are slightly increasing over time. The negative frequencies in the table are due to the conjugate complex eigenvalues, thereby only the positive oscillation frequencies are concerned. The energies of the remaining modes are apparently less than the dominated one, these modes are fictitious modes generated by DMD to better approximate the evolution of the input signals.

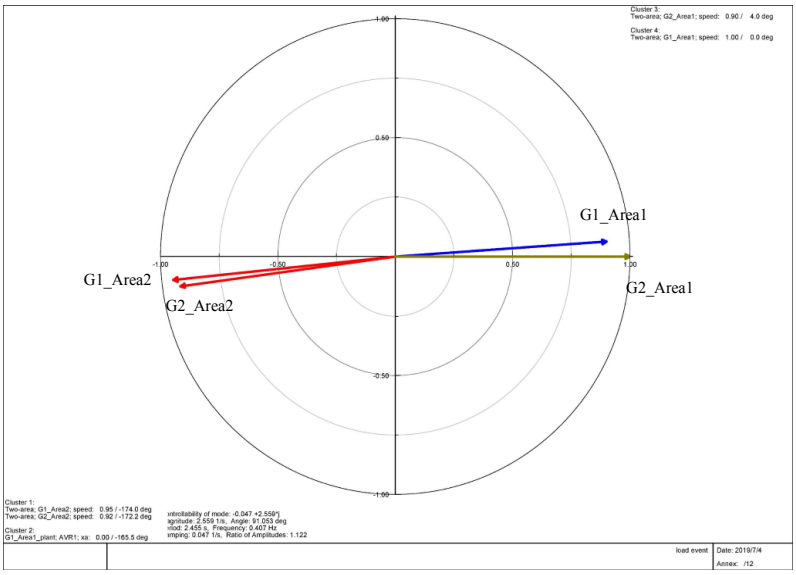

Figure 4.1 Interarea mode f=0.407 Hz, ζ=0.0184 obtained by mode-based method

Figure 4.2 displays the mode shapes of the voltage angle measurements. It can be seen that the voltage angles of the busbars in area1 are swinging against those in area2. The voltage angle of the interarea busbar situates exactly in the middle of the figure, whose amplitude is quite small. So, we can confirm that this event is an interarea event.

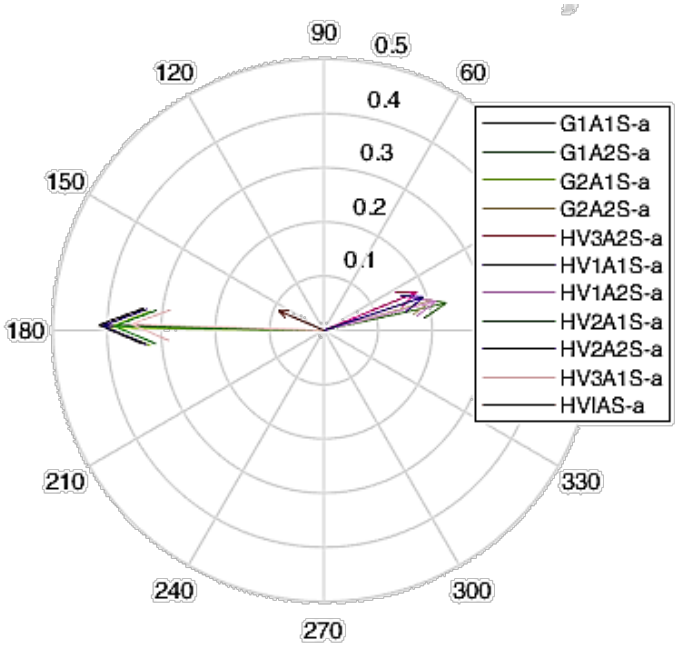

Figure 4.2 Mode shape using the angle measurements:

Table 4.1 DMD modes of Load event 3

Damping ratio	Frequency	Energy
1.0000	0	228.4490
-0.0078	0.3936	84.9225
-0.0078	-0.3936	84.9225
0.6707	-0.3259	1.4085
0.6707	0.3259	1.4085
0.2582	-0.6142	0.4594
0.2582	0.6142	0.4594
0.1239	-4.4398	0.2844
0.1239	4.4398	0.2844
0.2188	-0.8667	0.2699
0.2188	0.8667	0.2699
0.1940	1.2361	0.1995
0.1940	-1.2361	0.1995
0.3959	-2.6645	0.1610
0.3959	2.6645	0.1610
1.0000	0	0.1462
0.5543	25.0000	0.0546
0.9844	-0.5097	0.0457
0.9844	0.5097	0.0457
0.8638	1.1241	0.0425
0.8638	-1.1241	0.0425
1.0000	0	0.0363
1.0000	0	0.0073
0.0618	18.0417	0.0070
0.0618	-18.0417	0.0070
1.0000	0	0.0004

Moreover, we can reconstruct the data using DMD and compare them with the original ones. As shown in figure 4.3, no filters were applied here, but DMD can easily reconstruct the noisy signals: reconstructed curves match with curves of measured data.

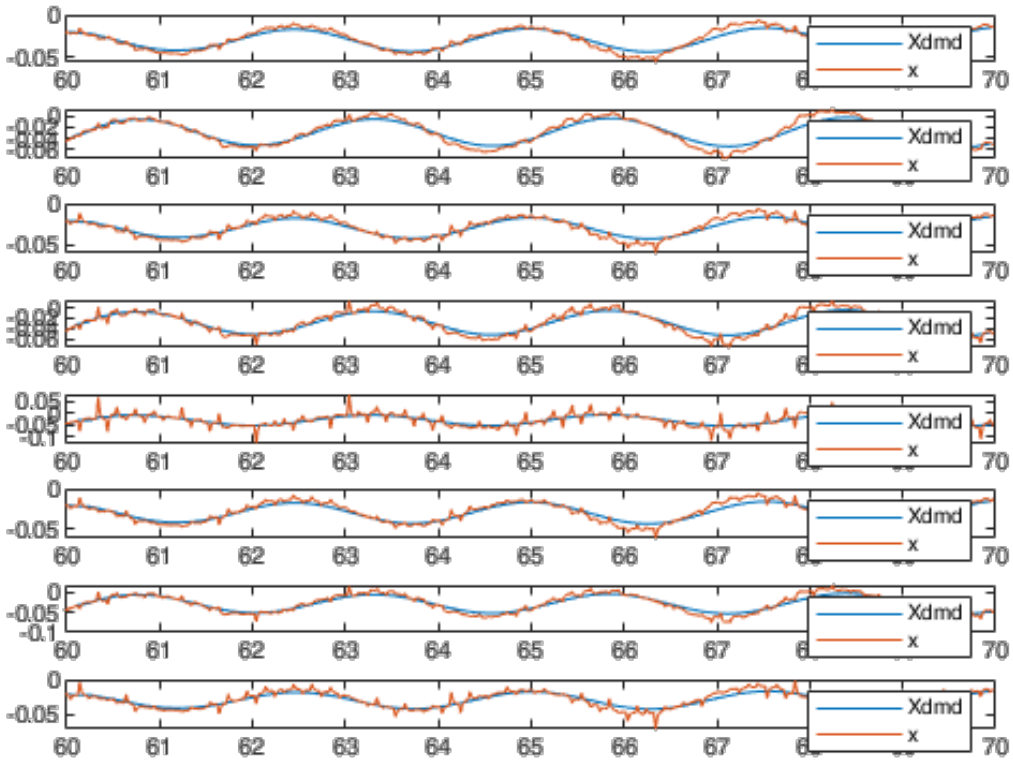

Figure 4.3 Comparison of reconstructed data and original data

4.3.2 Case 2: short-circuit event1

- Three-phase short-circuit fault is applied to Inter_Area_L1a at t=10 s, and removed at zero crossing after a power frequency cycled (0.02s), using COI as reference.

Similarly, the same variables are kept as inputs. The extracted modes are sorting in a descending order of energy, as shown in Table 4.2. The reason for negative frequencies is the same as mentioned in Case 1. In this case, the dominant mode is an inter-area mode with a frequency of 0.539 Hz and a damping ratio of 0.045. The mode damping is positive, which means the oscillations are decreasing over time. Still, the remaining modes are fictitious modes generated by DMD for a better approximation of the input signals. The frequency and damping ratio of the identified mode are quite close to the inter-area oscillation mode represented in Table 3.6, which is obtained by conventional modal analysis method.

In Figure 4.4, the clusters of coherent generators are identified with rotor speeds. Both figures represent the interarea oscillation mode that generators in area 1 are

swinging against those in area 2. The coherent groups identified by DMD and mode-based method are in good agreement with each other.

Table 4.2 DMD modes of Short-circuit event 1

Damping ratio	Frequency	Energy
0.0450	-0.5392	32.8133
0.0450	0.5392	32.8133
-0.3394	0.0347	2.0657
-0.3394	-0.0347	2.0657
0.9828	5.1952	1.6860
0.9828	-5.1952	1.6860
0.1733	1.0193	1.1289
0.1733	-1.0193	1.1289
0.0938	1.0199	0.8266
0.0938	-1.0199	0.8266
0.4184	2.6673	0.2668
0.4184	-2.6673	0.2668
0.2602	1.8800	0.1741
0.2602	-1.8800	0.1741
1.0000	0	0.1735
1.0000	0	0.1722
1.0000	0	0.1673
0.3878	-4.5316	0.1421
0.3878	4.5316	0.1421
0.9190	5.2166	0.1161
1.0000	0	0.0855
1.0000	0	0.0630
0.8206	-3.1015	0.0476
0.8206	3.1015	0.0476
0.5690	25.0000	0.0203

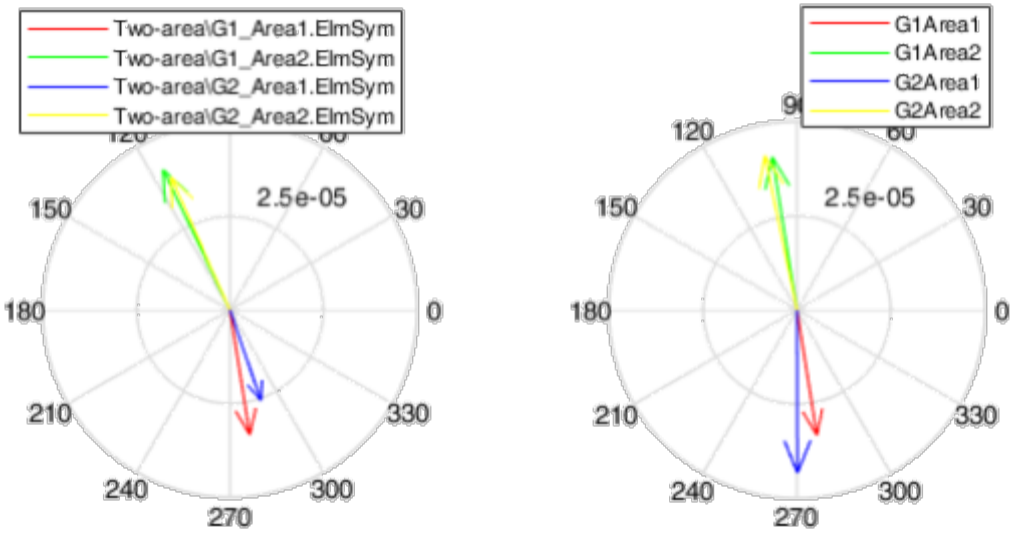

(a) Mode shape using Digslient

(b) Mode shape using the speed measurements

Figure 4.4 Comparison of mode shape

Similarly, we also reconstruct the noisy signals by DMD algorithm. In Figure 4.5, reconstructed curves are in coincident with curves of observable data, which also validate the ability of DMD.

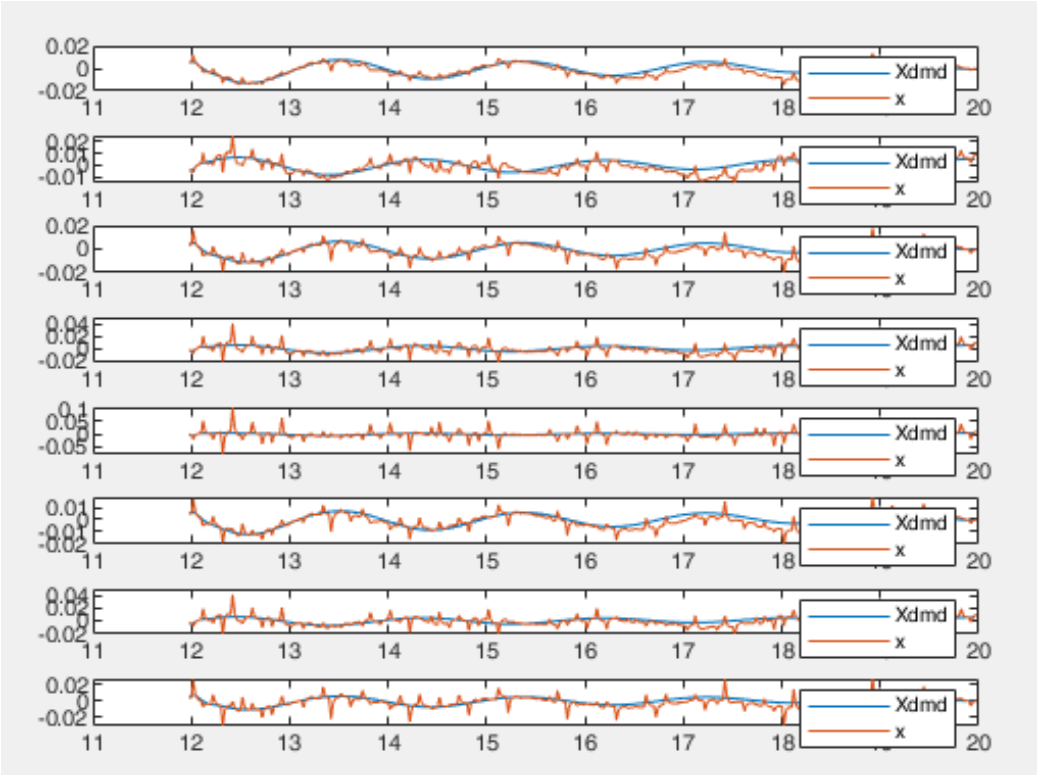

Figure 4.5 Comparison of reconstructed data and original data

5 Conclusions and Future Works

5.1 Conclusions

Conclusion

In this thesis, the effectiveness of dynamic mode decomposition technique for modal analysis of large data sets is validated.

Dynamic mode decomposition (DMD) is a mathematical method that aims at finding the low dimensional approximate matrix of the system to identify the oscillation modes and parameters. At this point, the underlying electromechanical oscillation modes of the power system could be extracted, without knowing the dynamic system matrix.

Firstly, a two-area system is simulated in the DigSILENT PowerFactory software. According to mode-based analysis method, eigenvalues and oscillation modes of the test system are calculated and identified.

Secondly, a perturbed dataset is generated for DMD analysis. Given the real-time load fluctuation, stochastic load deviations of 0.5% are added to the based loads. Five load events, three short-circuit events, three generator events and two switch events are applied to the tested system. Selected variables in different scenarios are extracted, simulating available measurements from PMUs in actual power systems.

Lastly, DMD technique is applied to identify oscillation modes of two typical events, on the basis of simulated data base. The results obtained by DMD algorithm are in coincident with conventional method, which validates the ability of DMD algorithm in electromechanical oscillation modes identification.

5.2 Future works

Experience with simulated data shows that DMD analysis can be efficiently used to analyze large datasets from multiple sources. Several aspects of the theory deserve further investigation including the physical interpretation of dynamic structures, mode-state relationships and the analysis of structural properties of the model. The effect of noise contamination, trends and other artifacts of the dataset and the application to measured data is to be investigated in future research.

REFERENCE

[1] Machowski J. Power system dynamics and stability[M]// Power system dynamics and stability /. 1997..

[2] Overschee P V, Moor B D. Subspace Identification for Linear Systems[M]. 1996..

[3] Pierre J W , Trudnowski D , Donnelly M , et al. Overview of System Identification for Power Systems from Measured Responses1[J]. IFAC Proceedings Volumes, 2012, 45(16):989-1000.

[4] Iswadi H R , Best R J , Morrow D J . Identification of Small Signal Oscillation Mode Parameters from Simulated and Actual PMU Ringdown Data[C]// Powertech, IEEE Eindhoven. IEEE, 2016.

[5] Marple S L J , Carey W M . Digital Spectral Analysis with Applications[J]. The Journal of the Acoustical Society of America, 1989, 86(5):2043.

[6] Williams M, Kevrekidis I, Rowley C. Extending Dynamic Mode Decomposition: A Data--Driven Approximation of the Koopman Operator[C]// Meeting of the Aps Division of Fluid Dynamics. 2014.

[7] Milanović J V, Duque A C S. Identification of electromechanical modes and placement of PSSs using relative gain array[J]. IEEE Transactions on Power Systems, 2004, 19(1):410-417.

[8] Antonio D L O S J , Ramirez J M , Zamora Mendez A , et al. Identification of Electromechanical Modes Based on the Digital Taylor-Fourier Transform[J]. IEEE Transactions on Power Systems, 2015:1-10.

[9] Han S, Zheng X U, Huang H Y. Research on Coherence Tracking for Inter-area Oscillation: An Integrated Algorithm Using Refined Emperical Mode Decomposition and Correlation Analysis[J]. High Voltage Engineering, 2011, 37(8):2045-2052.

[10] Vanfretti L, Dosiek L, Pierre J W, et al. Application of ambient analysis techniques for the estimation of electromechanical oscillations from measured PMU data in four different power systems[J]. International Transactions on Electrical Energy Systems, 2013, 21(4):1640-1656..

[11] Terms definitions I J F O S . Definition and Classification of Power System Stability[J]. IEEE TRANSACTIONS ON POWER SYSTEMS PWRS, 2004.

[12] Leandro R B , E Silva A S , Decker I C , et al. Identification of the Oscillation Modes of a Large Power System Using Ambient Data[J]. Journal of Control, Automation and Electrical Systems, 2015, 26(4):441-453.

[13] Mohapatra S. Techniques for determining hidden properties of large-scale power systems[J]. 2015.

[14] Sarmadi S A N , Venkatasubramanian V . Electromechanical Mode Estimation Using Recursive Adaptive Stochastic Subspace Identification[J]. IEEE Transactions on Power Systems, 2014, 29(1):349-358..

[15] Khalilinia H , Zhang L , Venkatasubramanian V . Fast Frequency-Domain Decomposition for Ambient Oscillation Monitoring[J]. IEEE Transactions on Power Delivery, 2015, 30(3):1631-1633.

[16] Trudnowski D J. Estimating Electromechanical Mode Shape From Synchrophasor Measurements[J]. IEEE Trans Power Syst, 2008, 23(3):1188-1195.

[17] Vanfretti L , Dosiek L , Pierre J W , et al. Application of ambient analysis techniques for the estimation

of electromechanical oscillations from measured PMU data in four different power systems[J]. International Transactions on Electrical Energy Systems, 2011, 21(4):1640-1656.

[18] Wang X , Bialek J , Turitsyn K . PMU-Based Estimation of Dynamic State Jacobian Matrix and Dynamic System State Matrix in Ambient Conditions[J]. IEEE Transactions on Power Systems, 2017:1-1..

[19] Eremia M, Shahidehpour M. Handbook of Electrical Power System Dynamics:Modeling, Stability, and Control[J]. Social Science Electronic Publishing, 2013, 1536(1):864-899.

[20] Pai M A . Energy Function Analysis for Power System Stability[M]. Kluwer Academic Publishers, 1989.

[21] Petrov N I, Dermendjiev V N, Rompolt B. Internal motions and oscillatory phenomena in a quiescent prominence.[J]. 1998.

[22] Tipping M E, Bishop C M. Probabilistic Principal Component Analysis[J]. Journal of the Royal Statistical Society, 2010, 61(3):611-622.

[23] Shlens J . A Tutorial on Principal Component Analysis[J]. 2014.

[24] Davis J L. Oscillatory Phenomena[J]. 1988.

[25] Hatcher L , O'Rourke N . A Step-By-Step Approach to Using SAS System for Factor Analysis and Structural Equation Modeling[J]. International Statistical Review, 2013, 83(2):325-326.

[26] Barocio E, Pal B C, Thornhill N F, et al. A Dynamic Mode Decomposition Framework for Global Power System Oscillation Analysis[J]. IEEE Transactions on Power Systems, 2015, 30(6):2902-2912.

[27] Bai Z, Kaiser E, Proctor J L, et al. Dynamic mode decomposition for compressive system identification[J]. 2017.

[28] Ni Yixin. Theory and Analysis of Dynamic Power System [M]. Tsinghua University Press, 2002.

[29] Mohapatra S. Techniques for determining hidden properties of large-scale power systems[J]. 2015.

[30] Schmid P J , Sesterhenn J . Dynamic Mode Decomposition of numerical and experimental data[J]. Journal of Fluid Mechanics, 2008, 656(10):5-28.

[31] Schmid P J . Application of the dynamic mode decomposition to experimental data[J]. Experiments in Fluids, 2011, 50(4):1123-1130.

[32] Schmid P J , Li L , Juniper M P , et al. Applications of the dynamic mode decomposition[J]. Theoretical & Computational Fluid Dynamics, 2011, 25(1-4):249-259.

[33] Mezi'c I . Spectral Properties of Dynamical Systems, Model Reduction and Decompositions[J]. Nonlinear Dynamics, 2005, 41(1-3):309-325.